Pharmaceutical water systems

A thermal-fluid analysis of pipe dead-legs

By

Benjamin L. Austen (B.Sc. (Eng.) Dip. Eng. MIEI)

Thesis presented at Dublin City University in fulfilment of the requirements for the degree of Master of Engineering

Under the supervision of

Dr. Brian Corcoran

School of Mechanical and Manufacturing Engineering,
Dublin City University,
Ireland.

April 2005

Declaration

I hereby certify that this material, which I now submit for assessment on the programme of study leading to the award of Degree of Master of Engineering is entirely my own work and has not been taken from the work of others save and to the extent that such work has been cited and acknowledged within the text of my work.

Signed: Benjamin Austen ID No.: 51183323

Date: 9/5/05

Table of contents

Abstract

Title: Pharmaceutical water systems
A thermal-fluid analysis of pipe dead-legs
By

Benjamin L. Austen (B.Sc. (Eng.) Dip. Eng.)

The most commonly used technique for flow exchange, fluid isolation and removal in pharmaceutical water systems, is the installation of a branch tee with a conventional two-way outlet port valve. This however can create a stagnant or "dead-leg" zone, which is particularly hazardous as bacteria can accumulate and contaminate the entire water system. This project has involved the study of the thermal and fluid dynamics considerations within pipe dead-legs and their impact on high purity water systems. A detailed literature review of the technology surrounding pharmaceutical water systems was carried out to set the background for the analysis of pipe dead-legs.

An experimental test rig was designed and constructed to represent a typical single loop water system incorporating a dead-leg test section. Results were obtained for a 6d, 4d and 2d branch tee configuration under dead-leg flow conditions. The effect of the main pipe loop velocity and temperature on the dead-leg end temperature was investigated. Determination of the temperature distribution along the axis of the dead-leg branch under steady state conditions was also investigated.

It was shown that the maximum dead-leg end temperature increased for an increase in loop velocity for each configuration. Reducing the dead-leg length from a 6d to a 4d and 2d configuration respectively was shown to significantly increase the dead-leg end temperature. It was found that a zone of uniform temperature and a temperature decay region were present in each branch configuration respectively. It was shown that stagnant fluid was present at the end of the dead-leg for the 6d and 4d configurations. The 2d dead-leg was found to be the most effective configuration to achieve full loop temperature penetration and mixing of the dead-leg fluid. The 6d rule was shown to be inadequate for both fluid mixing and loop temperature penetration.

List of Figures

List of tables

Nomenclature

ρ	Density
π	Dimensionless Buckingham group
μ	Dynamic viscosity
°C	Degrees Celsius
°F	Degrees Fahrenheit
μm	micrometers
A	Pipe cross sectional area
d	Internal pipe diameter of dead leg branch pipe
D	Internal pipe diameter of distribution pipe
h	Heat transfer coefficient
k	Thermal conductivity
L	Dead-leg length
l	length along dead-leg
*l*p	Thermal penetration depth
mA	milliAmps
mV	millivolts
P	Pipe Perimeter
Re	Reynolds number
T	Temperature
U	Mean distribution loop water velocity

Subscripts

a	ambient
dl	dead-leg
edl	end dead-leg
mdl	maximum dead-leg
e	experimental
l	distance along dead-leg
L	loop
m	mean
p	predicted
w	water

Abbreviations

ASAI	American Society of Architectural Illustrators
CFD	Computational fluid dynamics
CFR	Code of federal regulations
CFU	Colony forming Units
cGMP	Current good manufacturing practice
CIP	Clean-in-place
DI	Deionised
EMEA	European Agency for the evaluation of medicinal products
EU/ml	Endotoxin Units per mililitre
FDA	Food and Drug Administration
GAC	Granular activated carbon
GMP	Good manufacturing practice
LVP	Large volume parenterals
ME	Multiple effect
Ph Eur.	European pharmacopoeia
PIV	Particle image velocimetry
PW	Purified Water
RTD	Resistance temperature detector
RO	Reverse Osmosis
SIP	Steam-in-place
TOC	Total organic carbon
USP	United States pharmacopoeia
UV	Ultraviolet
WFI	Water for injection

Chapter 1. Introduction

1.1 Pipe dead-legs in pharmaceutical water systems

Any section of pipe connected to another pipe in which water is flowing may contain relatively stagnant water. This non-flowing water is of major concern in pharmaceutical water systems because of the high planktonic organism counts found in such water. These unused sections of pipe are known as system dead-legs. In general, fluid isolation and take-off in pharmaceutical water systems is achieved by the installation of a T-piece (fig.1.1) with a two-way outlet port valve [1]. This technique, however, creates a stagnant or "dead-leg" zone, which is particularly hazardous as biofilm and free-floating bacteria can accumulate in this area growing readily and contaminating the entire water system.

1.2 The 6d rule

Attention was first given to pipe system dead-legs in 1972 by the Food and drug administration when the Guide for Large Volume Parenterals (LVP), Code of Federal Regulations (CFR) section 212.49 CFR 21 was circulated for comment. This document contained a paragraph that has become known as the "6d Rule".

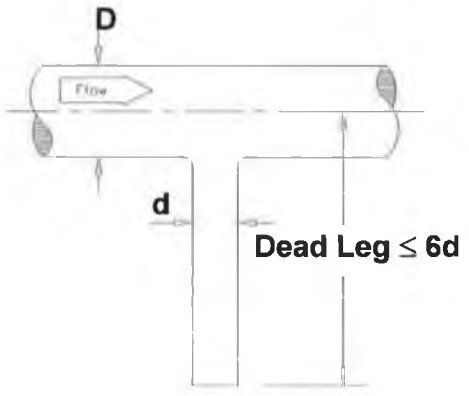

Figure 1.1: Classic dead-leg Configuration

The formal definition of a pipe dead-leg (fig.1.1) as given by the FDA requires that;

'Pipelines for the transmission of purified water for manufacturing or final rinse should not have an unused portion greater in length than 6 diameters of the unused portion of pipe (d) measured from the axis of the pipe (D) in use' [2].

The 6d rule has become a "rule of thumb" in industry with no substantial scientific data to support it. As a consequence dead-legs are a topic of great debate within industry but unusually no significant attempts until recently have been made to analyse closely their fluid and thermal characteristics [3].

As part of the research for this project three industrial site visits were undertaken to investigate current pharmaceutical water systems in operation within the Republic of Ireland. These companies included Yamanouchi Ireland, Leo laboratories and Archport Ltd. respectively. It was observed that dead-legs were evident in all the water systems being used particularly at sampling points and points-of-use for batch make-up and production purposes. It was found that continual flushing at these points was required to ensure bacterial limits were maintained. The dead-legs were considered the main cause for increases in bacterial counts in all cases. Leo laboratories were found to have a hot Water for Injection (WFI) loop in place with a distillation system installed to produce the required water quality. Dead-legs were present at almost all points-of-use within the system. Discussions with the facilities management and Quality department (QA) revealed continual contamination problems in the area of the dead-leg.

In order to have a full appreciation of pipe dead-legs and the potential threat they pose to the production of pharmaceutical products it is important to understand the technology surrounding pharmaceutical water systems so as to set the background for any subsequent dead-leg analysis.

1.3 Pharmaceutical water

'Water is one of the major commodities used by the pharmaceutical industry. It may be present as an excipient, or used for the reconstitution of products, during synthesis, during production of the finished product or as a cleaning agent for rinsing vessels, equipment and primary packaging materials' [4].

Different grades of water quality are required depending on the different pharmaceutical uses. Control of the quality of water, and in particular, the microbiological quality, is a major concern and the pharmaceutical industry devotes considerable resources to the development and maintenance of water purification systems.

Water that is found within the pharmaceutical industry would include high purity process water, water for personnel, utility grade water for heating and cooling and waste water [5].

1.4 Regulatory bodies

The pharmaceutical industry places a high priority on the quality of water used in the production of finished product, intermediate reagent preparation and analytical processes. Ensuring that consistency in the quality of waters produced is absolutely critical for pharmaceutical facilities.

'The high technology and cost of water purification/distillation equipment is negated if the distribution system cannot maintain the quality of water stipulated by the user quality department standards' [6].

The United States pharmacopoeia (USP), and the European pharmacopoeia (Ph Eur.) set the high purity water standards for the pharmaceutical industry. Both the USP and Ph Eur. work closely with the Food and Drug Administration (FDA), the European Agency for the evaluation of medicinal products (EMEA), the pharmaceutical industry, and the health professions, to establish authoritative pharmaceutical standards. These standards are enforceable by the FDA and the governments of other countries, and are recognised worldwide as the hallmark of quality. The FDA enforces current good manufacturing practice (cGMP), as well as the current USP monographs.

1.5 Purified water

Purified Water (PW) is water used in the process of production of medication for dosage. In general, either distillation or Reverse Osmosis (RO) can be used in the manufacture of purified water [7].

1.6 Water for injection

Water for Injection (WFI) is purified water used for the preparation of injectable pharmaceutical products. The USP 23 (p. 1635) monograph states: "Water for injection (WFI) is water purified by distillation or reverse osmosis." [8].

The EU pharmacopoeia only allows WFI to be produced by distillation. 'In 1999, in response to requests from major national delegations to permit the use of RO for WFI production, a major international symposium was organised to discuss the issue. The meeting concluded that there was insufficient evidence at the present time to support the use of RO to produce WFI and in view of the safety concerns, WFI should be prepared only by distillation as laid down in the European Pharmacopoeia' [4]. High purity water is categorised in accordance with the US and European Pharmacopoeias, as either Water for injection (WFI) or purified water (PW). Table 1.1 shows the difference between these waters based on maximum allowable microbiological and pyrogenic contamination [9].

Type of water	Upper bacterial limit (CFU/ml)	Upper Endotoxin Limit (EU/ml)
WFI	0.1	0.25
Purified water	100	0.25

Table 1.1: US and EU pharmacopoeia bacterial limits.

Bacterial contamination is quantified as "Colony Forming Units" (CFU), a measure of the total viable bacterial population. Pyrogens are substances that can induce a fever in a warm-blooded animal. Pyrogens are quantified as Endotoxin Units per millilitre (EU/mL). The most common pyrogenic substance is the bacterial endotoxin. They are more stable than bacterial cells and are not destroyed by standard conditions, such as autoclaving, that kill bacteria

1.7 Production of Pharmaceutical water

Waters that are found in nature will have had contact with their surroundings, and as a consequence will have adsorbed contaminants such as gases, minerals and organic materials, some naturally occurring and others man.

These waters require purification into high purity waters before use in a pharmaceutical or semi-conductor process. Impurities in water fall into three categories. These include dissolved solids, suspended solids and dissolved gases [10].

Dissolved solids are dissociated ionic salts and typically includes calcium, sodium, potassium, manganese, chloride, bicarbonate, sulphate as well as heavy metal traces and soluble silica.

Suspended solids are undissociated particles including silt, microbes, and cellular material suspected of causing the well-known pyrogen reaction.

Dissolved gases are typically limited to carbon dioxide and oxygen but occasionally also including ammonia.

A typical water treatment system used to produce pharmaceutical water is shown in Figure 1.2. The water system will be fed from the local mains water supply. A break tank is included to provide a reserve of water for the purification equipment and to maintain a constant pressure head to the system feed pump.

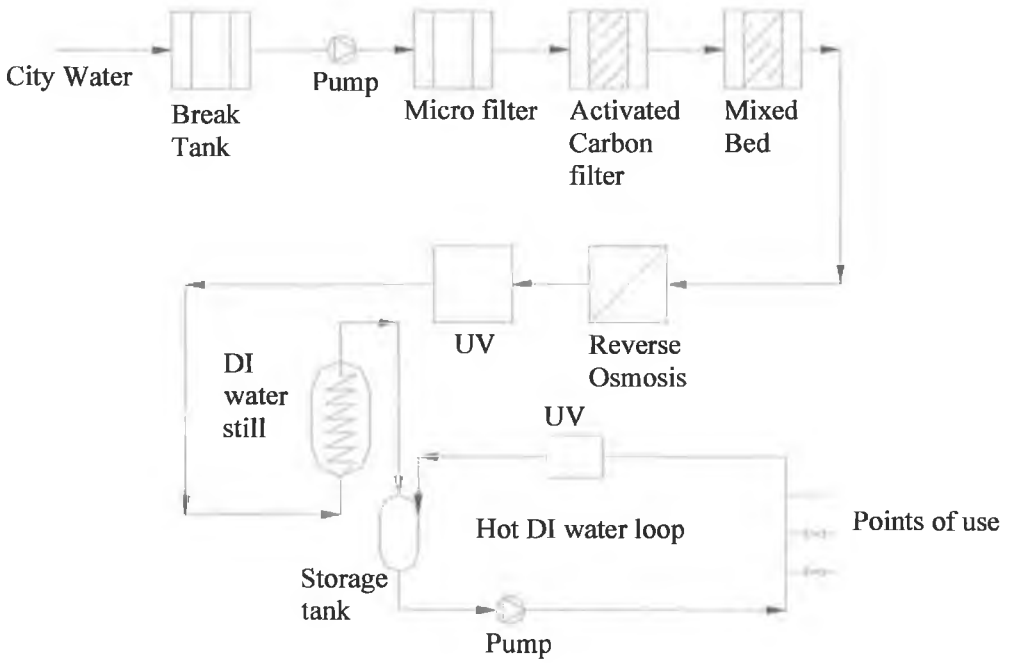

Figure 1.2: A pharmaceutical water purification system

After the break tank and pump a series of pre-treatment facilities are installed to eliminate bulk particulates and microorganisms. The water is then treated using either reverse osmosis and/or distillation depending on the water quality required by the particular pharmaceutical facility.

1.7.1 Pre-treatment of pharmaceutical waters

A number of pre-treatment facilities are adopted to ensure the required quality of water that is demanded by a particular pharmaceutical process prior to Distillation and Reverse Osmosis including microfiltration, Adsorption, Deionisation and Ozonation.

Microfiltration separates suspended particles from water by passing the water through a porous membrane or medium. The conventional and still the principal type of filter used for cleaning bulk water is the sand bed filter [11].

Adsorption removes organic constituents and residual disinfectants in water supplies using granular activated carbon (GAC) [12]. This not only improves taste and minimizes health hazards; it protects other water treatment units such as reverse osmosis membranes and ion exchange resins from possible damage due to oxidation or organic fouling. Most activated carbons are made from raw materials such as nutshells, wood, coal and petroleum.

Deionisation is used to remove scale forming minerals from water such as calcium and magnesium ions. The ion exchange water softener is one of the most common tools of water treatment. Ionic impurities are removed by passing water through a bed of synthetic resins, which have an affinity for dissolved ionized salts and gases. There are three types of deionisers: two-bed weak base, two-bed strong base, and mixed bed [13]. Two-bed deionizers have separate tanks of cation and anion resins. In mixed-bed deionizers the two resins are blended together in a single tank or vessel. Generally mixed-bed systems will produce higher-quality water, but with a lower total capacity than two-bed systems.

Ozonation is used to reduce colour, eliminate organic waste, reduce odour and reduce total organic carbon in water (TOC). Ozone is created in a number of different ways, including ultra violet (UV) light, corona discharge of electricity through an oxygen stream (including air), and several others [14]. In treating small quantities of waste, the UV ozonators are the most common, while large-scale systems use either corona discharge or other bulk ozone-producing methods.

After the water has been pre-treated, purified water can be produced in a number of ways, however, water for injection may only be produced by either Reverse Osmosis or Distillation.

1.7.2 Reverse Osmosis

It was found by Stadnisky [15] that the cost of producing pharmaceutical grade water in recent years with conventional distillation had significantly increased because of escalating energy costs. As a result, Reverse Osmosis (RO) has become a more attractive alternative. A typical Reverse Osmosis system is shown in figure 1.3.

Figure 1.3: Typical Reverse Osmosis system [16].

They are generally self-contained in design with all control features, pumps and filter membranes mounted on a frame. Ninety-eight to ninety-nine percent of organic compounds, dissolved ions, heavy metals, and microorganisms (bacteria, fungi, and viruses) can be removed from water with reverse osmosis. Reverse Osmosis utilizes hydraulic pressure to force pure water through a membrane.

Two types of membrane configurations are shown in figure 1.4. They can be either from flat sheets formed into spiral wound structure or from hollow fibres formed into a tube bundle configuration.

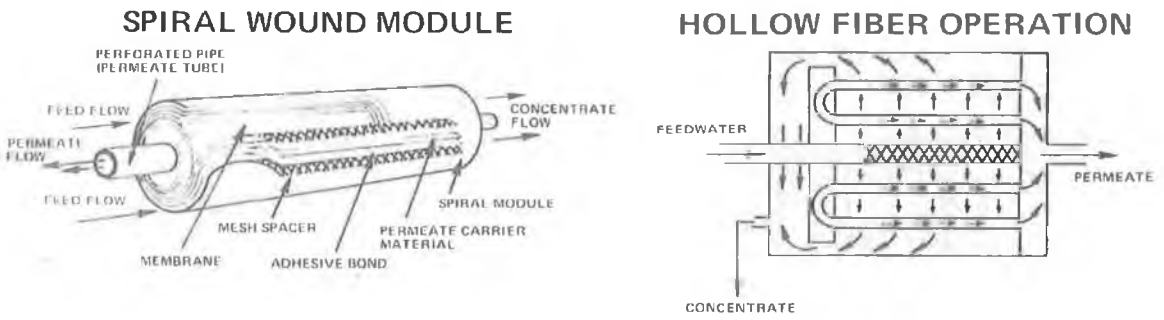

Figure 1.4: Reverse Osmosis membrane configurations [10].

1.7.3 Distillation

Distillation removes impurities from water by converting a liquid to a gas and then recondensing it as distilled water. This change of state process is used to purify water since most contaminants do not vaporise and therefore do not pass to the distillate upon condensation. Distilled water is free of all pyrogens, bacteria and viruses except dissolved ionised gases. A range of water stills are available including single effect, multiple-effect Stills (ME) or vapour compression [17]. Organic materials with a boiling point near that of water are very difficult to remove, due to carry over into the vapour. In these situations an ME still is often required for complete pyrogen removal.

The single-effect still is the oldest type of still and due to their high consumption of energy and cooling water, they are today only used in the small laboratory applications. The preferred alternative to the single effect still is the vapour compression still (fig. 1.5) due to a lower energy consumption, particularly if cold distillate is required. However, there are high maintenance costs associate with this system due to the large number of moving parts such as compressor, pumps, gears, belts etc. It was concluded by Kuhlman [13] that as the vapour compression still has a number of moving parts that are in contact with the distillate, they may with time wear and cause contamination in the distillate, particularly oil, which will not be detected by conductivity instruments.

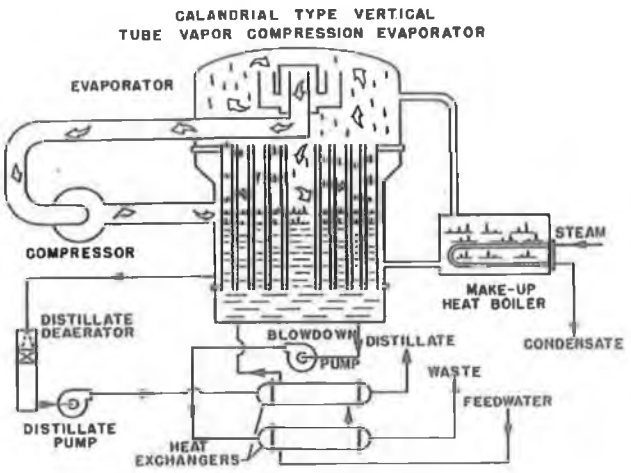

Figure 1.5: Vapour compression still [10].

The multi effect stills were originally based on the single effect. They can have as few as three effects, and as many as eight. Each effect decreases the energy and cooling water consumption. (figure 1.6).

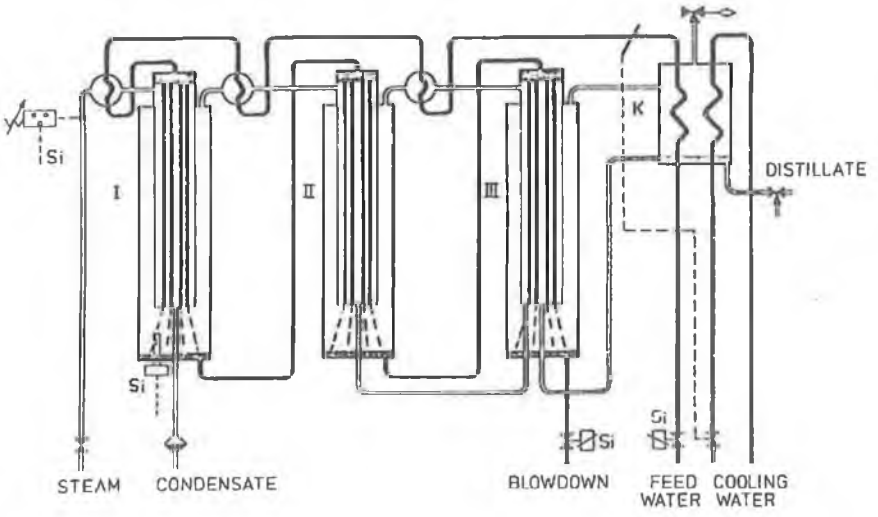

Figure 1.6: Multiple effect Still [13].

The multiple effect stills have no moving parts and can, therefore, be expected to have few breakdowns and maintenance problems. They are generally made of ASAI 316 stainless steel so they can be cleaned in place.

1.8 Recirculating pipe loop design

High purity water systems within the pharmaceutical industry are designed to continually recirculate the water in order to maintain a required microbiological limit.

1.8.1 Circulation temperature

'The circulation temperature of the water system is dictated by either the required microbiological specification or the required temperature for usage. To achieve a microbial limit of less than 10 CFU/100 ml, a minimum continuous temperature of at least 80 degrees Celsius is required (80 ^{0}C is the accepted minimum temperature that self sanitization will occur)' [6].

However, this will only limit bacterial proliferation, it will not entirely eliminate bacteria from the water. Ambient systems often incorporate a periodic sanitization by raising the loop temperature for a given period of time.

1.8.2 Circulation velocity

Stagnant or low fluid flow regions within distribution systems may promote bacterial growth. It is generally recognised within the pharmaceutical industry that a minimum circulation velocity in the region of 1.0 –3.0 m/s is required to maintain strict bacterial limits [18].

There are three main types of recirculating pipe loop. These include the single pipe loop, double pipe, flow and return loop and the double pipe, flow/reverse return loop. The factors affecting the ultimate selection will include user requirements, plant physical layout and the economic issues.

Figure 1.7 shows a schematic of a single pipe loop commonly installed in pharmaceutical plants. The system consists of a storage tank, pump, flow regulation devices, sampling and outlet ports and a number of heat exchangers to provide some points-of-use with different outlet temperatures. This system is used where only a small number of variable temperature outlets are required and most points-of-use within the pipe network are required at the loop temperature. This pipe system has the least amount of pipe work quantities of all system designs and will maintain an equal flowrate/velocity around the loop. This type of system however may be prone to high system pressures and difficulty in flow balancing [19].

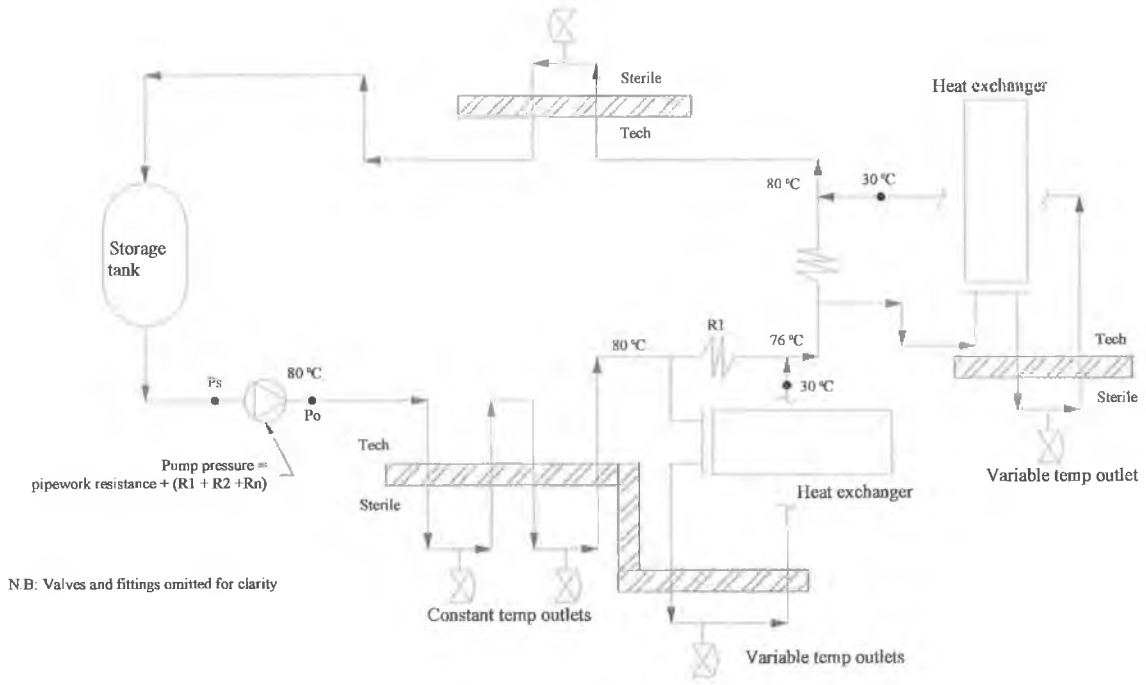

Figure 1.7: Single pipe distribution loop [6].

Double Pipe distribution loop arrangements are most suited to hot circulation systems where there is a requirement for a high number of variable temperature outlets/point-of-use heat exchangers [6]. The essential difference is that the return lines from the heat exchanger sub-loops are routed directly back to the storage tank for heating rather than being feed back into the main distribution loop pipe. This allows easier control over the flowrate across the system and does not require inline flow regulation devices, which provide a potential source for bacterial contamination. However, there will be a greater amount of pipework compared to the single loop system.

1.9 Components of a recirculating pharmaceutical loop

Many of the design characteristics associated with high purity water distribution systems are incorporated for hygienic reasons ensuring bacterial limits are maintained and the integrity of the system is not undermined.

1.9.1 Pipework

Piping in pharmaceutical water systems usually consists of a high polished stainless steel. Stainless steel has excellent corrosion resistance properties.

Chemical sanitising agents such as chlorine or hydrochloric acid can be very corrosive especially at high temperatures (60-80 ^{0}C), therefore, 316 stainless is generally used for this reason. Other materials include polypropylene and Teflon® Perdluoroalkoxy [20].

The ability to polish stainless steel to a specific pipe roughness reduces the risk of bacteria present in the water system lodging in microscopic crevices were it can grow and contaminate the system. All pipe joints are constructed using either sanitary fittings or are butt-welded using an orbital welder. Threaded fittings are not used as they create crevices for bacteria to accumulate and also give regions for pipe corrosion to take place [2]. Sanitary fittings are used where the piping meets valves, tanks and other equipment for ease of removal during maintenance or where components are replaced regularly.

Figure 1.8 shows a sketch of T-piece fittings that are used within the pharmaceutical industry. They are constructed with either a sharp entry or a small radius of curvature between the branch and main pipe [4].

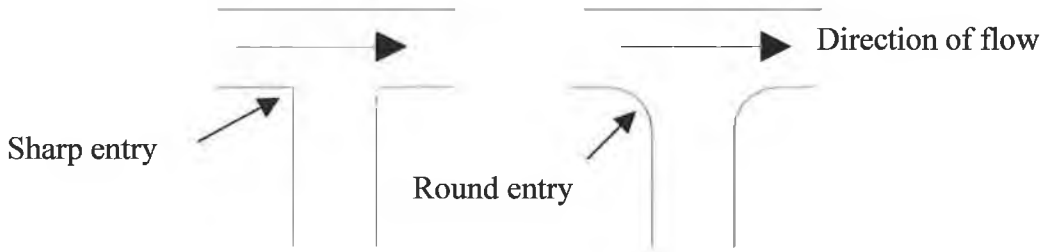

Figure 1.8: Sketch of round and sharp entry tee.

1.9.2 Storage tanks

Tanks that are constructed for storing large volumes of pharmaceutical water are made from 316 stainless steel due to the corrosive properties of water, particularly at elevated temperatures. Also the ability to highly polish tank surfaces to eliminate the possibility of bacteria lodging onto surfaces is of significant importance.

During a site visit to Leo laboratories Ireland Ltd., it was found that a storage tank included a vent filter, spray-balls, instrumentation, and flash steam heating.

The vent filter ensured that, during venting of excessive pressure from the storage tank, harmful air-born contaminants to personnel would be filtered out before entering the surrounding atmosphere. Sprayballs were installed to assist in cleaning of the storage tank during clean-in-place (CIP) processes. Instrumentation included pressure gauges, level sensors and volume flowmeters. Flash steam from the distillation process was used to assist in maintaining the required temperature in the tank. The heating was by way of an indirect heating coil.

1.9.3 Pumps

Both constant speed and variable speed centrifugal pumps are used within the pharmaceutical industry for transportation of pharmaceutical waters [21]. Variable speed pumps avoid over pressurising the distribution system and can also reduce excessive energy demands during periods of low water usage [22]. As the pump is one of the few moving parts within a water system, particulates that may become detached from the normal wear and tear of the pump during operation must be filtered out prior to the water entering the pipe loop to avoid contaminating the water system.

1.9.4 Valves

It was found by Carvell [1] that valves and actuators incorporated into a purified water system, while in operation, must not only isolate the sterile process area from the external environment but also prevent the process from polluting the external environment, particularly where genetically manipulated organisms are being produced. Like most of the materials used within pharmaceutical water systems, 316L stainless steel is the preferred material choice for valve construction.

'Valve components should be constructed of materials, which remain inert when in contact with process fluids. Seals, gaskets and flexible diaphragm materials must be capable of withstanding the rigours of "in-situ" steam sterilisation at temperatures of up to 140^0C. In most cases the diaphragm valve and ball valve are the choice of many pharmaceutical companies'.

Figure 1.9: Sanitary Valve [1]

Dead legs are often found at a point-of-use in a purified water system due to the installation of a T-piece and a diaphragm valve. To help to eliminate dead-legs in valve installation, zero dead-leg valves such as those shown in figure 1.9 are installed.

1.10 Contamination in pharmaceutical water systems

The main cause of bacterial contamination in pharmaceutical water systems is the development of Biofilm. A review of Biofilm within the pharmaceutical industry by Fleming et al [20] found that biofilms could affect aseptic transfer by contaminating production batches, by contributing to line fouling, and by increasing cleaning problems and costs. Control of bacterial limits in pharmaceutical or biotechnology production lines must take into account the mechanics of biofilm formation, prevention and cleaning.

1.10.1 Formation of Biofilm

'A Biofilm is defined as a bacterial population composed of cells which are firmly attached as micro-colonies to a solid surface' [23]. The instant a clean pipe is filled with water, a biofilm will begin to form.

After a pipe surface comes into contact with water, an organic layer deposits on the water/solid interface and creates an adsorbed layer [24]. This adsorbed layer allows the transport of planktonic bacteria to the pipe wall to begin the formation of a biofilm (figure 1.10).

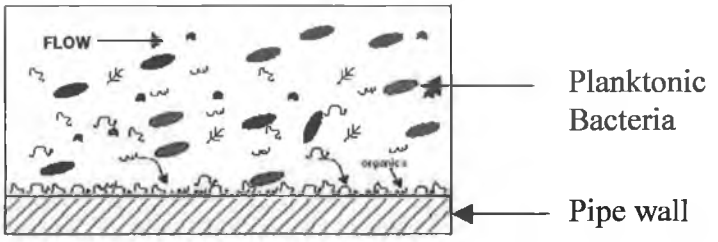

Figure 1.10: Adsorption of organic molecules on a pipe wall [25].

At this stage there is a process of detachment and attachment of microorganisms until a mature, fully functioning biofilm made up of a web of microbes and extracellular polymers has formed. It can spread at its own rate by ordinary cell division and it will also periodically release cells to colonize downstream sections of piping.

1.10.2 Effect of surface material on biofilm formation

It was reported by Meltzer [26] that the material of the pipe surface has little or no effect on biofilm development. Stainless steel is just as susceptible as plastic pipe. Studies have shown that bacteria will adhere as quickly to stainless steel as it will to Teflon and PVC pipework [20]. One major factor influencing biofilm development in purified-water systems is surface area. Industrial water systems offer a significant amount of surface area for biofilm attachment including RO membranes, storage tanks, cartridge filters, and piping systems.

1.10.3 Effect of loop velocity on Biofilm formation

Normal operating loop velocities were found to be in the region of 1.0-3.0 m/s to avoid bacterial proliferation [18]. However, not unlike other design criteria used in the pharmaceutical industry, a minimum loop velocity of 0.3 m/s was adopted as a rule of thumb to control biofilm growth on pipe walls [27]. It was found that this velocity was misapplied to recirculating loop systems as a means of controlling biofilm, were infact, it was originally proposed as a clean-in-place (CIP) guideline. It was found that there was no single velocity upon which recirculating high purity water systems could be designed and operated to control biofilm formation. It was shown that at high water flow rates biofilm growth would be altered but would not prevent the attachment of bacteria to pipe surfaces [26].

Regardless of the mean velocity, the water in the loop pipe will flow slowest close to the pipe surface due to the boundary layer developed between the fluid and the wall of the pipe. It was shown that the shear forces within the laminar sublayer were insufficient to dislodge a bacteria cell typically found in a biofilm [27].

1.11 Bacterial control in pharmaceutical water systems

The cleaning of pharmaceutical manufacturing facilities and production equipment has become of paramount importance in the pharmaceutical industry with the primary function of reducing or eliminating the possibility of cross contamination [28]. It was reported by Reidewald [23] that mechanical cleaning techniques, or the shear forces induced by fluids may be used to control the level of bacterial growth

Noble [29] found the methods most commonly used to achieve and maintain microbiological control included:

- Maintenance of the piping at elevated temperatures.
- Use of chemical disinfecting agents.
- Use of sterilizing radiation.
- CIP (clean-in-place), which also renders the piping chemically clean.
- SIP (steam-in-place) followed by the use of sterile barriers.

1.11.1 Sanitization

Sanitization describes the process of reducing viable microbial population using chemical or thermal treatments. The important issue is to contact the entire pipe surface area with the sanitizing agent to ensure that the system is maintained within the desired bacterial limits (table 1.1). Common sanitization agents would include caustic, bleach, hydrogen peroxide/peracetic acid and hot water.

Purified water systems can be either a hot water distribution system (80 ^{0}C) or an ambient cold water system. Heating water to a high temperature naturally kills bacteria and these systems are therefore self-sanitizing [30]. If the distribution system is at ambient temperature it will require chemical sanitization or raising the temperature to 80 ^{0}C for a period of time and then cooling back to distribution temperature.

1.11.2 Cleaning-in-Place (CIP)

'Clean-in-Place is the process used to ensure that process lines, vessels and reactors are free of inorganic and organic contaminants' [31]. In small scale laboratory practices, apparatus are generally disassembled, cleaned and if necessary, sterilized using an autoclave. On an industrial scale this is not possible and hence, CIP systems were developed to handle the complex nature of industrial cleaning processes.

Clean-In-Place (CIP) is an automated method of cleaning process plants, involving little or no dismantling of piping or equipment. In the cleaning cycle, CIP allows the cleaning solution to be brought into contact with all the soiled surfaces of the water system by a process of draining, rinsing, cleaning, washing and rinsing [32]. The cleaning process involves both chemical and physical aspects, and utilises the already present water recirculation system to minimize water, chemical and waste-treatment costs.

1.11.3 Steam-in-place (SIP)

In conjunction with the sanitization of pharmaceutical water systems is the use of process steam [31].

The production of parenteral solutions, and the variety of new pharmaceutical products has made it necessary to consider more rigorous cleaning procedures, replacing distilled water rinsing with chemical based CIP procedures followed by steam-in-place (SIP) sterilisation [33]. 'A system designed for CIP is readily adaptable to SIP. It is necessary only to properly incorporate additional hardware to accomplish and control the steam sterilisation cycle; i.e., steam traps, vent valves, and resistance temperature devices (RTD)' [34].

During an initial investigation of pharmaceutical water systems at a number of pharmaceutical plants, it was noted that CIP, SIP and sanitisation processes varied from one manufacturer to another. The main reason for this is that water quality requirements varied from one plant to another and as a consequence in-house water testing and cleaning validation techniques were considerably different. There was no specific literature available in relation to heating time requirements and this information is very much in the hands of the individual manufacturers.

1.12 Research of pipe system dead-legs

The contamination problems associated with dead-legs affect the design and operation of pharmaceutical water systems.

Due to an ever expanding and increasingly regulated pharmaceutical market, the need to scientifically examine water system design problems such as dead-legs has become essential to ensure the satisfactory production of pharmaceutical products.

During cleaning-in-place (CIP) through chemical and/or heat treatment, it was found that dead-legs caused problems in relation to diffusion of chemicals and the transfer of heat to the bottom of the dead-leg [6]. Firstly, the cleaning chemicals may not diffuse down the entire length of the dead leg resulting in areas that do not see the required concentration for the required amount of time and temperature. Secondly, they create pockets of cleaning chemicals that do not get properly rinsed from the system. Conduction is considered the primary method of heat transfer to the dead-leg in liquid sanitisation. This type of transfer can create localised pockets in the system that may not reach the distribution loop temperature. This localised temperature drop enables water bound bacteria to grow adding to the problem of contamination.

Noble [29] analysed transport in dead-legs for two common disinfection methods: thermal and ozone treatment. It was assumed that the mixing created by the turbulent Reynolds stresses in the main distribution pipe flow would have a dominant effect on the velocity field in the dead-leg entry region leading to good fluid mixing or a turbulent zone.

Forced convection was assumed to be the main form of heat transfer in this region. The turbulence was considered to reduce in magnitude with distance into the dead-leg. At the end of the branch pipe a stagnant region was assumed to be dominant with diffusion (conduction) as the mode of heat transfer. It was shown that the length of the turbulent zone, l_t, was a function of the loop velocity, U, if fluid properties remained constant and the tee was the same diameter as the main distribution pipe. The mathematical model presented suggested a significant drop in temperature within this diffusion zone.

Steam-in-place (SIP) sterilization of pharmaceutical equipment is one method of assuring an aseptic environment in purified water systems.

Steam sterilisation for example, requires the presence of adequate moisture and temperature to assure rapid and reproducible sterilisation. Entrapped air is the greatest impediment to steam sterilisation because it retards heat and moisture penetration. Dead-leg geometries present a severe challenge for air removal.

Young et al [35] studied the effect of tube diameter on steam-in-place sterilization of dead-legs, by examining temperature profiles and rates of kill of Bacillus stearothermophilus spores. Time required for sterilization was determined for 9.4 cm branches with various inside diameters from 0.4 to 1.7 cm.
It was found that sterilization time increased with decreasing tube diameter. For smaller diameter tubes, entrapped air remained after 2 hours and rates of kill were very dependent on position within the tube, tube diameter, and tube orientation with respect to the gravitational vector.

As is the case with most engineering problems, much of what is understood about the problem is determined through vast engineering experience. However, more recent attempts are being made to establish computational modelling solutions to engineering problems [36]. Although beyond the scope of this project a number of useful computational references are included in the following text to assist in understanding the complexity of a pipe system dead-leg.

Haga et al studied the cleaning of a dead-leg with several pipe diameter to length ratios, l/d, and loop liquid velocities [28]. A computational flow simulation was performed to investigate the cleaning mechanism of the dead-leg.

It was noted that more than 2 m/s liquid velocity was required to remove chemical residue from an l/d=6 dead-leg immediately. A velocity of 0.5 m/s liquid velocity was enough to remove residue from an l/d=2.8 dead-leg. It was shown that liquid velocities in the main pipe of 2.5 m/s produced a circulating flow in the dead-leg, which drew a stagnant region of liquid from the dead-leg back into the main flow. The higher the main liquid flow rate the higher the circulating flow in the dead-leg.

Corcoran et al researched a computational model to study turbulent flow in a 50mm diameter 90^0 pharmaceutical tee-junction during divided flow conditions and also under dead-leg flow conditions [3].

Numerical predictions were compared with previously presented experimental results based on particle image velocimetry (PIV)[37]. It was shown that regions of low turbulence were present within the dead-leg branch. The wall region, which is critical to biofilm formation, was found to have low velocity under dead-leg conditions and of low shear stress.

Nakamori et al [38] studied the thermal and flow characteristics of dead-leg branch pipes of a nuclear power plant. The research focused on the use of computational modelling and experimental analysis to study the depth of penetration of a cavity flow in order to evaluate temperature distribution and thermal cycling in the branch pipe.
It was found that cavity flow penetration increased with increase in the main loop velocity. Results obtained for cavity flow penetration from experiment were comparable to computational modelling.

Deutsch et al [39] studied isothermal flow in dead-legs commonly found in pressurised water reactors. Experimental data was obtained using PIV. Computational fluid dynamics (CFD) studies were carried out and compared to the experimental results. It was shown that a vortex penetration extended along the auxiliary line in a helicoidal fashion. Computational results obtained using the second moment closure turbulence model were in agreement with those obtained from experiment.

From a design and installation point of view the 6d rule as stated by the Guide for Large Volume Parenterals (LVP) [2], is poorly written. The problem with this specification is that it measures the length of the dead-leg from the centre line of the main loop pipe. Figure 1.13 shows the relationship of the 6d rule to three different branch pipe diameters. Branch A represents a tee with a loop to branch pipe diameter ratio of 1:1. Branch B and C represent 2:1 and 4:1 pipe ratios respectively.

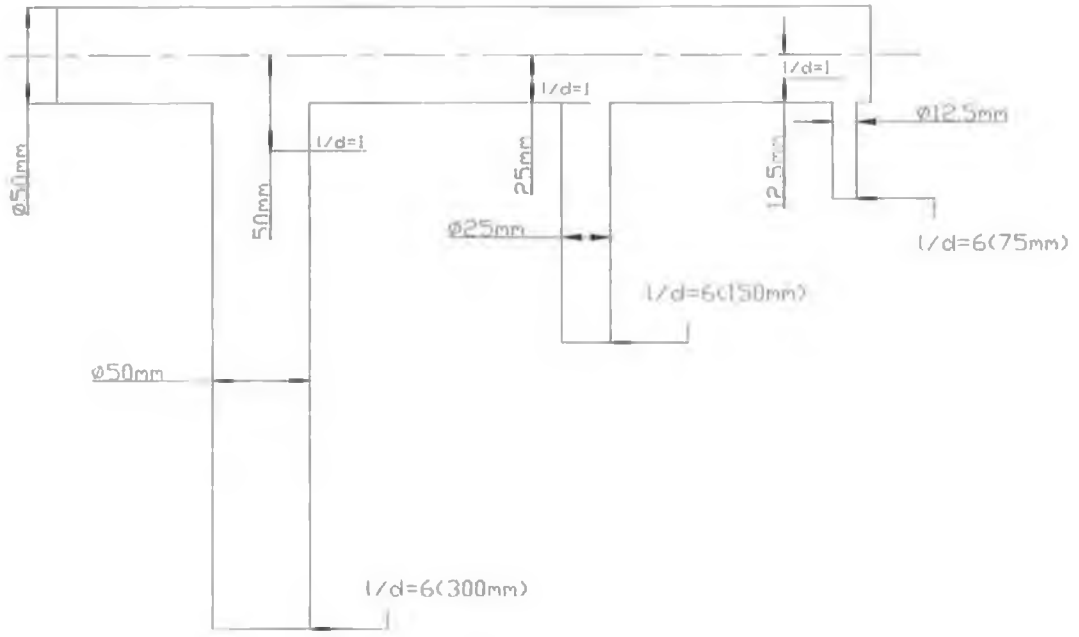

Figure 1.11: Relationship of 6d rule to three branch pipe diameters

This makes no sense from a physical standpoint and creates a problem when installing small branch pipes off much larger distribution pipes. If, for example, a 12.5mm diameter sample line was required off a 50mm diameter main, 2d is already at the tube wall. The addition of any kind of weld fitting would tend to put the dead-leg well beyond the 6d rule.

1.13 Objectives of this thesis

The main objective of this research was to investigate the effect of loop flow velocity on the thermal and fluid dynamic considerations within pipe dead-legs and their impact on high purity pharmaceutical water systems.

This required the design and construction of an experimental test rig to represent a typical single loop water system incorporating a dead-leg test section.

Results were obtained for a 6d, 4d and 2d dead-leg configuration with equal branch and loop pipe diameters. The experimental discussion was based around the following areas for each dead-leg configuration:

1. Investigation of the effect of loop velocity and temperature on the dead-leg end temperature.

2. Determination of the temperature distribution along the axis of the dead-leg branch under steady state conditions.

Chapter 2. Materials and Methods

An experimental test rig was designed and constructed to study the thermal characteristics of a pipe system dead-leg. The rig included a storage tank, recirculating pump, pipe network, dead-leg test section, instrumentation, temperature control and data acquisition. Figure 2.1 shows a schematic diagram for the initial testing rig including the flow path of the rig fluid.

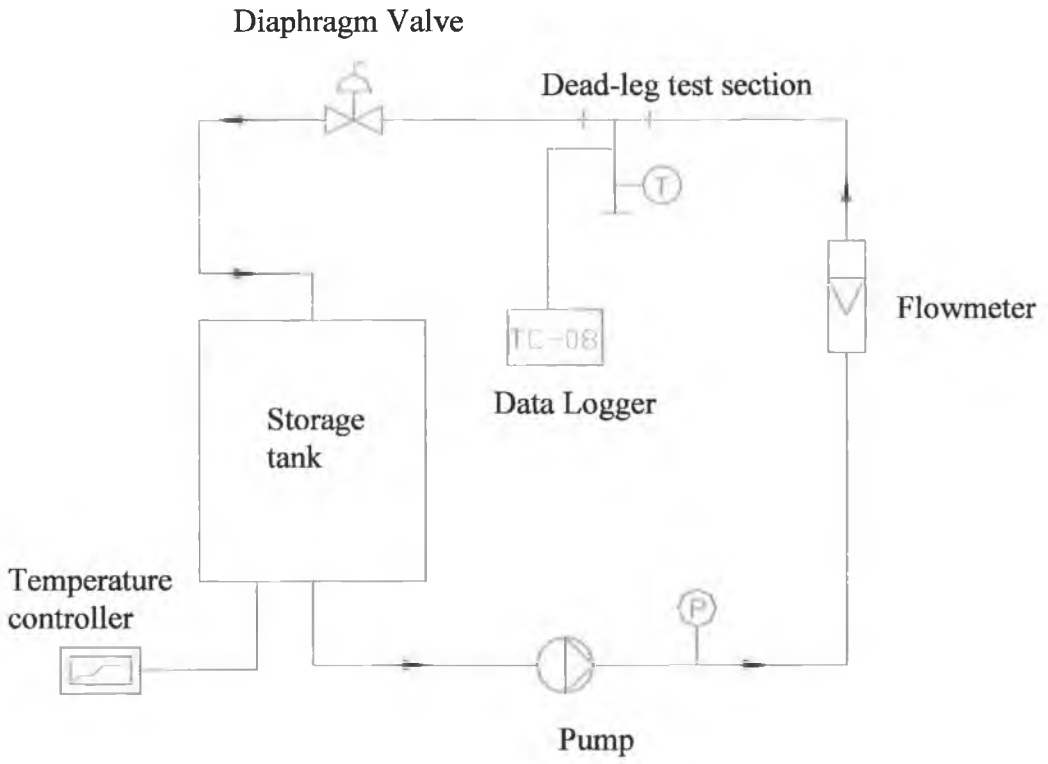

Figure 2.1: Piping and instrumentation on experimental rig

The rig was designed to operate as a recirculating hot water single pipe loop. A pump was used to recirculate hot feed water from a heated storage tank, through a pipe network and dead-leg test section and return the fluid back to the tank for reheating. A flowmeter was used to determine the required volume flowrate of the operating fluid and the flow was regulated using a diaphragm valve. Temperature data from the dead-leg test section was logged using a data acquisition system.

2.1 Storage tank

The storage tank was supplied by Heiton Buckley Ltd., and was manufactured from polyethylene with dimensions of 800 × 460 × 460mm (l×b×h).

The working capacity of the tank was 100 litres. It was mounted on a custom-built stainless steel frame that was also used to house the pump and control panel.

Because of a system operating temperature of 80°C, a lid was constructed for the tank and the sides, base and lid were fully insulated using 13mm foam sheet insulation supplied by Marr insulation Ltd.

2.2 Distribution loop pipework

All pipework and fittings were supplied by Leslie Reynolds & Co., and were manufactured from 316L stainless steel with a 50mm outer diameter. Pipe sections were constructed to make connections from the storage tank to the pump, the pump and the flow meter and also entry and exit lengths for the dead-leg test section and tank return pipework. The FDA [2] recommend the use of butt welded or sanitary fittings for all pipework. The piping was cut to the required length, deburred and the necessary fittings were butt welded at the pipe ends using a Tungsten Inert Gas (TIG) welder. Gas purging was used on the internal pipe area to ensure that the internal weld was clean and flush with the pipe wall.

Figure 2.2: Sanitary pipe fittings *(hand pen for scale)*

A selection of sanitary fittings are shown in figure 2.2. Pipe sections were clamped together using a tri-clamp (1). A PTFE seal (2) was placed between two adjoining pipe ferrules (3,4) to achieve the required watertight seal. A series of 90° elbows (5) were used to route the pipework in the required order.

The pipe assembly was wall mounted using 50mm galvanised brackets supplied by BSS Ireland Ltd. This allowed accurate levelling and sloping of the pipework were necessary.

It was found by Meltzer [21] that both constant and variable speed pumps were used within the pharmaceutical industry. A Grundfos CHI 12-10 constant speed centrifugal pump supplied by Grundfos Ireland Ltd., was selected to circulate the water through the pipe network. The pump was constructed from 316 Stainless steel and was specified with 1 ½" BSP female inlet and outlet connections. The rated head was 15 metres and the rated volume flowrate was 10 m^3/h. 50mm tri-clover fittings were retrofitted in-house to allow connection between the pipe network and connection ports of the pump.

A stainless steel ball valve with 2" BSP female connections and a 0-4 bar pressure gauge supplied by Radionics Ltd., were placed at the outlet port to allow pump isolation and visual inspection of outlet pump pressure during operation. The ball valve was placed in-line with the pipework and the pressure gauge was self-supporting directly on to the pipework with a G ¼ pressure connection. The pump was powered by means of an isolation switch mounted on the rig frame.

After the pump, a variable area flowmeter supplied by Manotherm Ltd., was mounted vertically into the pipework to allow setting of the required water volumetric flow rate. A magnet in the float system was detected by the Flowtrak dial indicator to give a direct reading flowrate scale. The flow rate range was from 20 – 250 l/min with intervals of 10 l/min. All wetted parts were of 316 stainless steel and tri-ferrule ends were placed at either end of the flowmeter to allow ease of mounting into the pipe network. The flowmeter indicator accuracy was ± 2% of the full-scale reading.

A length of ten internal pipe diameters was placed upstream of the flowmeter and a further five diameters placed downstream of the device to minimise disturbance of the flow around the flowmeter thus ensuring steady readings from the magnetic dial.

It was found by Carvell et al [1] that diaphragm and ball valves were the most commonly used valves within the pharmaceutical industry for flow regulation. A diaphragm valve with 50mm tri-ferrule ends purchased from Leslie Reynolds & Co. was used for restricting and setting the required volume flowrate of water through the pipe system (figure 2.3).

Figure 2.3: Diaphragm valve.

All wetted parts were made of 316 stainless steel and the diaphragm was made from PTFE. The diaphragm valve was placed into the pipework after the dead-leg test section.

The pipework was routed from the exit of the diaphragm valve back to the storage tank to allow recirculation of the water in the system.

2.3 Dead-leg test section

Three different tee configurations were used to obtain the dead-leg temperature data from the experimental rig (figure 2.4). The tee sections supplied by Petrochem ltd., were constructed from 316L stainless steel with sharp entry construction between the inlet of the tee and the branch pipe (see Appendix 3).

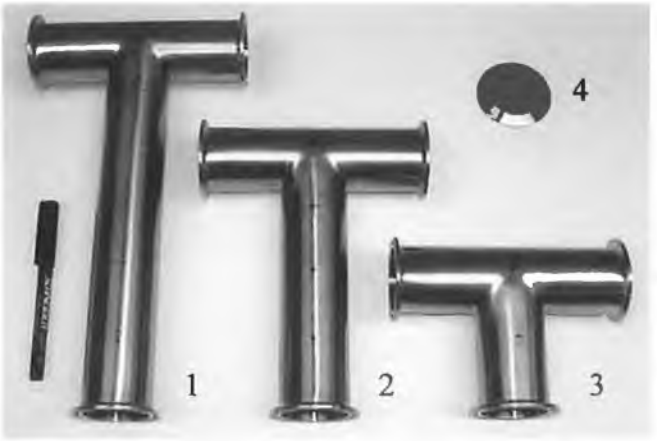

Figure 2.4: Image of 6d (1), 4d (2), 2d (3) tee configurations and blank cap (4)

A 6d configuration was designed in accordance with the FDA guidelines for pharmaceutical water systems (the 6d rule). The branch length was 300mm, specified from the centre line of the inlet pipe. 4d and 2d branch configurations were also specified with 200mm and 100mm branch lengths respectively. The branch pipe diameter, d, and the main pipe diameter, D, were both 50mm O.D for each configuration (figure 2.5).

The outside of the tee sections were finished to a sateen polish with a surface roughness of 0.8 – 0.9 μm and a maximum surface roughness of 0.5μm on the internal surface. Each was constructed in accordance with the American Society for Testing and Materials (ASTM), specification number ASTM A479 T 316L.

The inlet, exit and branch ends of each tee were specified with a ferrule end, as shown in figure 2.5, to allow ease of attachment and removal from the experimental rig when required. The branch tee section was fixed into position using a tri-clamp assembly. The branch of the tee was capped off using a blanking cap (figure 2.4. - item 4) and tri-clover assembly in order to obtain the dead-leg condition. The cap was machined to house a 3mm T-type thermocouple probe that was used to obtain the temperature data.

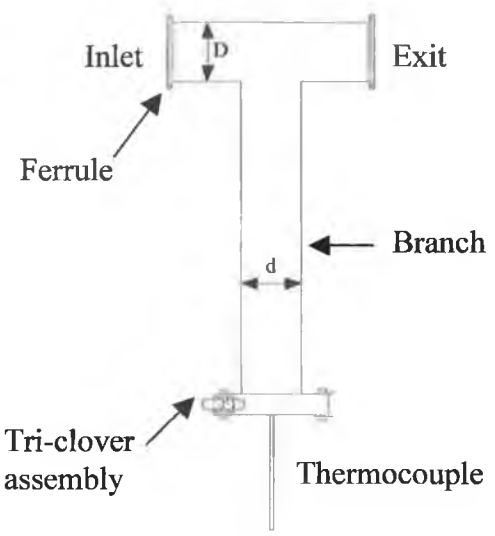

Figure 2.5: Schematic diagram of dead-leg configuration

A pipe length of ten internal pipe diameters was placed prior to the entry into the test section and also between the exit from the dead-leg and the diaphragm.

2.4 System heating and temperature control

All electrical components were supplied by John Denis Electrical Contracting Ltd. Electrical connections for the pump, heating element and temperature controller were housed within an IP 56 rated galvanised box. Each component was fused within the box to protect against electrical overload. The water temperature of the storage tank was achieved using a 9kW 3-Phase stainless steel industrial immersion heater element, supplied by Ideal Ltd. It was mounted to the side of the tank using a 2 ¼" BSP double flange arrangement. A Tecnologic TDF 11 temperature controller also supplied by Ideal Ltd., was used to control the heating element in the storage tank. The temperature measurement was achieved by way of a thermocouple that was housed in the side of the storage tank. The temperature reading was fed back to the controller and a contactor switch was used to power on and off the heating element to maintain the required temperature.

2.5 Data acquisition and software

A Pico TC-08 data acquisition system supplied by Pico technology Ltd., was used to retrieve the temperature readings from the experimental rig. The TC-08 signal converter was attached to the RS232 serial port of the local computer.

The specifications for the TC-08 are listed in table 2.1. T type thermocouples purchased from Instrument technology Ltd., were used to take temperature measurements for the dead-leg fluid and the ambient air temperature respectively. Each thermocouple was attached to a possible 8 input channels on the signal converter. The thermocouple probes were constructed from stainless steel and were 3mm in diameter. A thermocouple of 320mm in length was used to determine the dead-leg temperature measurements.

No. of channels	8
Connections	Miniature thermocouple
Reading Accuracy	The sum of ±0.3% and ±0.5°C (cold junction compensation)
Conversion time	200ms for cold junction compensation + 200ms per active channel
Resolution	20 bits

Table 2.1: Specifications for TC-08 data logger (Pico Technology Ltd.)

A Picolog software interface was loaded onto a local computer to capture and analyse the data obtained from the signal converter. The interface consisted of a 'recorder' and 'player' option. Recorder was selected during actual data logging.

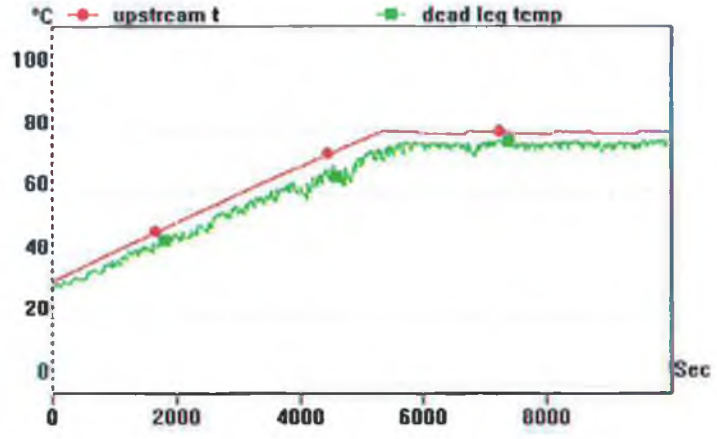

Figure 2.6: Typical display from Pico software interface

Initial setup required the specification of the number of samples required, assignment of thermocouples to a recording channel and the type of thermocouple type in use.

A data file was assigned during the recording phase to save the data. For data analysis purposes such as graph plotting and data retrieval the 'Player' interface was used.

The Picolog software allowed real-time display and recording of results with a sampling rate of one sample per second. A typical image of the screen display during recoding from the TC-08 data acquisition package is shown in figure 2.6.Temperature (°C) was assigned to the y-axis and sample time in seconds was assigned to the x-axis. This plot shows the data recorded for the dead-leg temperature and the main loop upstream temperature. Further graphing and data analysis was performed using SigmaPlot 8™.

2.6 Preliminary testing

To test the rig design a number of initial trials were performed (figure 2.7.). These trials tested for any leakage within the pipe system, that all instrumentation was working correctly and to determine the operation of the system. Also, an initial set of experimental data was obtained for the 6d dead-leg configuration. A digital image of the experimental test rig is shown in figure 1.

Figure 2.7: Experimental test rig

Initially, the storage tank was filled with cold water to the correct level and all connections made to the tank were inspected visually for leaks. The centrifugal pump was then primed as per the installation and operation manual. The pump was switched on and the diaphragm valve was opened slowly in order to prime the pipe system and dead-leg test section. After priming, the flowrate was adjusted from 20 l/min up to 160 l/min in intervals of 10 l/min. The system was allowed to run for 10-15 minutes and all pipe work and instruments were checked for correct operation over the flowrate range. The diaphragm valve was then closed and the system was checked under pressure. The pump was then switched off and the heating element was turned on. The tank temperature was allowed to reach the setpoint temperature of 80 ^{0}C and the system was rechecked under the elevated temperature.

Once, the system had been tested for operation an experimental procedure was developed and a first set of experimental data was obtained.

2.7 Preliminary experimental procedure

Dead-leg end temperature profiles were obtained for a 6d dead-leg configuration respectively for a range of distribution loop velocities. Figure 2.8 shows the position of the thermocouple probe used to measure temperature within the dead-leg. The tip of the probe was positioned 2mm into the dead-leg fluid to ensure the fluid temperature was measured and not the surrounding steel material temperature.

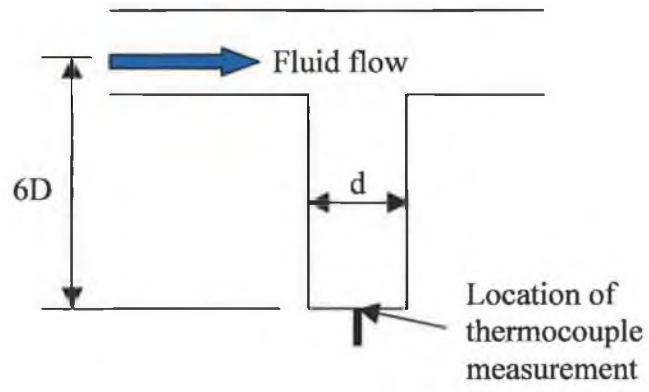

Figure 2.8: Dead-leg temperature measurement

Initially, the diaphragm valve was set to the closed position. The tank level was checked and filled where necessary and the lid placed back into position.

The temperature controller was set to 80^0C and the heating element was switched on. When the water temperature in the tank reached approximately 80^0C the pump was switched on. The diaphragm valve was then slowly opened until the desired flowrate was achieved on the flowmeter. A file was then assigned to the Pico data logger and recording of the dead-leg temperature was initiated. The experimental rig was allowed to run for 120 minutes ($7*10^3$ samples). After data logging was completed the diaphragm valve was closed and the pump and heating element were switched off. The recorded data was then exported to Sigmaplot for further analysis.

2.8 Preliminary operating problems

As with most experimental analysis this research rig was not without problems. During the initial operation of the rig, it was noted on the flowmeter that there were continual changes in the flowrate and also pulsations were noted in the flow during the first phase of experimental analysis. Figure 2.9 represents the data obtained for two experimental runs under the same operating conditions at a loop flowrate of 60 l/min for the 6d dead-leg configuration.

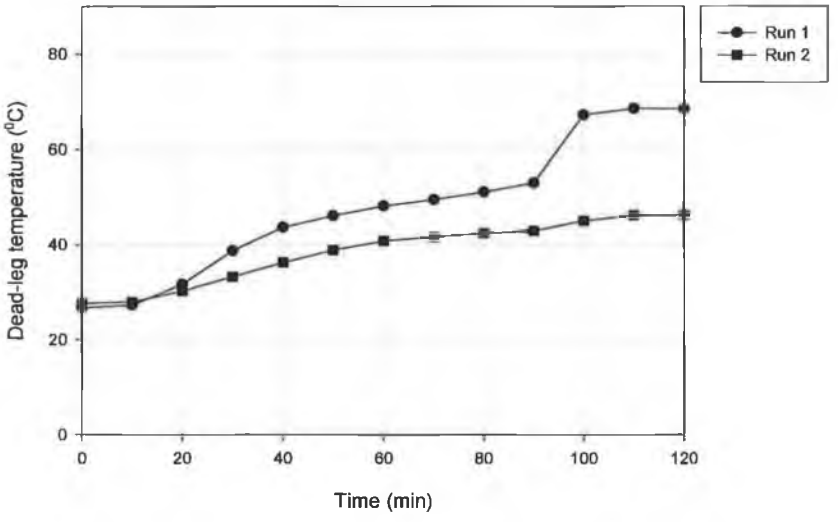

Figure 2.9: Temperature profiles for 60 l/min (6d)

The fluid at the end of the dead-leg for run 1 was shown to exhibit a larger temperature increase over time and a sudden increase in temperature after approximately 90 minutes. The final temperature reached for this run was shown to be considerably higher than the second run.

The fluctuations in the flowrate were considered to be a direct cause of this temperature increase. The possible causes of the dynamic changes in the flowrate are outlined below.

2.8.1 Flow control

Although diaphragm valves are one of the most commonly used for water systems in the pharmaceutical industry they are not considered to have fine flow control characteristics. It was found by McWilliams et al [6] that the diaphragm valve does not exhibit a linear slope for opening position against flowrate. The flowrate was difficult to set accurately using the diaphragm valve during operation. It was noted that after a period of time during an experimental run, the flowrate was shown to increase or decrease by as much as 10 l/min. The coarse actuation of the valve was considered the reason for this change in flowrate. Also, the pipe system was not considered to remain flooded during operation due to the position and horizontal orientation of the valve within the pipe network.

At low flowrates the exit pipe between the valve and the storage tank was found to drain creating a siphon effect on the system. This was caused by insufficient submerging of the exit line into the storage tank. The change in pressure across the diaphragm valve due to the siphon effect was found to change the flow characteristics of the pipe loop.

2.8.2 Pump operation

Air bubbles were also noted at the exit line in the storage tank during operation. This was primarily caused by the drain effect in the exit line. It was found that the air bubbles were carried through the system causing the pump to intermittently cavitate and cause large fluctuations in the flow through the pipe network.

Due to the initial experimental procedure used, the sudden change in temperature of the liquid at the start of the run as the diaphragm valve was opened required the materials in the pump to expand and adapt to the new operating conditions. It was noted that the pump became noisy in operation during this period. The sudden increase in temperature was shown to momentarily cause the pump to lose head.

2.9 Final rig design

As a result of the problems encountered in the rig, the initial and final rig designs differed considerably as changes were made to eliminate the problems encountered during operation. Figure 2.10 shows a schematic of the final rig design and fluid flow path.

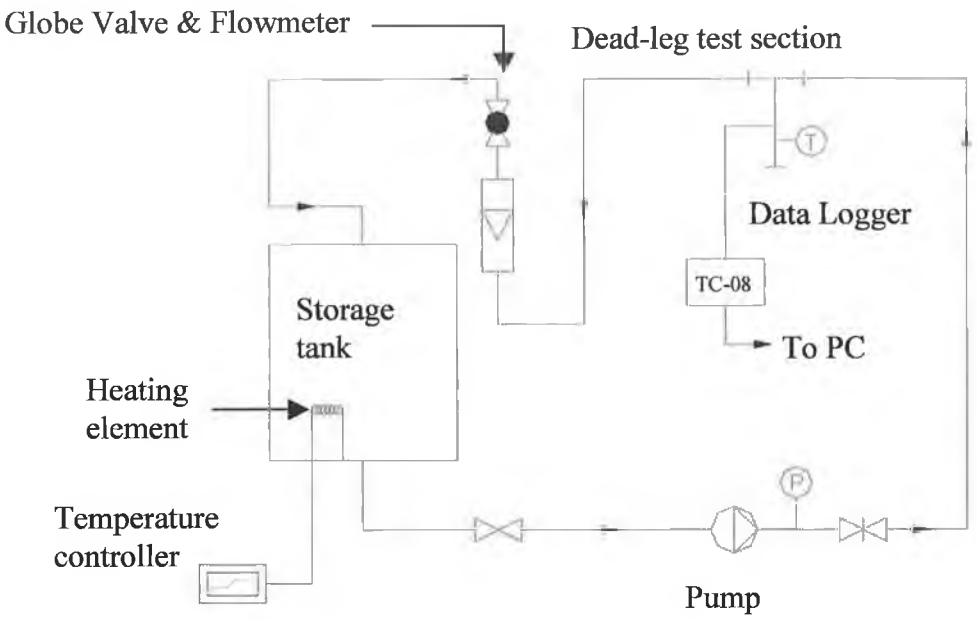

Figure 2.10: Schematic of final rig design.

The modifications to the experimental rig included adjustments to the loop pipework, pump and storage tank facilities, flow regulation and instrumentation and data Acquisition.

2.9.1 Loop pipework

A pipe entry length of 3m was placed before the dead-leg test section and an exit length of 1.5m was placed after the dead-leg (figure 2.11). The specifications of the pipe sections are shown in appendix 3. The new pipe entry length fulfilled the requirement of fully developed turbulent flow entering and exiting the dead-leg test section over the range of fluid velocities used [40]. These specifications where also in line with those used by Bates et al [41] and were required for the purposes of future computational modelling research.

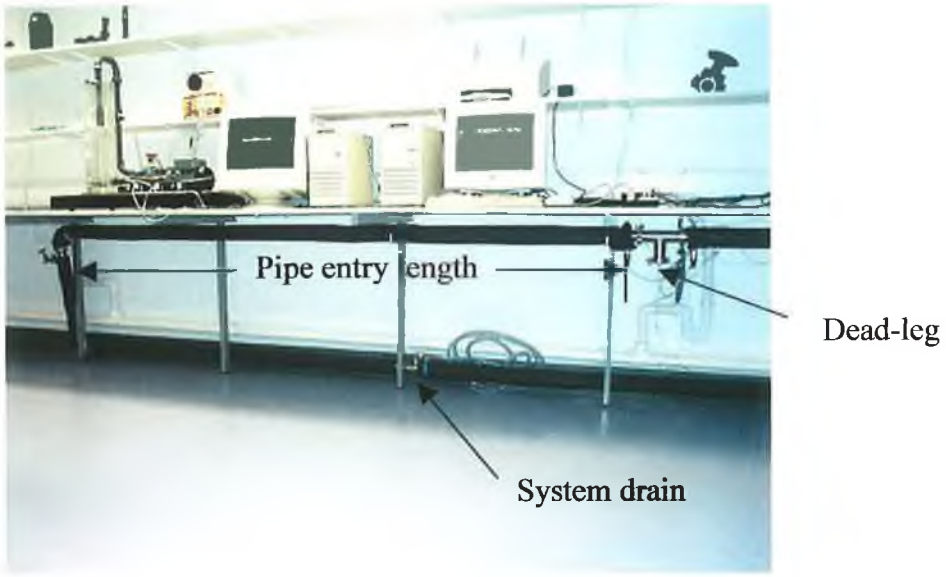

Figure 2.11: Final rig entry and exit lengths

A drain was placed in the pipe work after the pump exit to allow draining of the system during changing of the dead-leg test section and for maintenance purposes. A piping diagram for the final rig arrangement is shown in appendix 1.

The pipe network was hung in the laboratory using support brackets made in-house (figure 2.12). The brackets were made from aluminium, with an adjustable fixing slot to allow accurate levelling of the pipework.

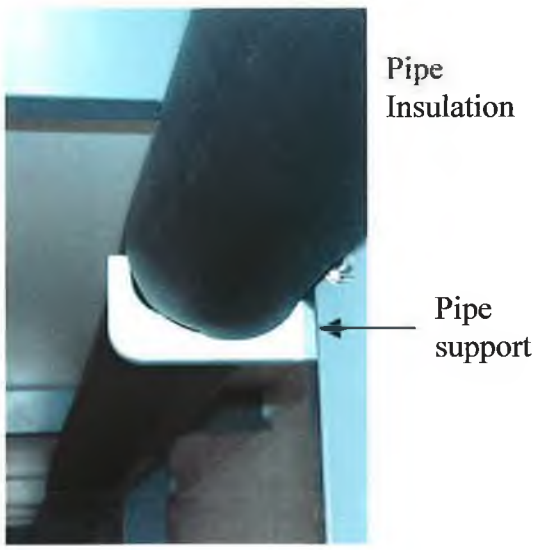

Figure 2.12: Pipe supports with insulation

2" 13mm tube foam insulation Class O, supplied by Mar insulation Ltd., was used on the pipework due to an increased heat load from the extended pipe system and also to prevent operator injury through burning.

2.9.2 Pump & storage tank facilities

Figure 2.13 shows the modifications made to the pump arrangement. The feed and return lines for the dead-leg test section are shown. The supply line from the storage tank (1) was connected to the pump (2) using a 1 ½" BSP 90^0 elbow and tri-ferrule sanitary fittings.

Figure 2.13: Pump arrangement

A pressure gauge (3) was fixed to the pipework to measure the pump outlet pressure. The pump isolation switch (4) was mounted directly onto the pump housing. A gate valve (5) supplied by radionics Ltd., was used to replace the ball valve to allow steady increase of water flow into the system and finer control over the pump priming. A thermocouple (6) was mounted to the pipework to measure the pump outlet temperature.

Figure 2.14 shows the tank, pump and exit line arrangement for the experimental rig. A stainless steel storage tank, provided in-house, was used to supply adequate volume to the extend pipe system. The tank lid and sides were fully insulated using 13mm and 25mm insulation respectively to avoid excessive heat loss. The dimensions of the tank were 600mm diameter and 1500mm in height with a working volume of 150 litres.

The tank was fitted with a butterfly valve located at the exit point to provide tank isolation during maintenance and drainage of the pipe system. The feed line to the pump was sloped down from the storage tank to ensure any air bubbles present were not drawn into the pipe network. The exit line between the globe valve and the storage tank was fully submerged into the tank to ensure the exit line did not drain, as was the case with the preliminary experimental rig.

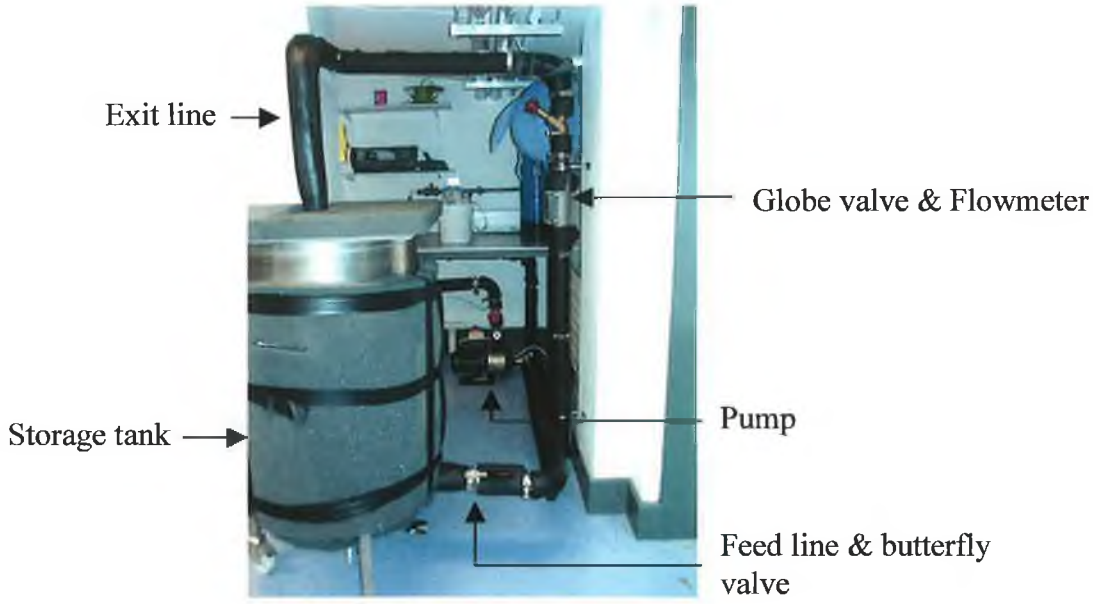

Figure 2.14: Tank, pump, feed & exit line arrangement

A shorter vertical section of pipe in the exit line ensured the pipe remained fully flooded during operation.

2.9.3 Flow regulation

The diaphragm valve was replaced by a Crane™ globe valve supplied by BSS Ireland ltd. The valve had 1 ½" BSP female connections and tri-ferrule fittings were adapted in-house to allow connection of the valve into the pipe network. The specification sheet for this valve was shown to have a characteristic linear pressure drop with increase in flowrate thus allowing a finer tuning of the flow through the system.

The globe valve and flow meter were both placed after the dead-leg test section and the pipe entry length placed before the flowmeter was increased to fifteen internal pipe diameters as specified by the manufacturer to reduce local disturbances of the measuring device (figure 2.15).

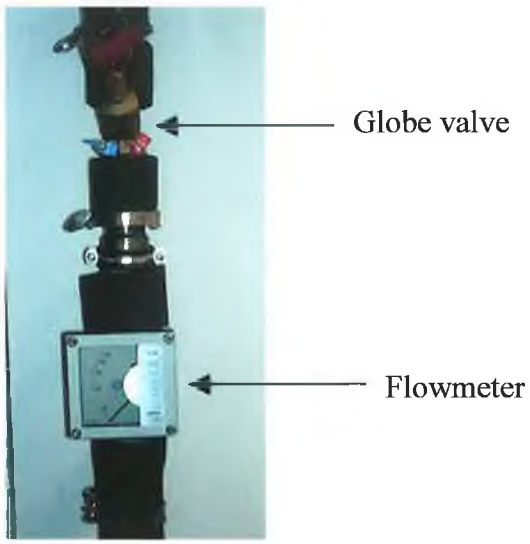

Figure 2.15: Flow regulation

Flow disturbances experienced at the flow meter in the preliminary rig design were removed and the flow settings were found to be stable on visual inspection. This ensured the accuracy of measurement during experimental runs.

The valve was orientated vertically and placed at the highest point of the rig to ensure that all parts of the pipe network remained fully flooded at all times during operation.

The flowmeter and globe valve were wall mounted using 50mm galvanised wall brackets supplied by BSS Ireland Ltd.

2.9.4 Instrumentation and Data Acquisition

Figure 2.16 shows the positions of the pressure and temperature sensors for the final experimental rig design.

Thermocouples (1, 2) were placed 100mm upstream and downstream of the dead-leg respectively to measure the temperature drop across the dead-leg. A thermocouple (3) was used to measure the ambient air temperature.

The dead-leg temperature was determined using a thermocouple (4) mounted in the blank cap of the branch pipe. Two Gems™ pressure transducers (5,6), supplied by Manotherm Ltd., were placed 100mm upstream and downstream of the dead-leg respectively. The transducers were of 2-wire construction requiring a 24-volt excitation voltage to produce the output signal. The output range from the transducer was 4 –20 mA and the operating pressure range was 0-2.5 bar absolute. Measurement accuracy was ± 0.25 % of full scale reading.

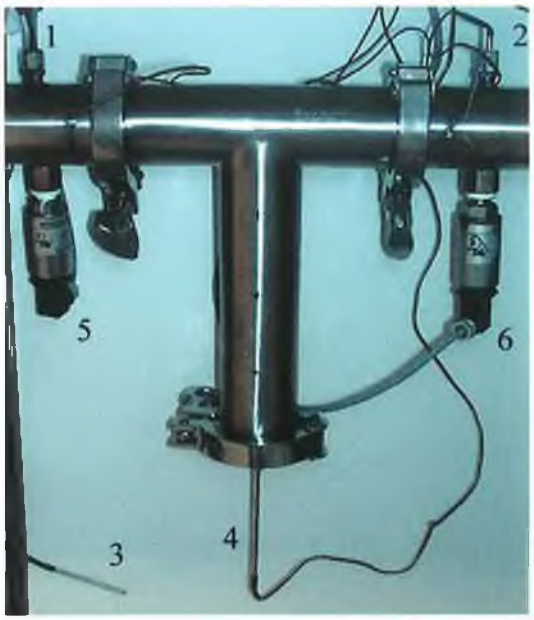

Figure 2.16: Pressure and temperature data acquisition

The pressure transducers were used to measure the system pressure and any sudden changes in pressure during operation. Any change in pressure would be mirrored by a sudden change in flowrate.

This was used as the basis of ensuring that small deflections in the dial on the flowmeter were purely local changes and did not reflect an overall change in the mean flowrate of the system. An ADC-16 data acquisition system, purchased for Pico technology, was used to retrieve the pressure readings from the experimental rig (figure 2.17).

A signal converter was built to condition the 4-20 mA signal from the pressure transducers to a ± 2.5 mV signal required by the ADC-16.

Figure 2.17: TC-08 signal converter and ADC-16 with 4-20 mA converter

2.10 Final rig validation

The final rig design was tested in a similar fashion to the initial design including tests for any leakage within the pipe system, correct instrumentation operation and to determine the operating procedure of the rig. Also, the flow characteristics through the pipe loop were tested over time using the pressure transducers installed into the pipework and by visual inspection using the flowmeter. Figure 2.19 represents the gauge pressure and temperatures recorded for the loop flow over time for a flowrate of 20 l/min and a 4d dead-leg configuration.

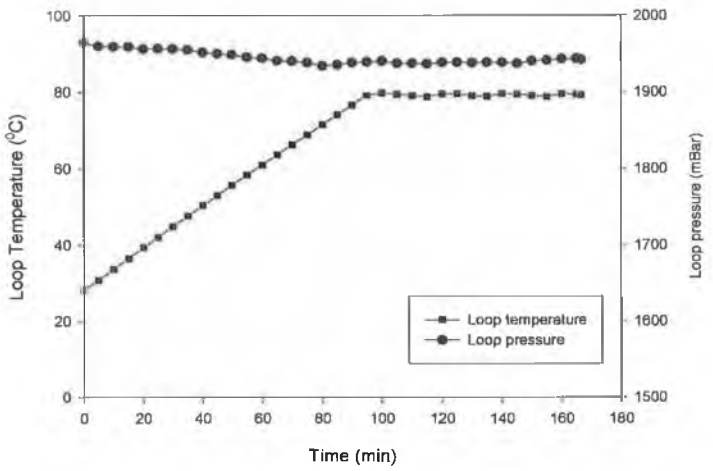

Figure 2.18: Loop pressure and temperature measurement.

The initial loop pressure was found to be 1960 mbar with a minimum pressure of 1940 mbar recorded during operation. As can be seen from the plot, there was no significant change in the loop pressure during the experimental run. This data was found to be repeatable for all experimental runs performed on the final rig design. Also, it was found that there were no significant fluctuations upon visual inspection of the flowmeter suggesting that the modifications made to the rig were successful in achieving the desired steady turbulent flow characteristic through the pipe loop.

Temperature profiles for the loop temperature were also found to have good repeatability across all the data obtained for the final rig design and for all dead-leg configurations. Figure 2.19 represents an example of the change in temperature of the loop fluid for a velocity of 1.03 m/s for a 4d dead-leg configuration.

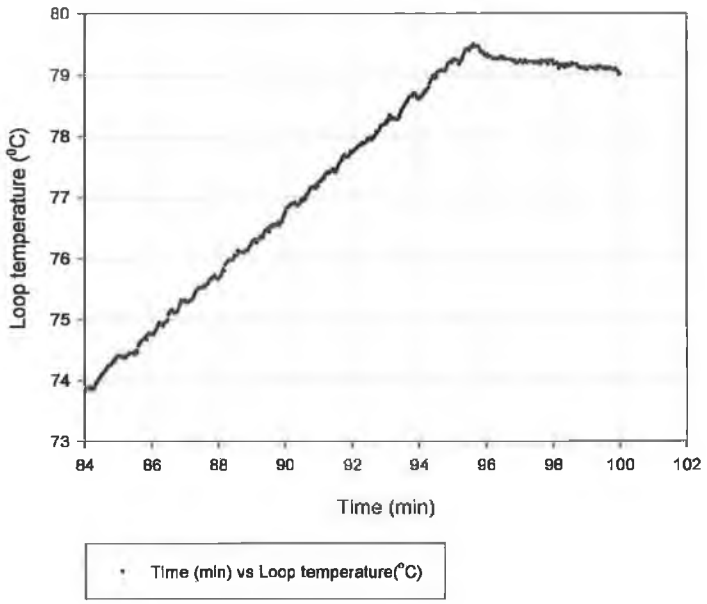

Figure 2.19: Loop temperature validation

The loop temperature profile was shown to exhibit a linear temperature increase and relative steady state phase with no notable scatter in the data.

2.11 Final rig operating procedure

After initial priming and testing of the final rig construction an operating procedure was developed to obtain the required temperature data. The procedure was as follows:

The globe valve and gate valve were set to the closed position after priming and before start up. The tank level was checked and filled where necessary ensuring the exit line was fully immersed in the tank water. The pump was switched on and the gate valve was opened slowly to the fully open position. The globe valve was then slowly opened in an anticlockwise direction and the required flowrate was set on the flowmeter. The experimental rig was allowed to run for approximately 10 minutes to ensure the system was fully primed and that the flowrate was at the desired value.

A log file was then assigned to the TC-08 and ADC-16 Pico data loggers for temperature and pressure measurement respectively, and recording was initiated. The temperature controller was switched on and the storage tank heating was started. The experimental rig was allowed to run for 166 minutes ($1*10^4$ samples). Temperature data was recorded for the loop temperature (figure 2.16 – item 1) and for the dead-leg end temperature (figure 2.16 – item 4).

After data logging was completed for the dead-leg end temperature profiles a new 'recorder' file was immediately assigned to record the temperature distributions throughout the dead-leg. Dead-leg distribution temperature was determined again using the thermocouple 4 shown in figure 2.16. Once the temperature distributions had been determined the heating element was switched off. The globe valve was closed followed by the gate valve and finally the pump was switched off. The recorded data was exported to Sigma plot for further analysis.

Dead-leg end temperature profiles were obtained for a 6d, 4d and 2d dead-leg configuration respectively for a range of distribution loop velocities for the final rig design.

2.12 Temperature distribution method

Temperature distributions were obtained for each dead-leg configuration for a range of distribution loop velocities.

The temperatures were recorded at the end of each experimental run performed for dead-leg end temperature measurement. The temperatures were recorded using a thermocouple probe that was inserted vertically upwards into the dead-leg branch pipe. A sketch of the temperature measurements that were taken are shown in figure 2.19.

C_{L1} represented the centre line of the main loop pipe and C_{L2} the centre line of the dead-leg branch pipe. The starting position for temperature measurement was at the end of the dead-leg. The thermocouple was moved into the dead-leg at specific graduations along C_{L2} and when fully inserted, extended to the centre line of the distribution loop pipe C_{L1}.

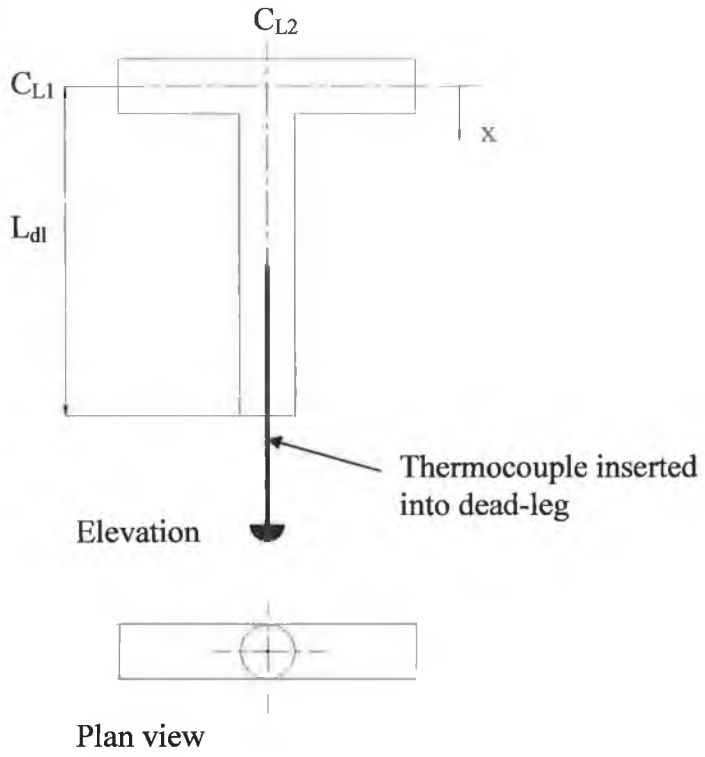

Figure 2.20: Schematic of temperature distribution measurement

It was found during experimental testing that the majority of the temperature change in the dead-leg occurred in the lower part of each dead-leg configuration. Thus, temperature measurements were taken at intervals of 2.5, 5 and 10mm until the temperature was approximately that of the loop temperature (appendix 3). Beyond this point a measurement was taken every 50mm or one pipe diameter into the dead-leg.

Chapter 3. Results and Discussion

3.1 Introduction to analysis

Results are presented for the preliminary and final experimental rig design. Preliminary results include dead-leg end temperature profiles over a range of loop velocities for a 6d branch tee configuration.

Results are presented for the final experimental rig for 6d, 4d and 2d branch tee configurations respectively. The following analysis was performed for each configuration over a range of loop velocities:

1. Analysis of the effect of loop velocity and temperature on the dead-leg end temperature profile.

2. Determination of the temperature distribution along the axis of the dead-leg branch under steady state conditions.

An analysis of the thermal-fluid characteristics within a dead-leg has been presented on the basis of the results obtained from the experimental rig. An empirical correlation to define the depth of thermal penetration into a dead-leg has also been presented.

An analysis of heating time requirements in relation to sanitisation of pipe dead-legs has been presented for each branch tee configuration. The effect of temperature limits has also been discussed with respect to dead-leg geometry.

3.2 Preliminary Analysis

The following analysis was performed on the data obtained from the initial rig design. Temperatures were recorded at the end of the dead-leg over time for a 6d dead-leg configuration for loop volume flowrates of 30, 50, 70 and 90 l/min respectively (see appendix 3). Each run was recorded over a time period of 120 minutes (7.2×10^3 samples).

Table 3.1 represents an overview of the geometric and fluid characteristics of the pipe system and dead-leg configuration.

Experimental Rig	**Fluid conditions**	**Fluid properties**
Equal Tee (D=d)	Steady flow	Water
50mm O.D.	80°C	$\mu = 3.51\times10^{-4}$ kg $m^{-1}s^{-1}$
47.5mm I.D.		$\rho = 972$ kgm^{-3}

Table 3.1: Characteristics of present measurements

The distribution loop flowrates of the water were converted to a mean loop velocity, U_m, based on the internal diameter of the pipe and the volume flowrate. The Reynolds number was used to determine the flow regime for each loop velocity and it was shown that each velocity was in the turbulent region [42]. The corresponding loop velocities and Reynolds numbers are shown in Table 3.2.

Flowrate Q (l/min)	**Velocity U_m (m/s)**	**Reynolds no. Re [-]**
30	0.28	3.71×10^4
50	0.47	6.18×10^4
70	0.66	8.66×10^4
90	0.85	1.11×10^5

Table 3.2: Flow characteristics of experimental rig

Figure 3.1 represents the temperature profiles recorded for the dead-leg end temperature, T_{edl}, and the loop temperature T_l for a loop velocity of U_m = 0.47 m/s.

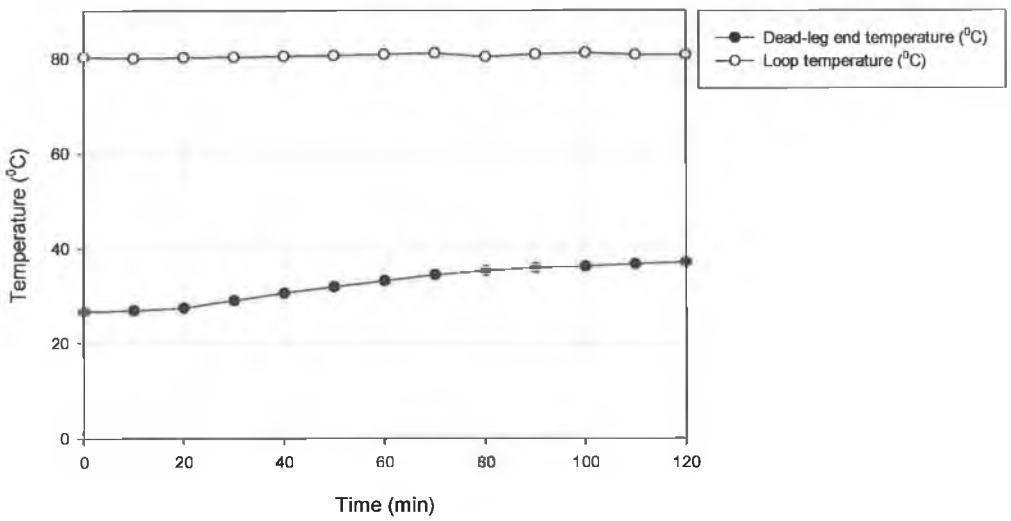

Figure 3.1: Preliminary temperature profiles at Um = 0.47 m/s (6d)

The loop temperature was set to 80°C with the pipe loop reaching an average of between 79 - 81°C. This was the case for all runs during the preliminary analysis. Time zero represented the point at which the flow control valve was opened. The fluid at the end of the dead-leg was shown to increase from 26.6°C to a maximum temperature of 34.84°C after 120 minutes.

Table 2.3 shows the relationship of time and dead-leg end temperature (T_{edl}) for a loop velocity for U_m = 0.47 m/s.

Time (min)	**Dead-leg end temperature T_{edl} (°C)**
0	26.6
20	27.1
40	29.74
60	32.52
80	34.79
100	36.10
120	36.84

Table 3.3: Relationship of time and dead-leg end temperature, U_m = 0.47 m/s (6d)

It can be seen from the results that there was no significant temperature change (+1°C) for approximately 30 minutes after the diaphragm valve was opened. The temperature was then shown to increase with time until a temperature of 36.10°C was achieved after 100 minutes. The temperature was shown to reach a relatively stable temperature with an increase of only 0.74°C noted over the remainder of the run.

Figure 3.2 represents the temperature change of the fluid at the end of the dead-leg with time for the four loop velocities used in this analysis (see appendix 3). It was shown from the results for each run that there was an initial period of time before the dead-leg end temperature began to increase. This was considered to represent a lag time or process lag [43]. Many processes have a delayed response to a process input due to transport lags such as fluid flow through pipes.

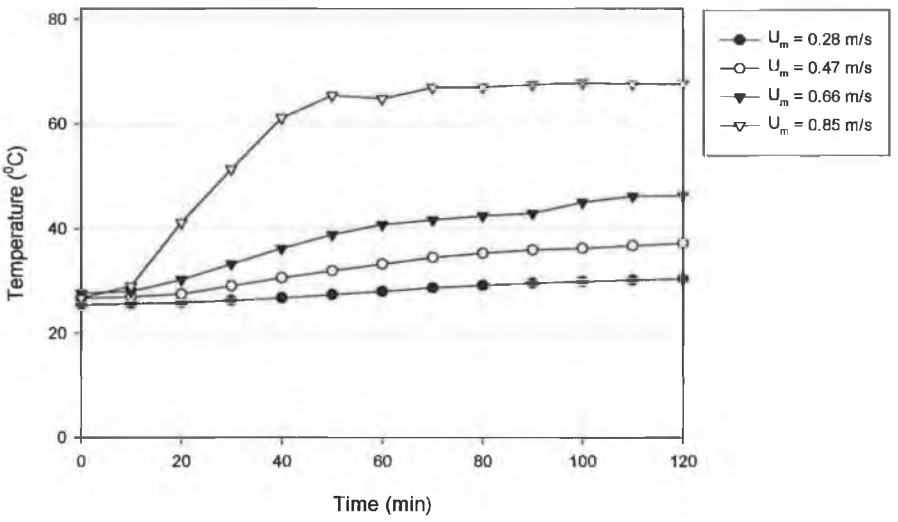

Figure 3.2: Preliminary temperature profiles for 6d configuration

This initial lag time was shown to be approximately 10 minutes for each run. The temperature at the end of the dead-leg was then shown to increase continually until a maximum temperature was achieved after 120 minutes for each experimental run. It was found for each run that the temperature at the end of the dead-leg began to stabilise before 120 minutes was reached suggesting that a relative state of thermal equilibrium throughout the length of the branch pipe had been achieved.

Table 3.4 shows the relationship between loop velocity and the maximum dead-leg end temperature (T_{mdl}) that was reached at the end of each run for the 6d configuration.

Velocity U_m (m/s)	**Maximum end temperature T_{mdl} (°C)**
0.28	30.25
0.47	36.84
0.66	46.18
0.85	67.13

Table 3.4. Preliminary relationship between loop velocity and maximum temperature (6d)

The results show that for an increase in the loop velocity, U_m, the maximum temperature at the end of the dead-leg also increased. The maximum temperature reached was 67.57°C for a loop velocity of U_m = 0.85 m/s. For each experimental run the setpoint temperature of 80°C was not reached within the given timescale of 120 minutes. It was shown that there was a significant temperature increase at the end of the dead-leg for loop velocities above 0.66 m/s.

It was noted in the materials and methods section (pp.36) that there were continual changes in the flowrate and pulsations were noted in the flow during the initial operation of the rig. The unsteady flow characteristics of the loop fluid were observed to cause large changes in the dead-leg end temperature and hence a change in the overall temperature profile.

Figure 3.3 represents the temperature profiles obtained for two experimental runs at a loop velocity of U_m = 0.66 m/s under the same operating conditions. The fluid at the end of the dead-leg for run 1 was shown to exhibit a sudden increase in temperature after approximately 90 minutes. The final temperature reached for this run was shown to be 68.48°C as opposed to 46.20°C for run 1.

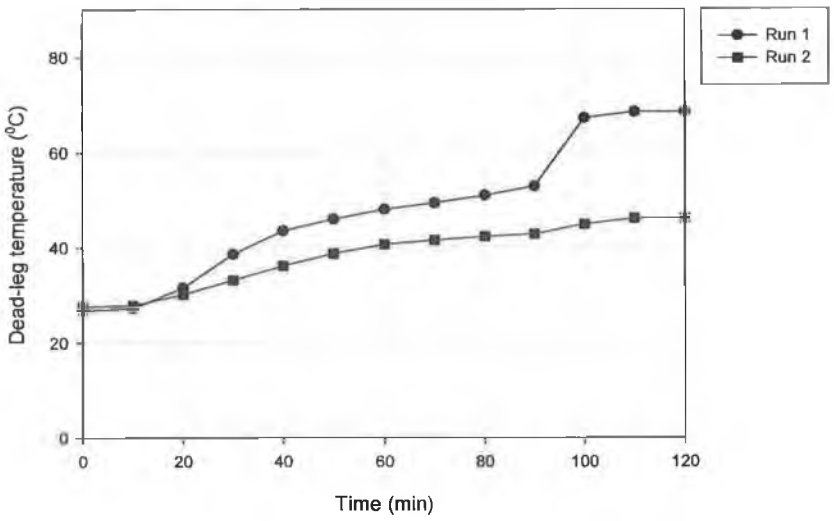

Figure 3.3: Preliminary temperature profiles at U_m = 0.66 m/s (6d)

The strong variability of data exhibited by the initial test rig would require a statistical analysis over the range of loop velocities used in this analysis, and at this stage in the research it was decided to redesign the test rig to provide for a more steady flow in the system.

3.3 Final experimental analysis

A number of alterations were made to the experimental rig as outlined in the materials and methods. These included changes to pipe loop layout, flow control, pump and storage tank facilities and data acquisition (figure 2.10). Temperature data was then obtained for 6d, 4d and 2d branch tee configurations for the final experimental rig and are presented in the following text (see appendix 3).

Part A. Temperature profile analysis

Analysis of the effect of loop velocity and temperature on the dead-leg end temperature profile has been presented. Data is presented for 6d, 4d and 2d dead-leg configurations respectively (see appendix 3).

A range of distribution loop flowrates were used for each dead-leg configuration and are shown in Table 3.5. The relationship between flowrate, velocity and Reynolds number for the flow conditions are also shown.

It was shown that each velocity was in the turbulent flow regime. The ambient air temperature was approximately 21°C ± 0.5°C for all experimental runs and the tank temperature set point was 80°C. The distribution loop temperature was shown to reach a temperature of 79°C ± 0.5°C.

Flowrate Q (l/min)	Velocity U_m (m/s)	Reynolds no. Re [-]
20	0.19	2.47×10^4
30	0.28	3.71×10^4
60	0.56	7.42×10^4
90	0.85	1.11×10^5
110	1.03	1.36×10^5
130	1.22	1.61×10^5
160	1.50	1.98×10^5

Table 3.5: Loop flowrate, Velocity and Re numbers for final rig design.

3.3.1 6d Temperature profile analysis

Figures 3.4 represents the temperature profiles for the change in loop temperature T_l and dead-leg end temperature T_{edl} respectively over time for a 6d dead-leg at a loop velocity of 0.19 m/s. The run time was set to 166 minutes ($1*10^5$ samples) with time zero representing the point at which the heating element was switched on. The maximum temperature recorded every 300 samples or 5 minutes were plotted for each profile.

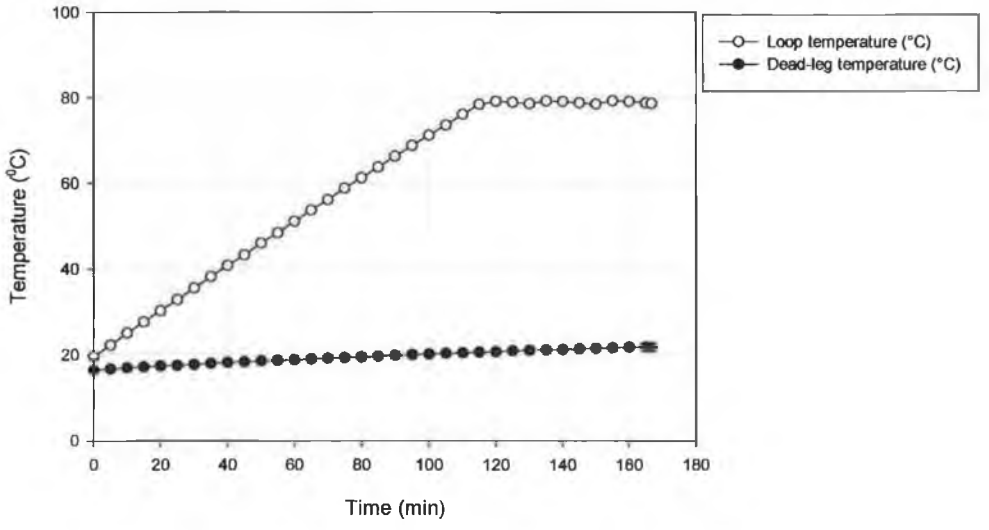

Figure 3.4: Temperature profiles for U_m = 0.19 m/s (6d)

The loop temperature profile was shown to consist of a heating or ramp phase followed by a constant temperature phase. The increase in the loop temperature during the ramp phase was linear until the setpoint of the tank was reached. The loop temperature was then maintained at 79°C ± 0.5°C. The characteristics of the loop temperature profile for 0.19 m/s was shown to be the same for all loop velocities used in this analysis. The water at the end of the dead-leg increased in temperature from 16.01°C (initial mains water temperature) at the start of the experimental run and reached a maximum temperature of 21.74°C. The final end temperature of the dead-leg was shown to be marginally above ambient conditions. This would suggest that the temperature at the end of the dead-leg was not significantly affected by the increase in loop temperature during the experimental run. The small temperature change of the dead-leg would suggest a poor mixing process between the dead-leg and loop fluids.

Figure 3.5 represents the temperature profiles for dead-leg end temperature over time for loop velocities of 0.28, 0.85 and 1.03 m/s. This plot clearly demonstrates an increase in the dead-leg end temperature over time for an increase in loop velocity.

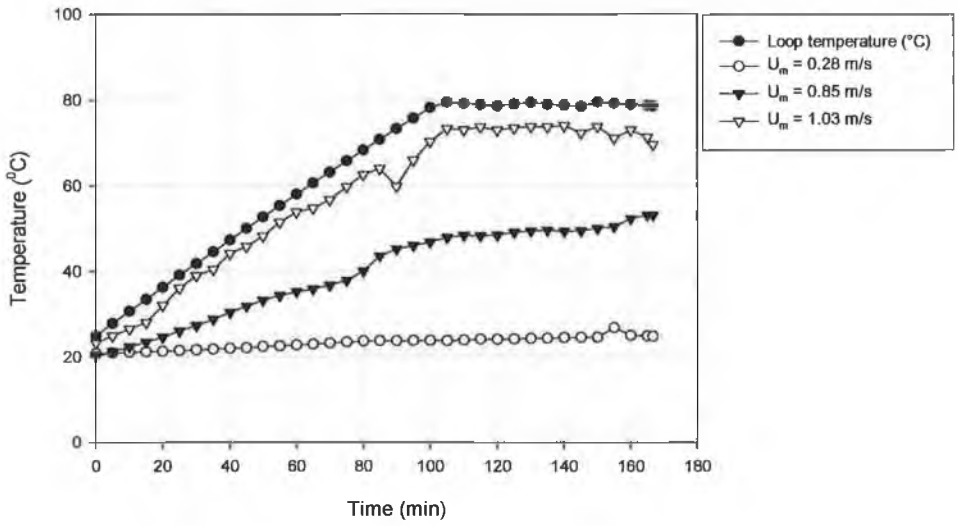

Figure 3.5: Dead-leg end temperature profiles for 6d configuration

For loop velocities U_m > 0.85 m/s there was a tendency for the dead-leg temperature profile to approach that of the loop temperature profile. This would suggest that there was an increase in the mixing process between the dead-leg and loop fluids.

This was comparable to the findings of Haga et al [28] were an increase in loop velocity was shown to increase the circulation of liquid within the dead-leg fluid.

Table 3.6 shows the relationship between loop velocity and the maximum temperature achieved at the end of the dead-leg after completion of each experimental run for a 6d dead-leg configuration.

Velocity (U_m) (m/s)	**Maximum end temperature 6d T_{mdl} (°C)**
0.19	21.74
0.28	24.79
0.56	34.35
0.85	53.13
1.03	69.56
1.22	76.29
1.50	75.97

Table 3.6: Relationship of loop velocity and maximum end temperature (6d)

It was shown that when the loop velocity was increased there was an increase in the maximum temperature achieved at the end of the dead-leg. The increase in temperature over this range of loop velocities would suggest that an increase in the Reynolds number has a significant affect in the mixing process of the fluid within the dead-leg.

The maximum temperature achieved for the 6d configuration was 76.29°C for a velocity of 1.22 m/s. It was noted that the difference in the maximum temperature achieved for loop velocities of $U_m \geq 1.22$ m/s was marginal, suggesting that a maximum temperature had been achieved for this dead-leg configuration. The loop temperature of 78°C ± 0.5°C was not achieved over the range of loop velocities used for the 6d configuration.

Figure 3.6 shows the temperature profiles obtained for a loop velocity of 0.85 m/s. There were large temperature increases noted at approximately 80 and 155 minutes respectively. This unusual characteristic would suggest a dynamic change in the fluid at the end of the dead-leg.

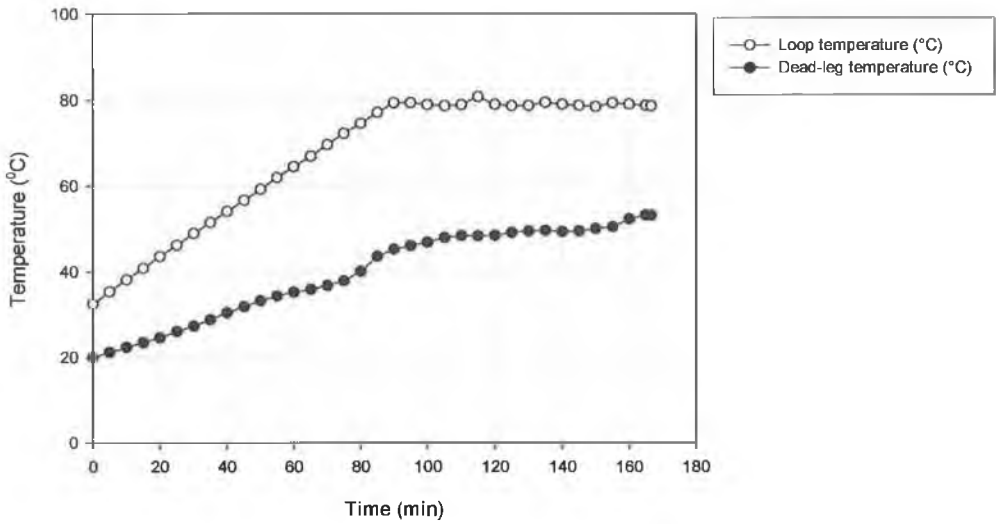

Figure 3.6: Temperature profiles at U_m = 0.85 m/s (6d)

The increase in loop velocity would appear to have increased the level of mixing in the dead-leg. However, the mixing process may not be uniform throughout the dead-leg length.

It was identified by Corcoran et al [3] that the magnitude of the circulation or cavity flow velocity of the fluid within the dead-leg was higher on the downstream wall of the branch pipe than the upstream wall. The varied velocity of the fluid within the dead-leg would give rise to hot and cold fluid regions within the dead-leg.

Figure 3.7 represents the temperature profiles for a loop velocity of 1.03 m/s. The dead-leg temperature profile was shown to exhibit a linear temperature increase and followed the profile of the change in loop temperature during the heating cycle of the loop fluid.

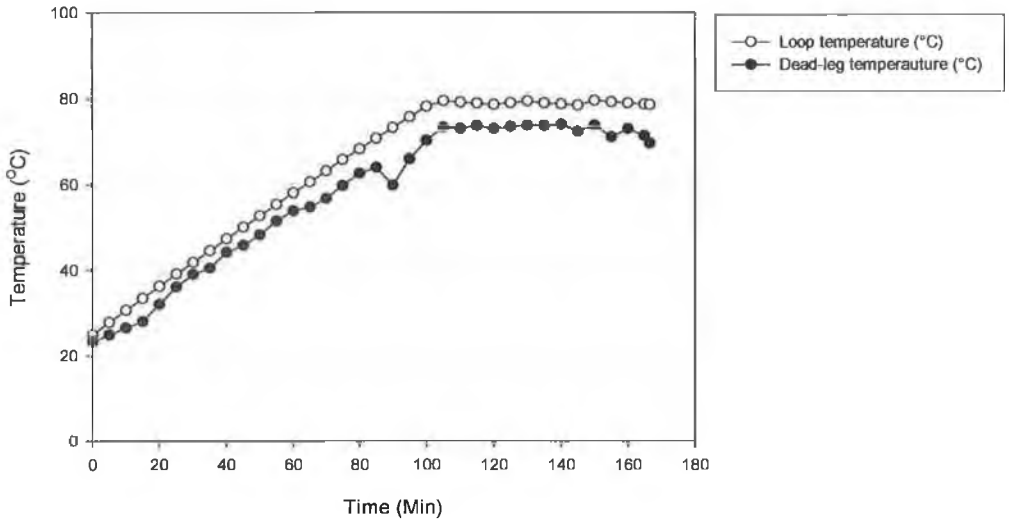

Figure 3.7: Temperature profiles at U_m = 1.03 m/s (6d)

However, a temperature drop and subsequent temperature rise is noted at approximately 90 minutes run time. The points at which the temperature changes over a short period of time would suggest further that the mixing process is not uniform. It was found by Robert et al [44] that a uniform cavity flow exhibited in the dead-leg was shown to break down creating a non-uniform helicoidal flow penetrating down the length of the dead-leg.

Although testing in this case was performed at higher loop velocities and a larger pipe diameter the change in the flow dynamics in the dead-leg would give rise to sudden changes in temperature.

Figure 3.8 shows the temperature profiles associated with 1.22 m/s. The dead-leg temperature profile was similar to that of the loop temperature profile with a distinct heating period and constant temperature or steady-state period.

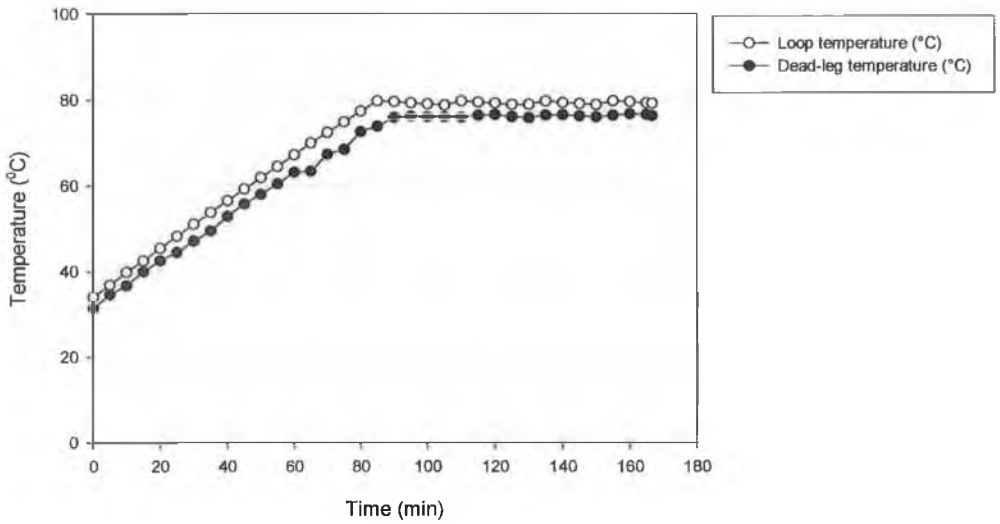

Figure 3.8: Temperature profiles at U_m = 1.22 m/s (6d)

The temperature difference during heating between the loop and dead-leg profiles for this velocity was significantly reduced with a maximum temperature difference measured at 6.5°C. This would suggest a more vigorous mixing of the dead-leg fluid at higher loop velocities.

Evidence of increased mixing of the fluid at the end of the dead-leg with increase in loop velocity was found by examining the data obtained during the heating phase of a number of experimental runs.

Figure 3.9 represents the change in temperature of the fluid at the end of the dead-leg during the ramp phase of the loop fluid for a velocity of 0.56 m/s. Data was plotted for temperatures between 66 and 83 minutes at one-second intervals. The data set clearly shows that there is no significant scatter in the data indicating that the temperature change is achieved predominantly by diffusional effects. However, for an increase in loop velocity, the temperatures recorded over the same time period show considerable temperature fluctuations.

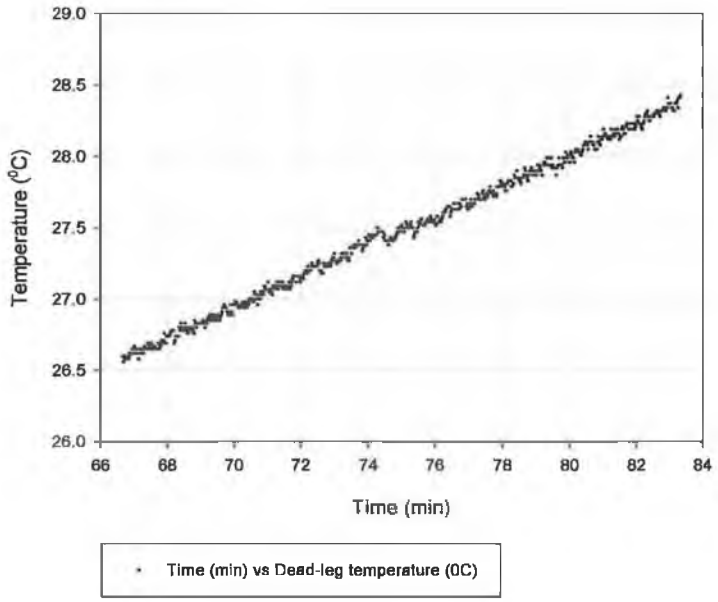

Figure 3.9: Ramp phase for dead-leg end temperature, U_m = 0.56 m/s (6d)

The line graph in figure 3.10 represents the change in temperature of the fluid at the end of the dead-leg during the ramp phase of the loop fluid for a velocity of 1.03 m/s. The loop temperature profile was shown to follow a linear increase with no notable scatter in the data.

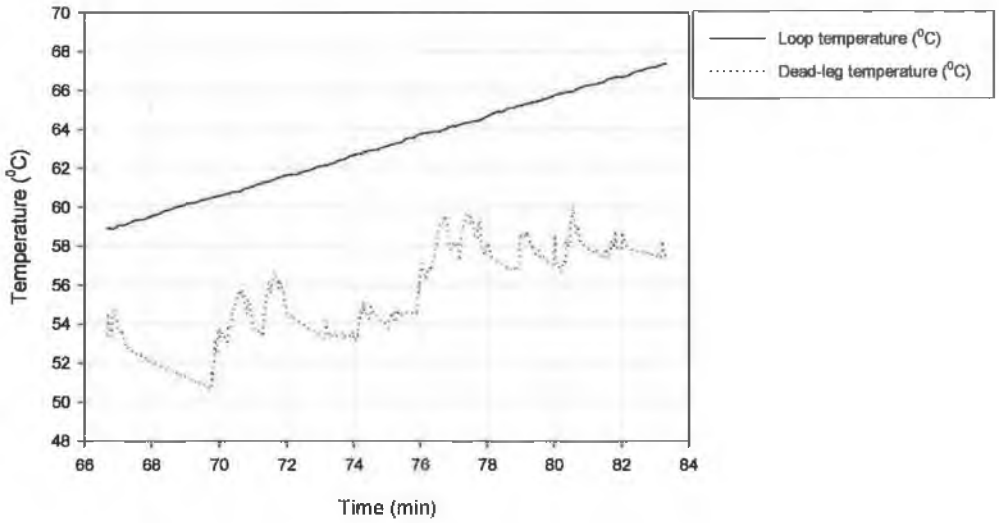

Figure 3.10: Ramp phase for dead-leg end temperature, U_m = 1.03 m/s (6d)

It was found, however, that the temperature at the end of the dead-leg was fluctuating by approximately 1-3°C during heating with approximately 16 peak values displayed during this time period. This would indicate that there was a continual change of fluid in this area of the dead-leg at this loop velocity and that heat transfer by convective processes become dominant over that of diffusion.

Figure 3.11 represents the dead-leg end temperature increase during the loop heating phase for a velocity of 1.22 m/s. The dead-leg end temperature was found to fluctuate more rapidly with time for this velocity with approximately 21 temperature peaks within the same time period.

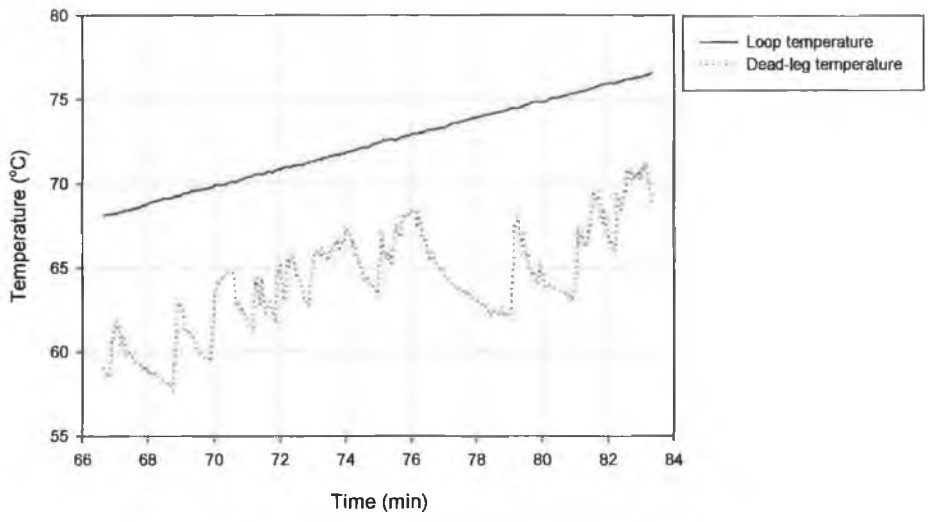

Figure 3.11: Ramp phase for dead-leg end temperature, U_m = 1.22 m/s (6d)

This would highlight that there was an increase in the motion of the fluid at the end of the dead-leg with an increase in the loop velocity.

3.3.2 4d Dead-leg temperature profile analysis

Figures 3.12 represents the temperature profiles for the change in loop temperature T_l and dead-leg temperature T_{edl} respectively over time for a 4d dead-leg configuration at a loop velocity of 0.19 m/s.

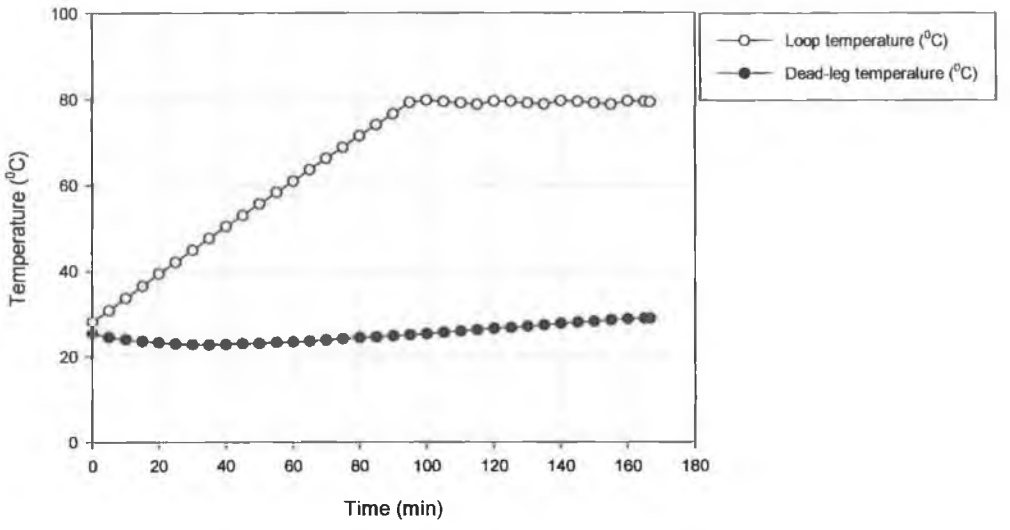

Figure 3.12: Temperature profiles at U_m = 0.19 m/s (4d)

As was the case for the 6d configuration, the loop temperature profile was shown to consist of a heating or ramp phase followed by a constant temperature phase. The water at the end of the dead-leg increased in temperature from 25.44°C at the start of the experimental run and reached a maximum temperature of 28.95°C. It was shown that for this velocity the temperature at the end of the dead-leg was not significantly affected by the increase in loop temperature suggesting there was little fluid motion within the dead-leg.

The most significant temperature change for the fluid at the end of the dead-leg in a 4d configuration was for loop velocities of 0.19 and 0.28 m/s. Figures 3.13 represents the temperature profiles for the change in loop temperature T_l and dead-leg temperature T_{edl} respectively over time for both velocities.

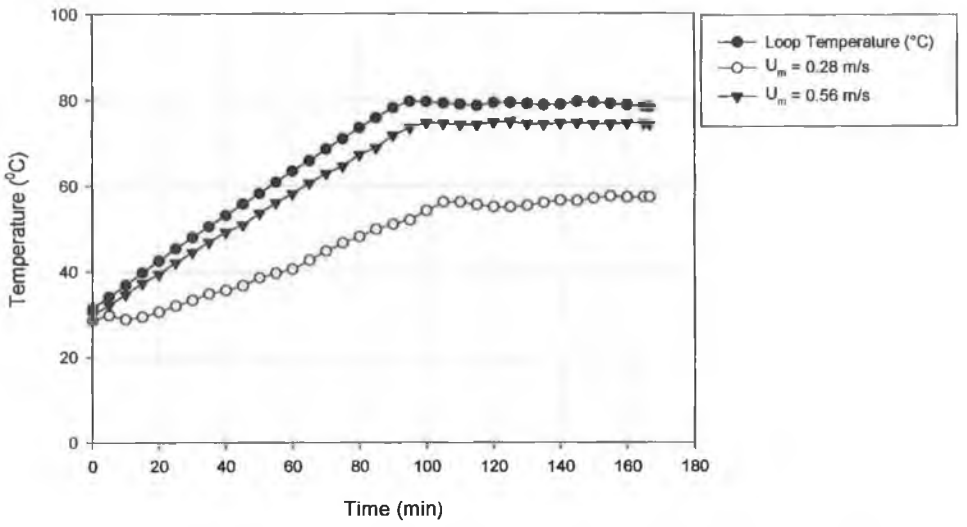

Figure 3.13: Temperature profiles at U_m = 0.28, 0.56 m/s (4d)

The dead-leg temperature profile was shown to approach that of the loop temperature profile more readily for the 4d configuration during the heating or ramp phase for loop velocities of 0.28 m/s and above. This would suggest a more vigorous mixing process of the dead-leg fluid for the 4d configuration compared to the 6d configuration. It was shown by Haga et al [28], that removal of chemical residue from dead-legs was shown to increase with reduced dead-leg length and at lower velocities.

Figure 3.14 represents a closer analysis of the heating phase for the fluid at the end of the dead-leg and loop fluid for a velocity of 0.56 m/s. The data was recorded from 66 to 83 minutes during the experimental run. The loop temperature profile was shown to follow a linear increase with no notable temperature scatter.

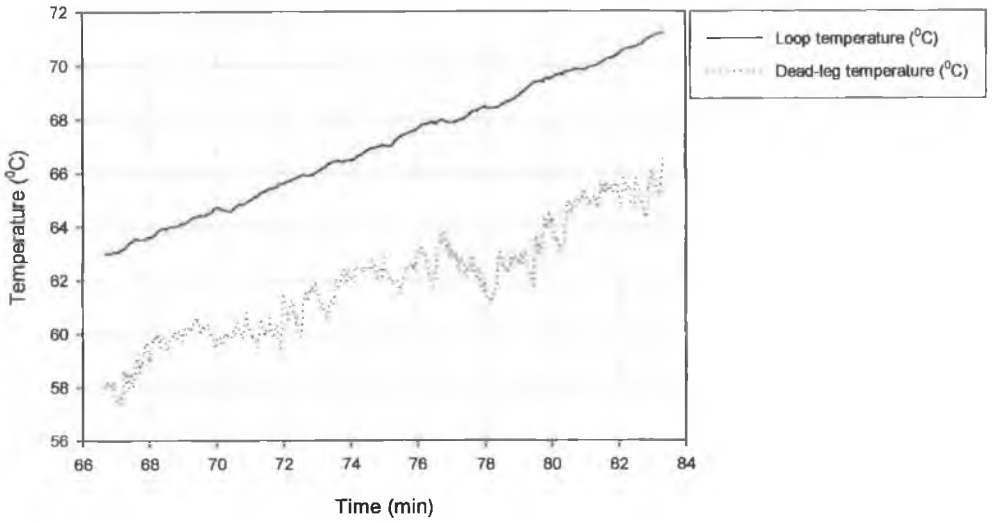

Figure 3.14: Ramp phase for dead-leg end temperature, U_m = 0.56 m/s (4d)

It was noted that there was a significant number of temperature peaks during this time period for the dead-leg end temperature. This was comparable to the 6d configuration, however, the time between peaks was reduced. This would indicate that there was an increase in fluid mixing for this dead-leg geometry.

Table 3.7 shows the relationship between loop velocity and the maximum temperature achieved at the end of the dead-leg after completion of each experimental run.

Velocity (U_m) (m/s)	**Maximum end temperature 4d T_{mdl} (°C)**
0.19	28.95
0.28	57.30
0.56	74.21
0.85	72.61
1.03	72.02
1.22	70.76
1.50	74.25

Table 3.7: Relationship of loop velocity and maximum end temperature (4d)

As for the 6d configuration, an increase in the maximum temperature of the 4d dead-leg configuration was noted for an increase in loop velocity.

The maximum temperature significantly increased for loop velocities of $U_m \geq 0.28$ m/s. However, the dead-leg end temperature was found to plane off for loop velocities of $U_m \geq 0.56$ m/s. It was shown that the maximum temperature achievable over this range of loop velocities for the 4d geometry was approximately 72°C ± 2°C. The maximum temperature recorded was 74.25°C for a loop velocity of 1.5 m/s. In all cases the loop temperature of 78°C ± 0.5°C was not achieved at the end of each experimental run.

3.3.3 2d Dead-leg temperature profile analysis

The loop temperature and dead-leg end temperature profiles are shown in figures 3.15 and 3.16 for loop velocities of 0.19 m/s and 1.5 m/s respectively.

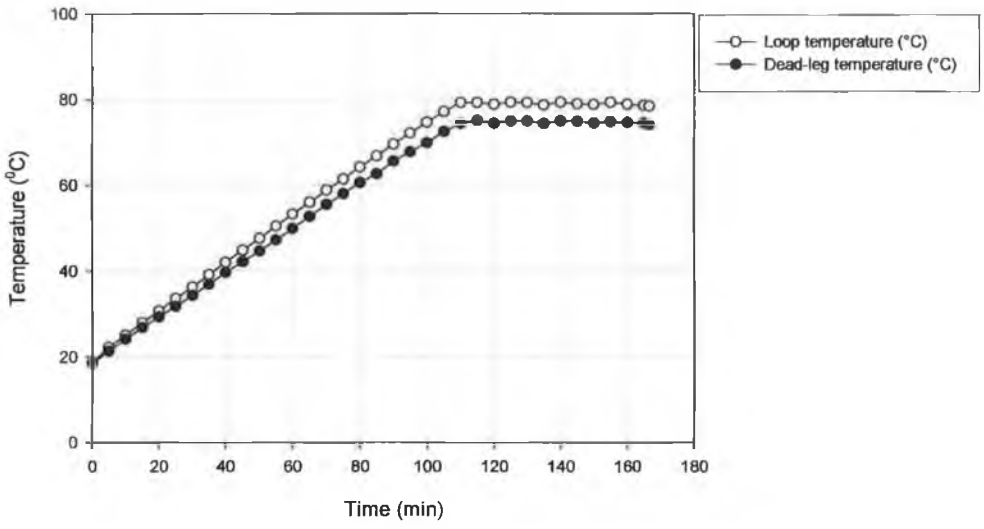

Figure 3.15: Temperature profiles for $U_m = 0.19$ m/s (2d)

The temperature change at the end of the dead-leg was shown to follow the loop temperature closely in each case. For each velocity the dead-leg temperature was shown to have a defined ramp phase and a constant temperature phase. The difference between the loop temperature and dead-leg temperature was shown to be small at all times in each experimental run.

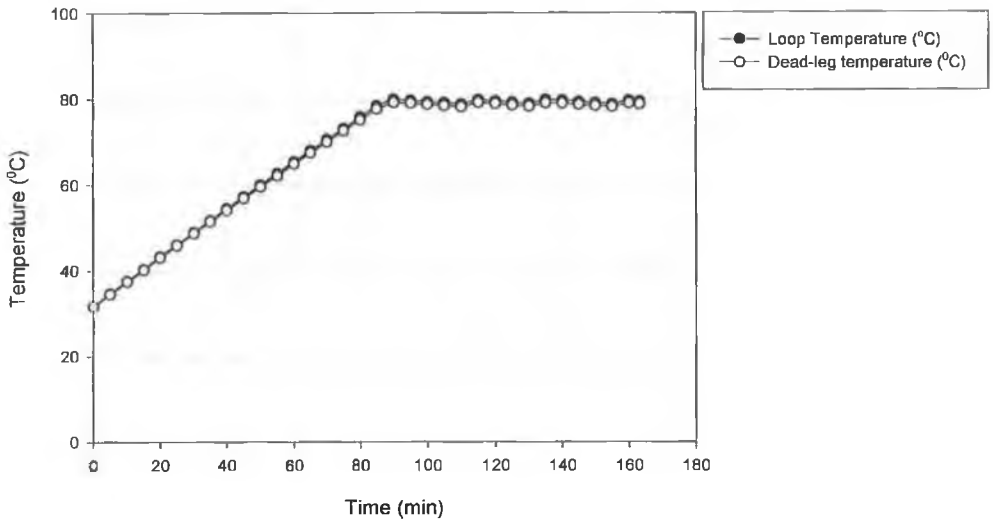

Figure 3.16: Temperature profiles for U_m = 1.5 m/s (2d).

The maximum temperature difference between the loop and dead-leg end temperatures during the heating phase was found to be 4.86°C for U_m = 0.19 m/s and 0.73°C for U_m = 0.56 m/s. The small temperature differences would suggest an efficient mixing process for the 2d geometry.

The temperature difference between the loop and dead-leg end temperature was found to be 4.13°C for U_m = 0.19 m/s and 0.77°C for U_m = 1.5 m/s at the end of each run.

Table 3.8 shows the relationship between loop velocity and the maximum end temperature of the dead-leg achieved after completion of the experimental runs for the 2d dead-leg configuration.

Velocity (U_m) (m/s)	**Maximum end temperature 2d T_{edl}(°C)**
0.19	74.00
0.28	77.18
0.56	78.21
1.03	78.17
1.50	78.84

Table 3.8: Relationship of loop velocity and maximum end temperature (2d)

It was found from table 3.8 that the dead-leg end temperature was approximately that of the loop temperature (78°C ± 0.5°C) for loop velocities Um ≥ 0.56.

In was shown that, in general, the maximum dead-leg end temperature recorded on completion of each experimental run increased with increase in loop velocity for each configuration. The increase in the Reynolds number in the loop pipe was shown to coincide with a significant increase in dead-leg end temperature for the 6d and 4d configurations. The small temperature changes recorded for low loop velocities for the 6d and 4d configurations would suggest that there was poor mixing between the loop and dead-leg fluid. For higher loop velocities there was an increase in the temperature at the end of the dead-leg during the heating phase of each experimental run suggesting a more vigorous mixing process. Reducing the dead-leg to a 2d configuration was shown to significantly increase the end temperature of the dead-leg and mixing of the fluid over the specified range of loop velocities.

Part B. Temperature distribution analysis

Temperature distributions were obtained for a 6d, 4d and 2d dead-leg configuration respectively for a range of distribution loop velocities (see appendix 2). The temperatures were recorded at the end of each experimental run described in Part A. It was found that the dead-leg end temperature and loop temperature were approximately constant at the end of each experimental run for each configuration. Therefore, each temperature distribution was considered to represent the steady state temperature throughout the dead-leg.

3.3.4 6d Temperature distribution analysis

The following results represent temperature measurements that were taken for a 6d dead-leg configuration.

The temperature along the centre line of the dead-leg branch pipe was plotted against *l*/d ratio where *l* represented the position along the centre line of the dead-leg and d represented the diameter of the dead-leg pipe. For this analysis, the temperature of the loop fluid was shown to be 78°C ± 0.5°C. Temperatures recorded in this range within the dead-leg were considered to have reached the main loop temperature.

Figure 3.18 shows the temperature distribution that was recorded for a loop velocity of $U_m = 0.19$ m/s. The temperature at the entry region to the dead-leg (l/d = 0) was shown to be that of the loop temperature of approximately 78°C ± 0.5°C.

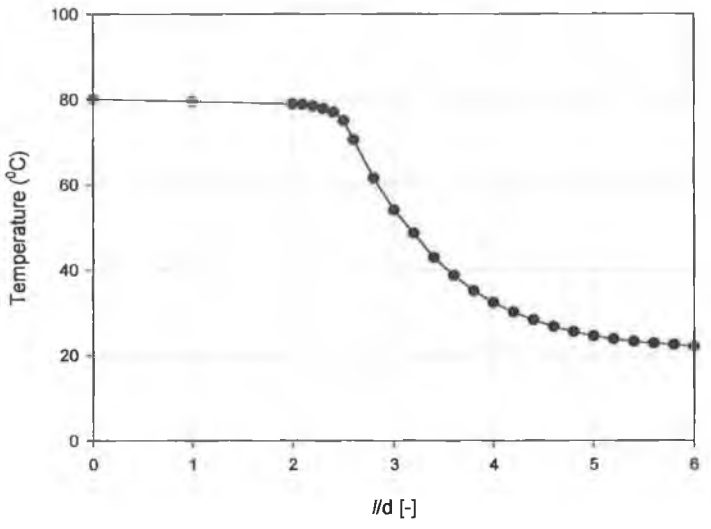

Figure 3.17: Dead-leg temperature distribution at $U_m = 0.19$ m/s (6d)

The loop temperature was shown to extend to an l/d ratio of approximately 2.3 into the dead-leg. There was a significant temperature drop with distance along the remainder of the dead-leg were the temperature was found to be 22°C at the end of the dead-leg (l/d = 6).

From $0 \leq l/d \geq 2.3$ the temperature was found to be uniform suggesting that there was a good mixing process between the loop and dead-leg fluids in this region.

From $2.3 \leq l/d \geq 6$ the temperature was found to decrease exponentially with distance along the dead-leg. Conduction is associated with an exponential temperature decay indicating that the fluid in the bottom part of the dead-leg was stagnant and was unaffected by the mixing process occurring between $0 \leq l/d \geq 2$ [40]. It was shown numerically by Noble [29] that the heat transfer in the lower part of a dead-leg was through conduction.

Figure 3.18 represents the dead-leg temperature distribution that was obtained for a loop velocity of 0.56 m/s. The loop temperature of 78°C ± 0.5°C was shown to extended further into the dead-leg penetrating to an *l*/d ratio of 4.2.

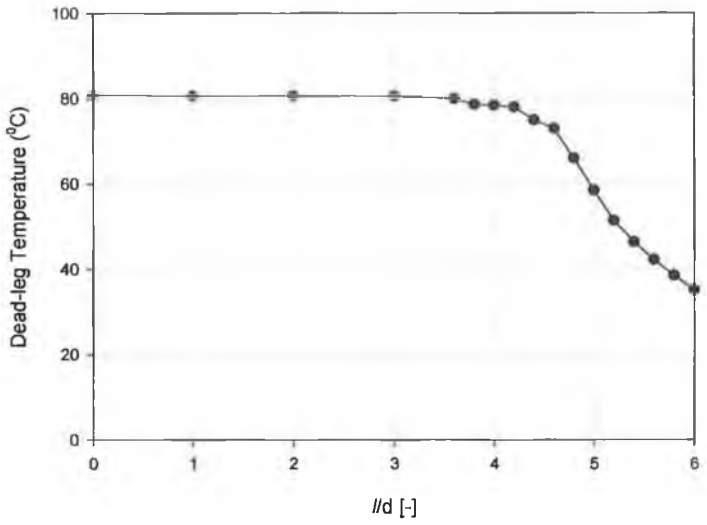

Figure 3.18: Dead-leg temperature distribution for U_m = 0.56 m/s.

The increase in loop velocity was shown to increase the depth to which the loop temperature extended into the dead-leg. This would suggest that the level of fluid mixing in the dead-leg had increased. A large temperature drop was still noted in the remainder of the dead-leg and represented a stagnant region of fluid.

The distance into the dead-leg to which the temperature was approximately that of the loop temperature can be described as a thermal penetration depth, *l*p/d, and is expressed in dimensionless form [38].

Table 3.9 shows the relationship of thermal penetration depth, *l*p/d, and loop velocity for the 6d configuration. Where *l*p is the distance along the dead-leg branch measured from the centre line of the loop pipe and d, is the diameter of the dead-leg branch pipe.

Loop Velocity U_m (m/s)	Thermal penetration Depth 6d *l*p/d [-]
0.19	2.3
0.28	3.2
0.56	4.2
0.85	5.0
1.03	5.1
1.22	5.5
1.50	5.8

Table 3.9: Relationship of loop velocity and loop temperature penetration (6d)

It was noted that for a 6d dead-leg configuration, an increase in loop velocity was found to increase the thermal penetration depth into the dead-leg. This would indicate that mixing of the dead-leg and loop fluids increased for an increase in loop velocity. However, full penetration of the loop temperature was not achieved for this range of loop velocities. The maximum depth of penetration was found to be 5.8 for a loop velocity of 1.5 m/s.

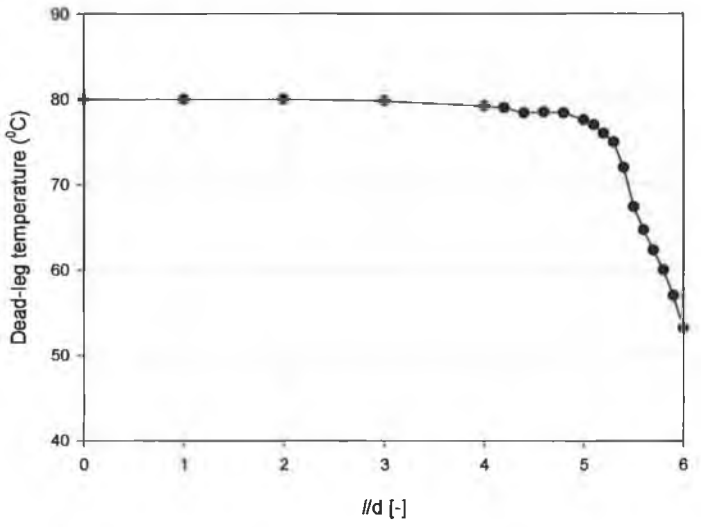

Figure 3.19: Dead-leg temperature distribution for U_m = 0.85 m/s (6d)

Figures 3.19 represents the temperature distribution for a loop velocity of U_m = 0.85 m/s. The depth of thermal penetration was found to be *l*p/d 5.0 into the dead-leg indicating good fluid mixing in the majority of the branch pipe.

The temperature decay region was significantly reduced, however, the profile was not found to be exponential in form indicating that there was some mixing of the fluid in his region.

Figures 3.20 represents the temperature distributions measured for a range of loop velocities for the 6d dead-leg configuration. It was shown that for an increase in loop velocity the loop temperature was shown to penetrate further into the dead-leg branch. The temperature decay region exhibited at low loop velocities was eliminated for velocities of $U_m > 1.03$ m/s suggesting that the fluid was no longer stagnant at the end of the dead-leg.

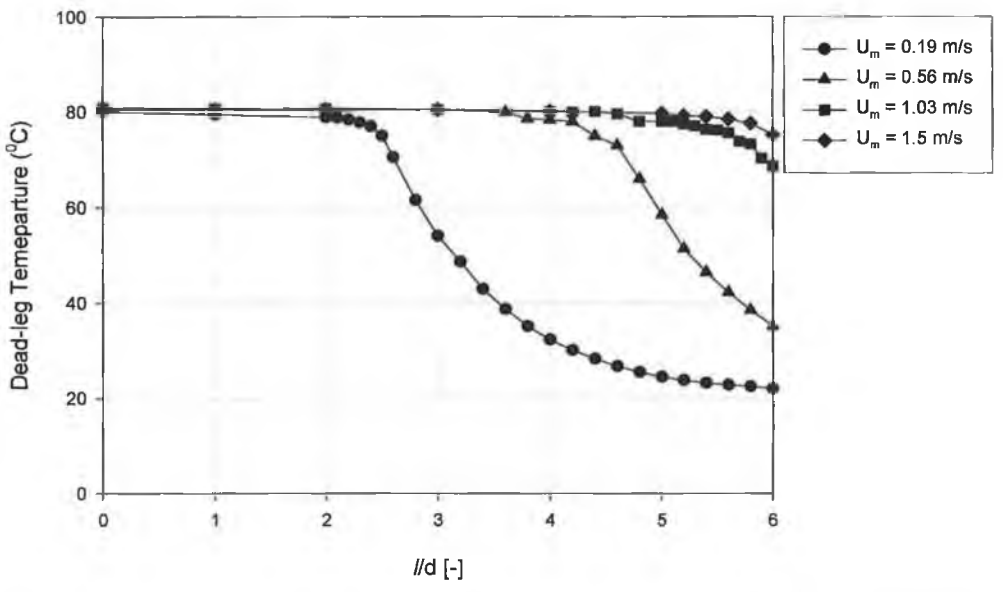

Figure 3.20: Dead-leg temperature distributions for a range of loop velocities (6d)

3.3.5 4d Temperature distribution analysis

The following results represent temperature measurements that were taken for a 4d dead-leg configuration.

Figure 3.21 shows the temperature distribution that was recorded for a loop velocity of 0.19 m/s. The temperature at the entry region to the dead-leg was shown to be approximately 78°C ± 0.5°C.

The loop temperature was shown to extend to an *l*/d ratio of approximately 2.2 into the dead-leg. A significant temperature drop was noted along the remainder of the dead-leg.

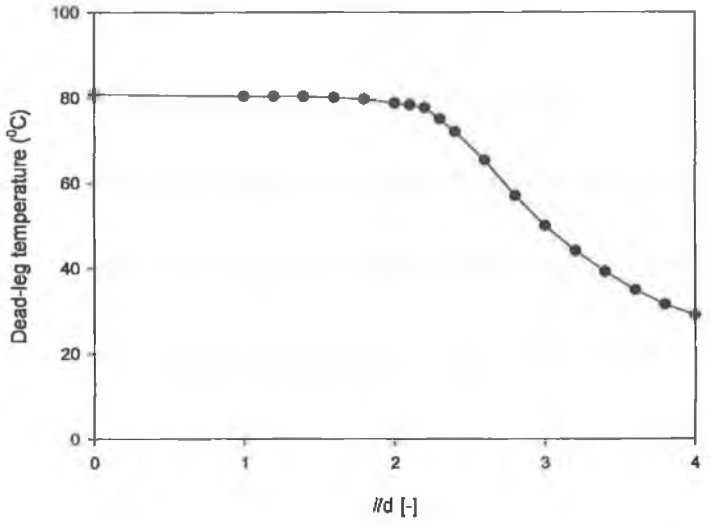

Figure 3.21: Dead-leg temperature distribution for U_m = 0.19 m/s (4d).

From $0 \leq l/d \geq 2.2$ the temperature was found to reach the loop temperature suggesting good mixing of the dead-leg fluid in this region. As for the 6d configuration the temperature was found to exponentially decay from *l*/d = 2.2 to *l*/d = 4 indicating that the fluid in this region was stagnant.

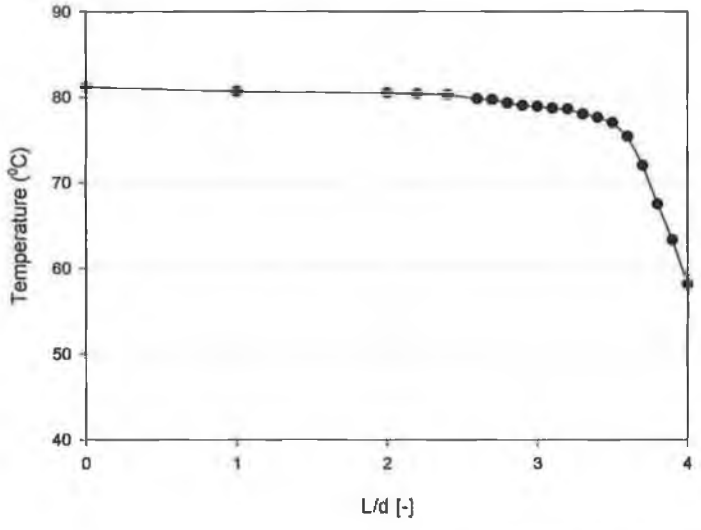

Figure 3.22: Dead-leg temperature distribution for U_m = 0.28 m/s (4d)

Figure 3.22 shows the temperature distribution that was recorded for a loop velocity of 0.28 m/s. The thermal penetration depth was shown to be *l*p/d = 3.4. A significant increase in thermal penetration was noted between 0.19 and 0.28 m/s and the dead-leg end temperature at *l*/d = 4 was also found to have greatly increased. The temperature drop in this region was no longer shown to exhibit an exponential decay suggesting that fluid mixing was occurring along the length of the dead-leg branch.

Figure 3.23 represents the temperature distributions for different loop velocities (U_m) for the 4d configuration. It was shown that for an increase in loop velocity the loop temperature was shown to penetrate further into the dead-leg branch.

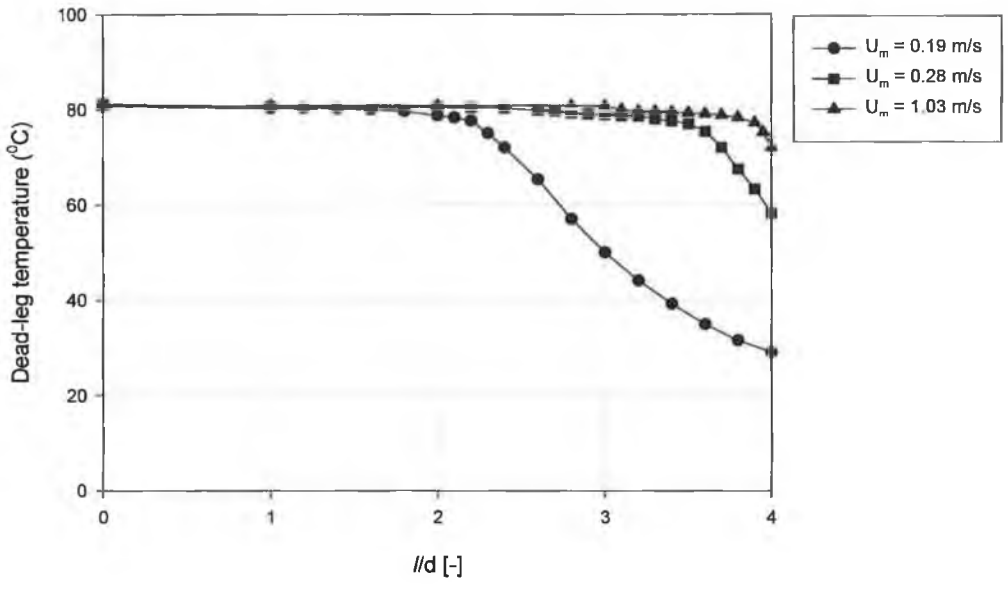

Figure 3.23: Dead-leg temperature distributions for a range of loop velocities (4d)

The temperature decay region exhibited at a loop velocity of 0.19 m/s was significantly reduced with an increase in loop velocity. It was observed that there was no notable change in the temperature distribution characteristics for loop velocities of $0.56 \leq U_m \geq 1.22$ m/s with an *l*p/d ratio of 3.8 maintained for each experimental run. This would suggest little change in characteristics of the mixing process of the dead-leg fluid for this range of loop velocities.

Table 3.10 shows the relationship of the thermal penetration depth for a range of loop velocities.

Loop velocity U_m (m/s)	**Thermal penetration Depth 4d *l*p/d [-]**
0.19	2.2
0.28	3.4
0.56	3.8
0.85	3.8
1.03	3.8
1.22	3.8
1.50	3.9

Table 3.10: Relationship of loop velocity and loop temperature penetration (4d)

A significant increase in thermal penetration depth was noted for loop velocities of $U_m \geq 0.28$ m/s. It was found that this increase coincided with a change from the transitional to turbulent flow regimes in the loop pipe. It was noted that full thermal penetration was not achieved for the 4d geometry over the specified range of loop velocities with a maximum value of 3.9 obtained for a loop velocity of 1.5 m/s.

3.3.6 2d Temperature distribution analysis

The following results represent temperature measurements that were taken for a 2d dead-leg configuration. Figure 3.24 shows the combined temperature distribution plot for loop velocities of U_m = 0.19 m/s and 0.56 m/s. It was noted that for each loop velocity the temperature at the entry region to the dead-leg was approximately 78°C ± 0.5°C. The loop temperature was shown to extend to an *l*p/d ratio of 1.8 for a loop velocity of 0.19 m/s.

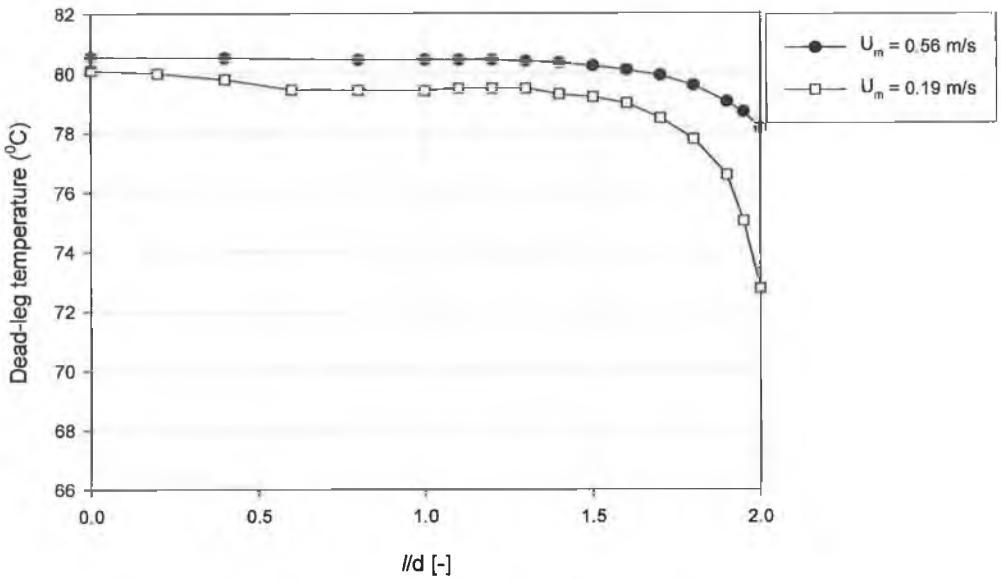

Figure 3.24: Dead-leg temperature distributions (2d)

For a velocity of 0.56 m/s the temperature throughout the dead-leg was approximately that of the loop temperature. The temperature recorded at the end of the dead-leg was shown to be 78.15°C.

It was noted that all temperature distributions measured for loop velocities above 0.56 m/s displayed similar characteristics and that the thermal penetration depth extended the full length of the dead-leg. There was no significant temperature decay region at the end of the dead-leg indicating that there was good fluid mixing throughout the 2d geometry. Table 2.11 shows the relationship of loop temperature penetration into the dead-leg for a range of loop velocities.

Velocity U_m (m/s)	**Loop penetration *l*p/d [-]**
0.19	1.8
0.28	1.9
0.56	2.0
1.03	2.0
1.50	2.0

Table 3.11: Relationship of loop velocity and loop temperature penetration (2d)

In general, for each branch configuration, it was found that a region of uniform temperature existed in the dead-leg. This was described as the thermal penetration depth and was representative of the region of the dead-leg encompassed by the loop fluid temperature. The thermal penetration depth was also found to represent the circulation flow region in the dead-leg. It was shown that the thermal penetration depth increased for an increase in loop velocity for each configuration.

A temperature decay region was also found for a number of experimental runs for each dead-leg configuration. The temperature drop in this region was found to be exponential for low loop velocities and was considered to be a region of stagnant fluid for the 6d and 4d configurations. The 2d configuration was shown to have no significant temperature decay region within the dead-leg for all loop velocities indicating that the fluid was well mixed along the branch length.

3.4 Evaluation of the thermal–fluid characteristics within a pipe dead-leg

Establishing the flow and temperature characteristics in a pipe dead-leg are essential in determining the efficiency of thermal sanitisation and hence, the ability to control bacterial contamination in a pharmaceutical water system. It was found from the results obtained from the experimental rig and within literature [28, 29, 38] that there were two identifiable regions of temperature and fluid flow in the dead-leg.

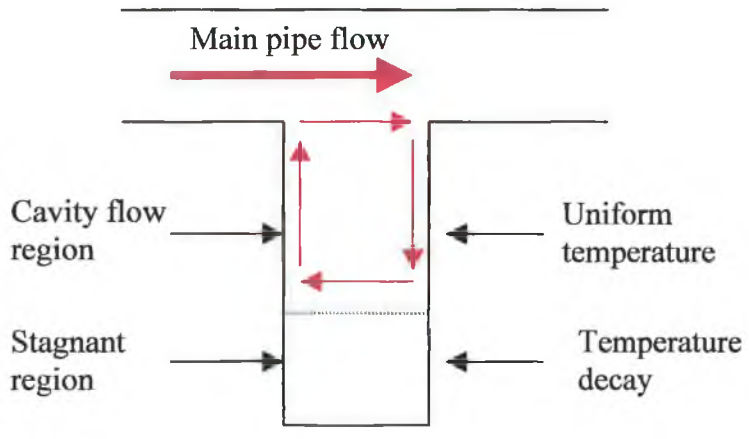

Figure 3.25: Schematic of dead-leg flow and temperature regions

A sketch of the two regions is shown in figure 3.25. The first was a region of uniform temperature with good fluid mixing and the second was a region of temperature decay indicating the presence of stagnant fluid.

3.4.1 Correlation of thermal penetration depth

It was found that for each dead-leg configuration the depth of thermal penetration increased for an increase in loop velocity. The thermal penetration depth was shown to encompass the region of the dead-leg that was at the loop temperature. This was also shown to be a measure of the cavity or circulation flow in the dead-leg [38].

A correlation using dimensional groups has been developed to predict the thermal penetration depth, *l*p/d, for the data obtained for each dead-leg configuration. The depth of penetration will provide a means of estimating the extent of the circulation flow region and an approximation to the extent of the stagnant region in the dead-leg branch pipe.

Dimensional analysis is a technique that is used widely in the field of engineering. This form of analysis is often used where it is recognised that some physical phenomena are so complex that they cannot be predicted from first principles. In these cases empirical correlations are developed from dimensional groups. Common dimensional groups would include the Reynolds number (Re) in fluid flow analysis or the Nusselt number (Nu) in heat transfer problems.

The rules of dimensional analysis were applied to the data obtained from the experimental rig to develop a correlation that would best describe the process of thermal penetration in a range of dead-leg configurations [45].
The thermal penetration depth, *l*p/d, was assumed to be a function of the following variables:

$$l\mathrm{p/d} = f(\mathrm{L}, \rho, \mathrm{v}, \mathrm{D}, \mu) \qquad (1)$$

Where L was the length of dead-leg, ρ the density of fluid, v the velocity of fluid in loop pipe, D the loop pipe diameter and μ the dynamic viscosity of the fluid.

Using the Buckingham Pi theorem, equation 1 was shown to reveal two dimensionless groups including:

$$\pi_1 = \frac{L}{d} \tag{2}$$

$$\pi_2 = \frac{\rho v D}{\mu} \tag{3}$$

Equation 2 was considered to be a length ratio. It defines the ratio between the length of the dead-leg to the diameter of the dead-leg. The length ratios for the three configurations were L/d = 6, 4 and 2.

Equation 2 was shown to be the Reynolds number which defines the characteristics of the fluid in the main distribution loop pipe. Table 3.12 shows the relationship of loop velocity and Reynolds number.

Loop velocity U_m (m/s)	**Reynolds no. Re [-]**
0.19	2.47×10^4
0.28	3.71×10^4
0.56	6.18×10^4
0.85	1.11×10^5
1.03	1.36×10^5
1.22	1.61×10^5
1.50	1.8×10^5

Table 3.12: Relationship of loop velocity and Reynolds number

The dimensionless penetration depth *l*p/d was assumed to be a power-law function of the other dimensionless groups. Non-linear regression was applied to the data obtained from the experimental rig using Sigmaplot™ (SSI, California, USA) and the following expression for thermal penetration depth was determined (see appendix 1).

$$\frac{l_p}{d} = 0.05\left[\frac{L}{d}\right]^{0.72}[Re]^{0.29} \tag{4}$$

Figure 3.26 shows the relationship between the experimental and predicted values for thermal penetration depth.

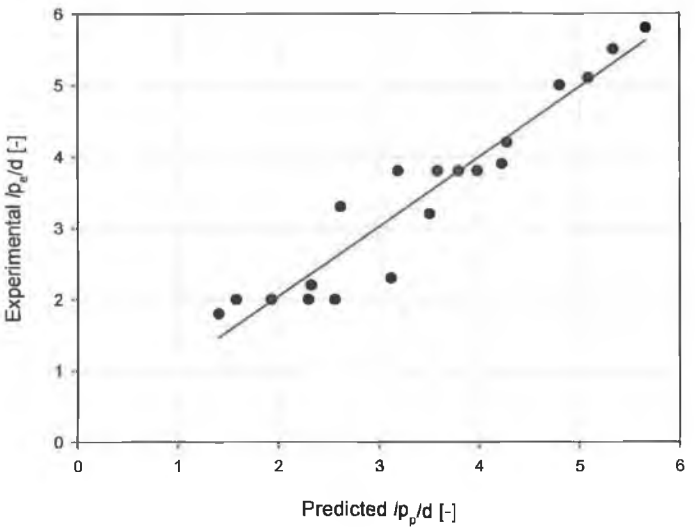

Figure 3.26: Relationship of predicted and experimental *l*p/d values

A measure of the quality of the data fit can be determined by finding the correlation coefficient or R^2 value. By applying a linear regression to the data, Sigmaplot™ returned an R^2 value of 0.91. The predicted data would appear to work best for the 6d configuration with only small differences between predicted and experimental values.

By applying equation 4 the results for predicted penetration depth were shown to be more scattered for the 2d and 4d geometries. However, the dimensional analysis approach to correlating thermal penetration depth would appear to present a useful tool in predicting loop temperature pentration and hence circulation flow within a pipe dead-leg. The relationship between experimental and predicted thermal penetration depth for a 6d, 4d and 2d dead-leg configuration are presented in tables 3.13 to 3.15.

Loop Velocity (m/s)	Experimental penetration depth l_{pe}/d [-]	Predicted penetration depth l_{pp}/d [-]
1.5	5.8	5.67
1.22	5.5	5.34
1.03	5.1	5.09
0.85	5	4.80
0.56	4.2	4.28
0.28	3.2	3.51
0.19	2.3	3.12

Table 3.13 Relationship of loop velocity to predicted and experimental thermal penetration depth (6d)

Loop Velocity (m/s)	Experimental penetration depth l_{pe}/d [-]	Predicted penetration depth l_{pp}/d [-]
1.5	3.9	4.23
1.22	3.8	3.98
1.03	3.8	3.80
0.85	3.8	3.58
0.56	3.8	3.19
0.28	3.3	2.61
0.19	2.2	2.33

Table 3.14 Relationship of loop velocity to predicted and experimental thermal penetration depth (4d)

Loop Velocity (m/s)	Experimental penetration depth l_{pe}/d [-]	Predicted penetration depth l_{pp}/d [-]
1.5	2.0	2.56
1.03	2.0	2.30
0.56	2.0	1.93
0.28	2.0	1.58
0.19	1.8	1.41

Table 3.15 Relationship of loop velocity to predicted and experimental thermal penetration depth (2d)

3.4.2 Analysis of the stagnant region

It was shown from the results that for low loop velocities the dead-leg end temperature did not increase significantly for the 6d and 4d configurations. It was shown that the loop velocity had little effect on the fluid at the end of the dead-leg indicating that the fluid was relatively stagnant. Temperature distributions were found to have a region of exponential temperature decay at the end of the dead-leg for the same loop velocities. This was comparable to the findings of Nakamori et al [38] and Noble et al [29] where temperature was shown to exponentially decay in a stagnant fluid region of the dead-leg.

The exponential temperature decay in the stagnant region can be shown to be analogous with extended surface theory applied to fin design [46]. By applying the one-dimensional heat conduction equation the variation of temperature along the length of the dead-leg branch can be shown as:

$$T_{dl} - T_a = T_a + (T_l - T_a)e^{-al} \quad (5)$$

where

T_{dl} = temperature along the dead-leg below the circulation region

T_l = loop temperature

T_a = Ambient air temperature

l = Distance along dead-leg

$$a = \sqrt{\frac{hP}{kA}} \quad (6)$$

where, k is the thermal conductivity of the fluid, h the heat transfer coefficient evaluated from experiment, P the perimeter of the dead-leg branch pipe and A is the cross sectional area of the dead-leg branch pipe.

Figure 3.27 shows the temperature decay region for a 6d dead-leg configuration at a loop velocity of U_m = 0.19 m/s. The dead-leg temperature T_{dl} is plotted against dimensionless position along the dead-leg.

By applying non-linear regression an exponential decay function of $(T_{dl} - T_a) = T_a + b*e^{-cl/d}$ was shown to fit the data where b and c were constants and $T_a = 20.7°C$ was the ambient air temperature for this run and l/d was the position within the dead-leg branch.

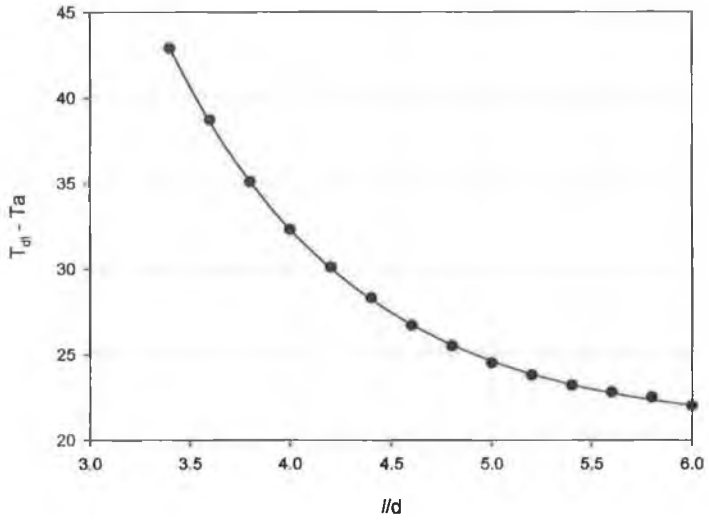

Figure 3.27: Exponential temperature decay for $U_m = 0.19$ m/s (6d)

The curve fit was shown to have an R^2 value of 0.999. The accuracy of this curve fit would suggest that stagnation of the fluid was dominant in this region of the dead-leg for this loop velocity. It was found that this exponential temperature decay region was reduced in the dead-leg for an increase in loop velocity for the 6d configuration. However, it was shown that this stagnant region of fluid was still present at loop velocities as high as 0.85 m/s.

Figure 3.28 shows the temperature decay region for a 6d configuration for a loop velocity of 1.03 m/s. The R^2 value returned for this data was 0.89 indicating the move away from an exponential temperature change. It was found for loop velocities above 1.03 m/s that the exponential function was eliminated.

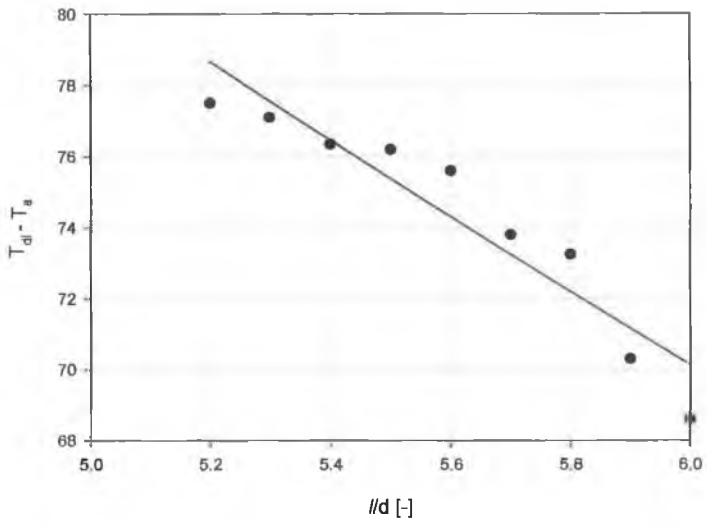

Figure 3.28: Exponential temperature decay for Um = 1.03 m/s (6d)

The temperature decay region was shown to be significantly reduced for a change in dead-leg geometry. Figure 3.29 shows the plot of the decay region for the 4d configuration at U_m = 0.28 m/s. An R^2 value of 0.94 was returned for this curve fit indicating that there was a breakdown of the decay region for low loop velocities for this geometry compared to the 6d configuration. It was found for the 4d configuration that for loop velocities greater than U_m = 0.28 m/s the exponential region was eliminated. The 2d configuration was found to have no significant decay region.

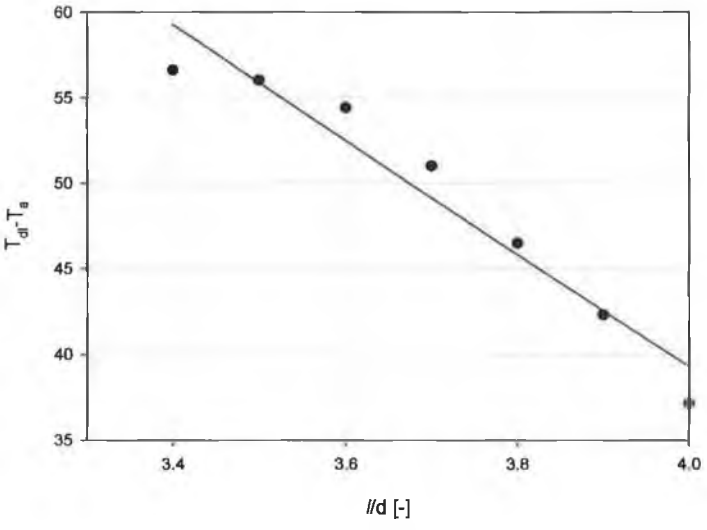

Figure 3.29: Exponential temperature decay for Um = 0.28 m/s (4d)

3.5 Application of results to the 6d rule

The formal definition of a pipe dead-leg as given by the Food and Drug Administration in GMP (LVP) section 212.49 CFR21 1972, requires that 'Pipelines for the transmission of purified water for manufacturing or final rinse should not have an unused portion greater in length than 6 diameters (the 6d rule) of the unused portion of pipe measured from the axis of the pipe in use' [2]. This definition was developed for heated systems running at 75 - 80°C to ensure all parts of the pipe network reached the required sanitisation temperature.

Figure 3.30 represents the relationship between dead-leg end temperature and loop velocity for the results obtained from the experimental rig for each dead-leg configuration.

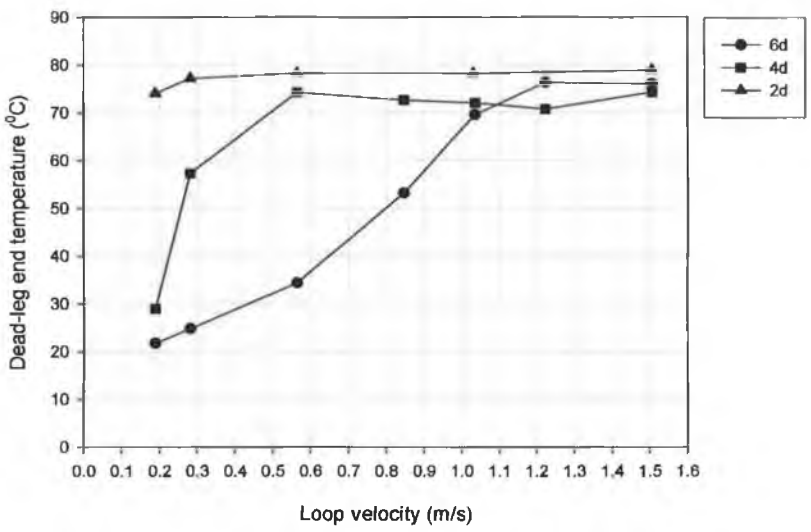

Figure 3.30: Relationship of loop velocity and dead-leg end temperature (2d, 4d, 6d)

It was shown from the results that the 6d rule was inadequate to achieve full thermal sanitisation of the dead-leg for loop velocities of 0.19 – 1.5 m/s with a loop temperature of 78°C ± 0.5°C. This was also the case for the 4d dead-leg configuration. It was found that a minimum loop velocity of U_m = 0.56 m/s was required to achieve a loop temperature of approximately 80°C at the end of the 2d dead-leg branch pipe.

If a dead-leg is present in the design of a pipe network there must not only be full loop temperature penetration but also full mixing and flushing of the fluid within the dead-leg during operation. This would ensure that microbial deposits and solids are not trapped within the water system. It was shown from the temperature distribution analysis that full thermal penetration and fluid mixing was not achieved for the 6d and 4d configuration over the range of velocities used in this experimental process. Thus, extensive flushing would be required during operation and cleaning. The 2d configuration was the only dead-leg geometry to achieve both full thermal penetration and fluid mixing.

These findings have significant implications to the design criteria of pipe system dead-legs. The present length of a maximum length of 6d as indicated by the FDA is unacceptable and in fact would require a reduction in length to 2d to ensure that the dead-leg is not only fully sanitised to the loop temperature but also flushed by the loop fluid at all times.

Chapter 4. Conclusions and future work

4.1 Conclusions

An experimental test rig was designed and constructed to study the temperature characteristics of a pipe dead-leg typically found in pharmaceutical water systems. An analysis was presented on the effect of loop velocity and temperature on the thermal characteristics for 6d, 4d and 2d dead-leg configurations respectively.

From the analysis of the results it was found that, in general, for an increase in distribution loop velocity there was an increase the dead-leg end temperature for all configurations. It was shown that the 6d and 4d geometries were inadequate to achieve full temperature penetration for loop velocities of 0.19 – 1.5 m/s at a loop temperature of 78°C ± 0.5°C. It was found that a minimum loop velocity of U_m = 0.56 m/s was required to achieve full thermal penetration of the loop temperature for the 2d dead-leg configuration.

Temperature distribution analysis identified two regions of temperature distribution. The first was referred to as a thermal penetration depth, *l*p/d, and defined a region of uniform temperature with good fluid mixing. The second was shown to be a region of temperature decay where there was the evidence of stagnant fluid in the dead-leg. For an increase in loop velocity, the thermal penetration depth was found to increase for each dead-leg configuration. The decay region was found to decrease with increase in loop velocity and was eliminated completely for the 2d configuration.

The empirical correlation developed to predict the thermal penetration depth, *l*p/d, into the dead-leg using dimensionless groups was shown to work best for the 6d configuration with only small differences between predicted and experimental values.

The 2d dead-leg was found to be the most effective configuration to achieve full temperature penetration and mixing of the dead-leg fluid for loop velocities of $U_m \geq$ 0.56 m/s. The 6d rule was shown to be inadequate for the range of distribution loop velocities used for this experimental analysis for both fluid mixing and thermal penetration requirements.

4.2 Future work

A number of observations were made during the analysis of the results obtained for the experimental rig that would be useful in future analysis of the problem of pipe system dead-legs. Future work in the field should include the following areas of investigation:

- Investigation into the effect of different loop to dead-leg pipe diameter ratios on the thermal-fluid characteristics of pipe system dead-legs.

- Investigation of surface temperatures to establish a heat transfer coefficient for various dead-leg configurations.

- The effect of increased loop velocity and hence flow regime on the dead-leg temperature and circulation flow penetration.

- The effect of dead-leg fluid flushing on the temperature of the fluid within the dead-leg.

- The effect of insulating the dead-leg using foam insulation and comparisons made to the results obtained for the current un-insulated case.

- Investigation of dead-leg flow structure using flow visualisation techniques.

Appendix 1. Publications and Presentations

Austen B, Corcoran B, (2003) The pharmaceutical industry – dead in the water, The Irish scientist yearbook, Oldbury Publishing Ltd., Co. Dublin.

Austen B, Corcoran B, (2004), 'Analysis of heat transfer within a pharmaceutical dead-leg', Proceedings, 7th Annual Sir Bernard Crossland Symposium and postgraduate research workshop, Institute of Mechanical Engineers of Ireland.

Austen B, Corcoran B, (2003) Analysis of Heat transfer within a pharmaceutical pipe dead-leg, 8th UK National Heat Transfer conference, Oxford, UK.

Austen B, Corcoran B, (2004), 'Analysis of heat transfer within a pharmaceutical dead-leg', Proceedings, 7th Annual Sir Bernard Crossland Symposium and postgraduate research workshop, Institute of Mechanical Engineers of Ireland.

Appendix 2. References

1. Carvell, J.P., 'Sterility and containment considerations in valve selection', Pharmaceutical Engineering, Vol. 12, No.1, pp31-35, 1992.
2. Food and drug Administration., 'Guide to inspection of high purity water systems', The division of field investigations, Office of regional operations, Office of regulatory affairs, FDA, Rockville MD, 1993.
3. Corcoran, B.G., Esmonde, H. and Hashmi, M.S.J., 'Investigation of turbulent flow in pharmaceutical pipe tee junctions', 1st international Conference on Heat transfer, Fluid Mechanics and Thermodynamics, Kruger park, South Africa 8-10 Aril 2002.
4. The European Agency for the evaluation of medicinal products (EMEA), 'Note for guidance on Quality of water for pharmaceutical use', 2002.
5. Fessenden B., 'A guide to water for the pharmaceutical Industry', Journal of validation technology, Volume 1, Part 1, pp 30-39, 1996.
6. McWilliam, A.J., 'The design of High purity Water Distribution Systems', Pharmaceutical Engineering, 1995.
7. European Pharmacopoeia, Directorate for the Quality of Medicines of the council of Europe (EDQM), Monographs, Volume 2, 5th Edition, pp. 4823-4828, 2005
8. Meltzer, T H., Pharmaceutical water systems, Tall Oaks publishing, Inc., pp 18, 1997.
9. Corcoran, B.G., 'Pharmaceutical water systems and the 6D rule, A computational fluid dynamic analysis', Thesis, pp. 3, 2003.
10. Riddle, R.A., 'Efficient Reliable Production of Water for injection', Pharmaceutical Engineering, pp. 30-31,3454, 1981.
11. Dickenson, C., 'Filters and filtration Handbook', Elsevier Advanced Technology, third edition, pp. 329-335, 1994.
12. DeSilva, F., 'Activated Carbon filtration', Water Quality Products Magazine, January 2000.
13. Kuhlman, H.C., 'Production of water for injection by the use of distillation' Pharmaceutical Engineering, pp. 22-24, 44, 1981.

14. Meltzer, T H., 'Pharmaceutical water systems', Tall Oaks publishing, Inc., pp 133, 1997.

15. Stadnisky W., 'Product-staged reverse osmosis system', Pharmaceutical engineering, pp16-18, 1981.

16. Edstrom Industries Incorporated, http://www.edstrom.com/products, January, 2005.

17. Corcoran, B.G., 'Pharmaceutical water systems and the 6D rule, A computational fluid dynamic analysis', Thesis, pp 12, 2003.

18. Meyrick, C.E., 'Practical design of a high purity water system', Pharmaceutical Engineering, Vol.9., No.5., pp 20-27, 1989.

19. Meltzer, T H., Pharmaceutical water systems, Tall Oaks publishing, Inc., Chapter 11, pp. 644-646, 1997.

20. Fleming J., Kemkes D., 'Biofilm contamination issues in pharmaceutical fluid-handling tubing', Pharmaceutical Engineering, 19, 5, pp. 36-38, 40, 42, 44 1999.

21. Meltzer, T H., 'Pharmaceutical water systems', Tall Oaks publishing, Inc., pp 637-640, 1997.

22. Mcnutt, J.L., Sinisgalli, P., Chafee, W., 'Ultrapure water system hydraulics 2', transcripts of fifth annual semiconductor pure water conference, San Francisco, January 16-17, pp.18-32, 1986.

23. Reidewald, F., 'Biofilms in pharmaceutical waters', Pharmaceutical Engineering, pp. 8,10,11-12,14,16,18-19. 1997.

24. Melo, L.F., Bott, T.R., 'Biofouling in water systems', Experimental thermal and fluid science, 14, pp 375-381, 1997.

25. Characklis, W.G.; Marshall, K.C., ' Biofilms', John Wiley & Sons, Inc., New York, 1990.

26. Meltzer, T H., Pharmaceutical water systems, Tall Oaks publishing, Inc., Chapter 2, pp. 94-97, 1997.

27. Gray, C., 'Recirculation velocities in water for injection (WFI) distribution systems', Pharmaceutical Engineering, pp. 28-32, 1997.

28. Haga, R., Murakami S., Ostrove S., Weiss S., 'Cleaning Mechanism study for bio-pharmaceutical plant design', Pharmaceutical Engineering, pp. 8-10, 11-14, 16-18, 21 1997.

29. Noble, P.T., 'Transport considerations for microbiological control in piping', Journal for pharmaceutical Science and technology, pp76-85, March-April, 1994.

30. Meltzer, T H., Pharmaceutical water systems, Tall Oaks publishing, Inc., pp. 65-70, 1997.

31. Forday, W.L., 'Clean in Place Technology', Singapore Microbiologist-Microbiology and Biotechnology News, July-September 5-7, 1995.

32. Seiberling, D.A., 'Alternatives to conventional Process/CIP design – for improved cleanability, Pharmaceutical Engineering, Vol. 12, No.2, pp.16-26, 1992.

33. Meltzer, T H., Pharmaceutical water systems, Tall Oaks publishing, Inc., pp. 115-116, 1997.

34. Seiberling, D.A., 'Clean-in-place & sterilize-in-place applications in the parenteral solutions process', Pharmaceutical Engineering, Vol. 6, No.6, pp30-35, 1986.

35. Young, Jack H., 'Sterilization of various diameter dead-ended tubes', Biotechnology and Bioengineering, v 42, n 1, pp 125-132. Jun 5, 1993.

36. Boyle F. 'Computational fluid dynamics in Engineering', The Engineers Journal – The Institute of Engineers of Ireland, Vol.58:02, pp. 112-116, 2004.

37. Sierra-Espinosa, F.Z., Bates, C.J., O'Doherty, T., 'Reverse and fully developed flow regions in an equally divided 90° pipe junction', ASME Fluids Engineering Division Summer meeting, June 22- 26, pp. 1-8, 1997.

38. Nakamori, N., Suzuta, T., Ueno, T., Kasahara, J., Hanzawa, K., Oketani, K., Ukai, O., 'Thermal stratification in a branch pipe', Proceedings of the international topical meeting on nuclear thermodynamics, Grenoble, pp. 415-424, 1993.

39. Deutsh, E., Barcouda, M., Rousset, J.L., Mallez, C., 'Numerical and experimental study in piping system dead-legs', Proceedings of the international topical meeting on nuclear reactor thermal hydraulics, Tokyo, pp. 782-790, 1997.

40. Cengal, Y.A., Turner, R.H., 'Fundementals of Thermal-fluid Sciences', McGraw Hill International edition, Mechanical engineering series, Chapter 12, pp. 513, 2001.

41. Bates, C.J., Zonuzi, F., Faram, M.G., O'Doherty, T., 'Experimental and numerical comparison of the flow in a 90° tee junction', ASME, Separated and complex flows, Vol. 217, pp. 43-50, 1995.

42. Douglas, J.F., Gasiorek, J.M., Swaffield, J.A., 'Fluid mechanics', Second Edition, Longman Scientific & Technical, pp. 100, 1992.

43. Pollard, A., 'Process control for the chemical and allied fluid-processing industries', Heinemann Educational, pp. 14-16, 1984.

44. Robert, M., Mattei, J.D., 'Thermal-hydraulic phenomena in a zero flowrate pipe connected to a high flowrate, high temperature circuit', International symposium on engineering, Turbulence modelling and measurements', Dubrovnik, pp. 819-827, 1990.

45. Geankoplis, C.J., 'Transport processes and unit operations', Allyn and Bacon Inc., Second edition, pp. 195-197, 1983.

46. Incropera, F.P., DeWitt, D. P., 'Introduction to heat transfer', John Wiley and Sons, Fourth edition, pp. 496-497, 2002.

Appendix 3. Specifications & Raw data

3.1 Branch tee configurations

3.1.1 2d Branch tee configuration

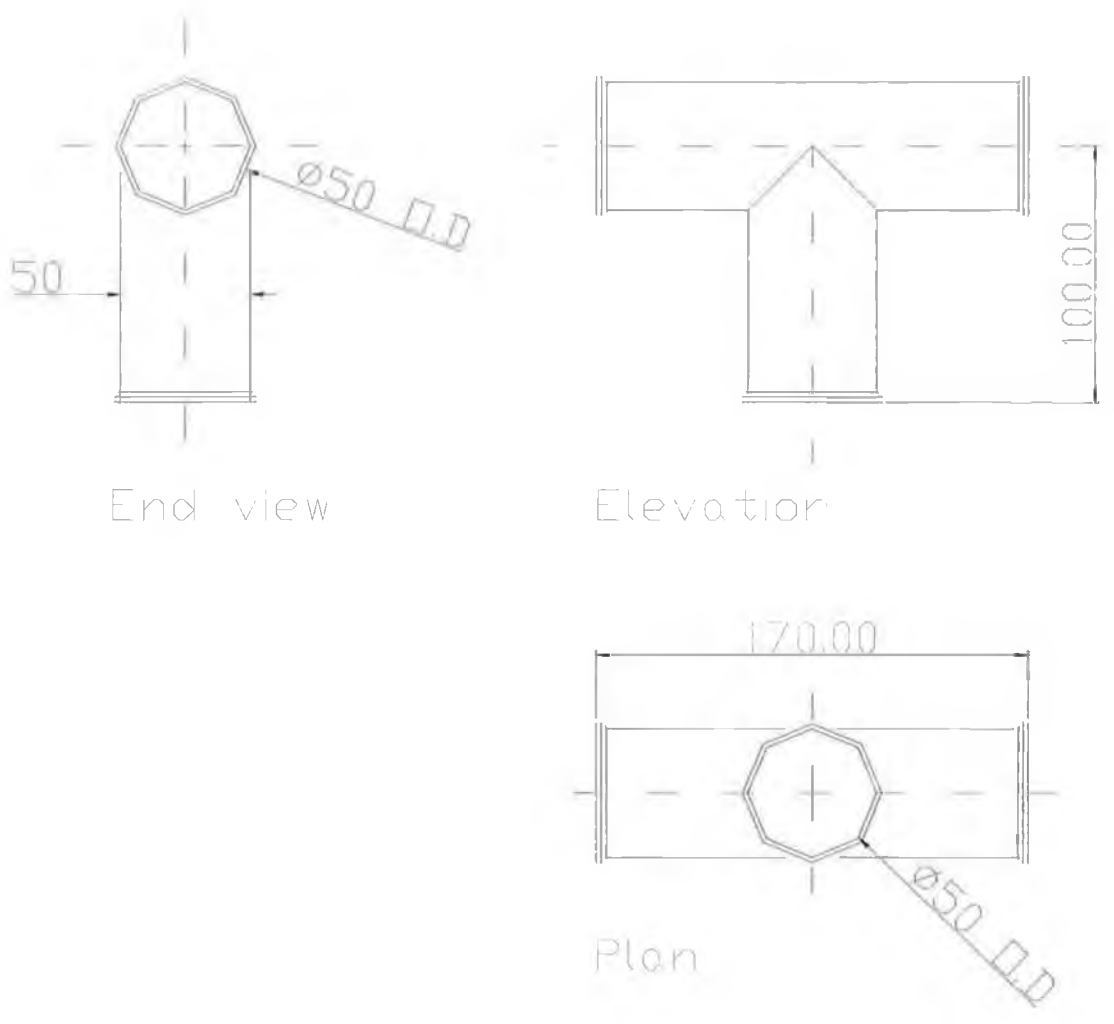

All dimensions in mm

3.1.2 4d branch tee configuration

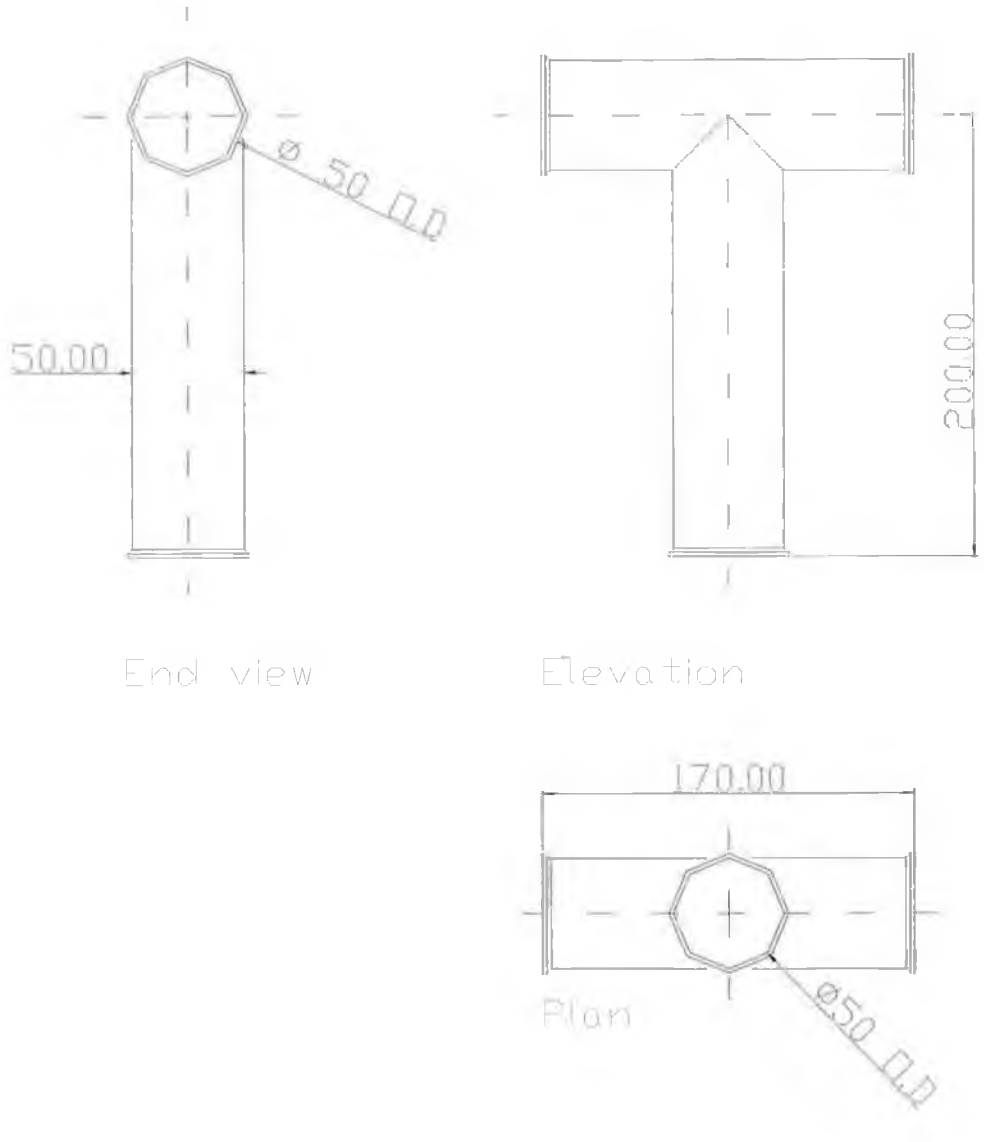

All dimensions in mm

3.1.3 6d branch tee configuration

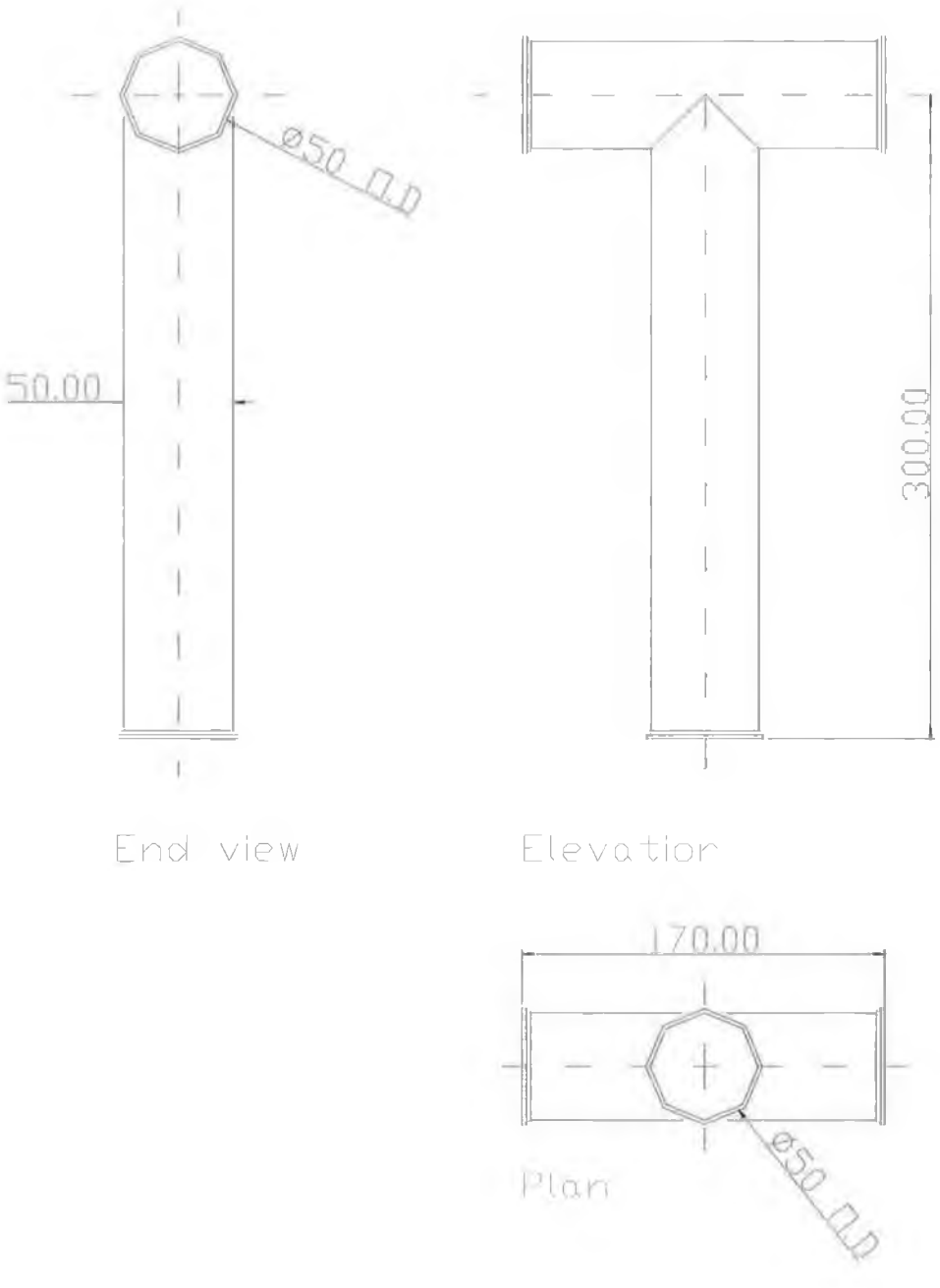

All dimensions in mm

3.2 Pipe sections

Pipe letter	Section
A	Pump feed pipe
B	Pump exit pipe
C	Loop feed pipe
D	Dead-leg entry pipe
E	Dead-leg exit pipe
F	Loop exit pipe
G	Flowmeter entry pipe
H	Flowmeter entry pipe
I	Globe valve exit pipe
J	Tank return pipe
K	Tank return pipe
L	Tank return pipe
1	Dead-leg test section
2	Pump
3	Tank

Key of pipe sections & equipment

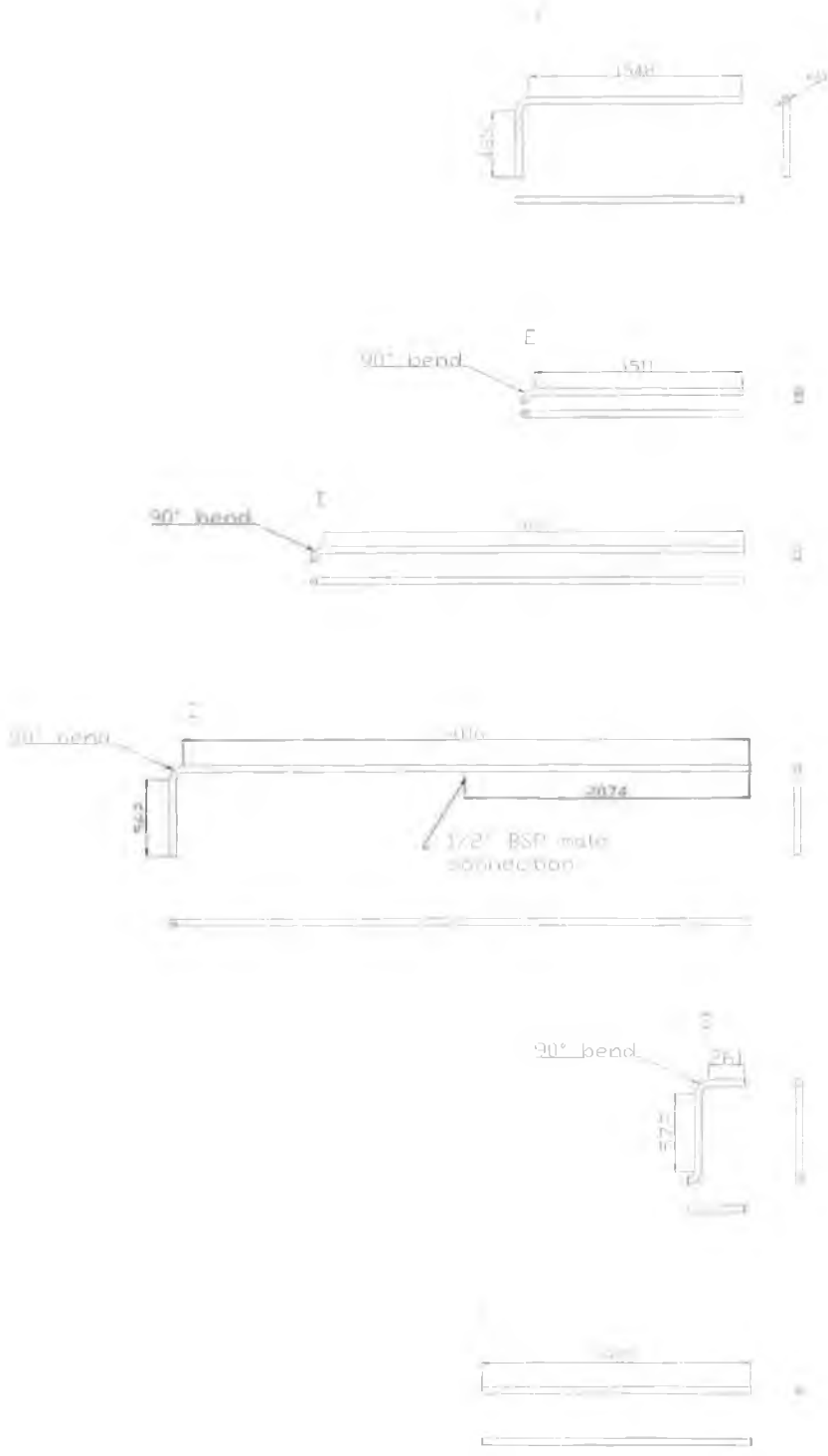

All dimensions in mm
All pipe sections with tri-ferrule ends
All pipe joints welded construction

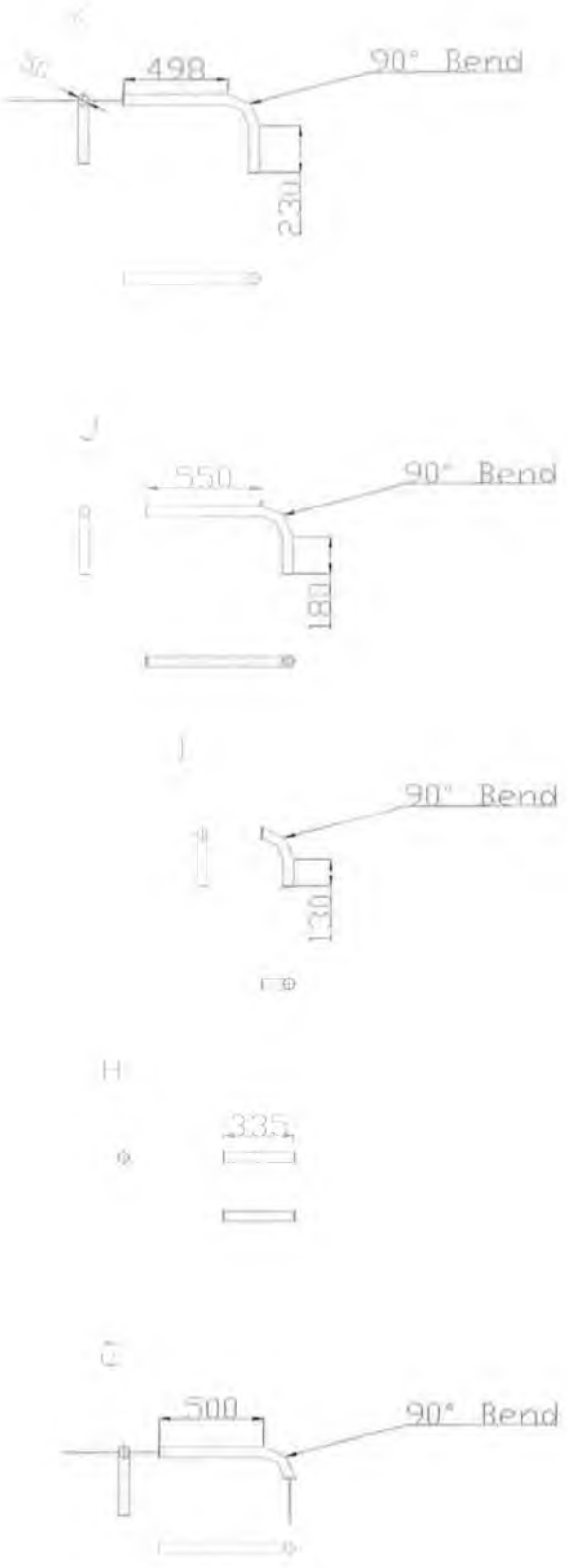

All dimensions in mm
All pipe sections with tri-ferrule ends
All pipe joints welded construction

3.3 Piping diagram

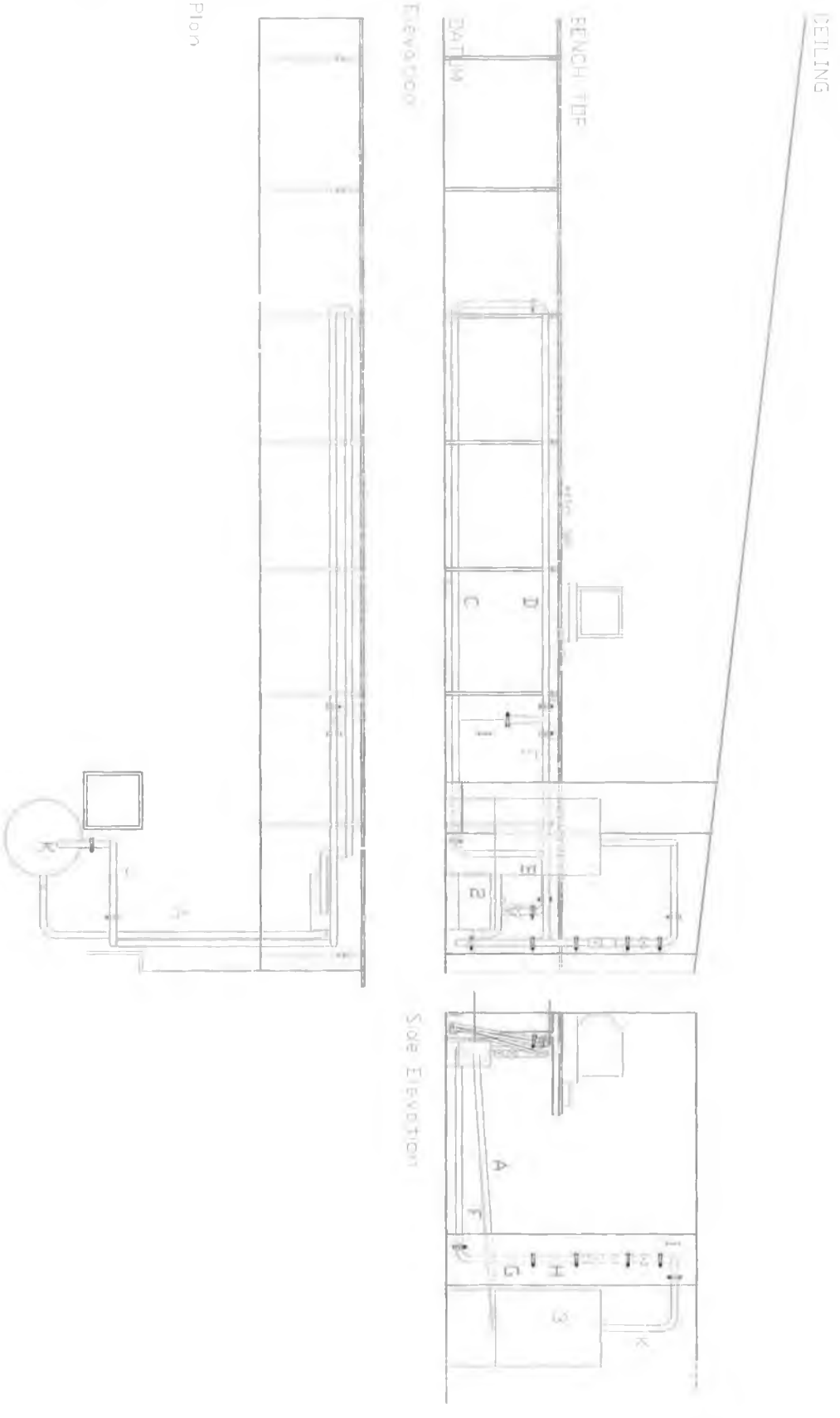

3.4 Results data

3.4.1 Preliminary temperature profiles

Preliminary temperature profiles at U_m = 0.28 m/s (6d)

Time (Sec)	Time (min)	Dead-leg (°C) Maximum	Loop (°C) Maximum
0	0	25.34	80.06
300	5	25.37	80.2
600	10	25.49	78.9
900	15	25.6	79.25
1200	20	25.66	79.38
1500	25	25.81	79.37
1800	30	26	79.3
2100	35	26.25	79.69
2400	40	26.42	79.73
2700	45	26.74	78.93
3000	50	27.03	79.49
3300	55	27.32	79.34
3600	60	27.63	79.73
3900	65	27.91	79.69
4200	70	28.19	79.12
4500	75	28.66	79.93
4800	80	28.92	79.03
5100	85	29.12	79.75
5400	90	29.36	79.43
5700	95	29.55	79.95
6000	100	29.68	79.03
6300	105	29.85	79.67
6600	110	30	79.49
6900	115	30.1	79.23
7200	120	30.25	79.56

Preliminary temperature profiles at U_m = 0.47 m/s (6d)

Time (Sec)	Time (min)	Dead-leg (°C) Maximum	Loop (°C) Maximum
0	0	26.6	80.31
300	5	26.69	80.2
600	10	26.78	79.72
900	15	26.94	80.04
1200	20	27.1	80.17
1500	25	27.47	80.14
1800	30	28.1	79.89
2100	35	29.01	80.21
2400	40	29.75	80.43
2700	45	30.56	80.32
3000	50	31.33	80.58
3300	55	31.9	79.86
3600	60	32.52	80.39
3900	65	33.15	80.8
4200	70	33.82	79.8
4500	75	34.43	81.06
4800	80	34.79	80.22
5100	85	35.27	80.28
5400	90	35.6	80.83
5700	95	35.89	80.3
6000	100	36.1	80.46
6300	105	36.19	81.18
6600	110	36.42	80.65
6900	115	36.69	80.72
7200	120	36.84	80.41

Preliminary temperature profiles at U_m = 0.66 m/s (6d)

Time (Sec)	Time (min)	Dead-leg (°C) Maximum	Loop (°C) Maximum
0	0	27.64	79.62
300	5	27.67	79.45
600	10	27.82	79.54
900	15	27.96	79.34
1200	20	28.72	79.51
1500	25	30.21	79.3
1800	30	31.72	79.64
2100	35	33.21	79.21
2400	40	34.61	79.8
2700	45	36.22	79.41
3000	50	37.71	79.45
3300	55	38.81	79.51
3600	60	40.02	79.51
3900	65	40.72	79.65
4200	70	41.26	79.55
4500	75	41.62	79.97
4800	80	41.88	79.69
5100	85	42.41	79.91
5400	90	42.65	79.81
5700	95	42.89	79.01
6000	100	44.02	79.75
6300	105	44.98	79.08
6600	110	45.61	79.71
6900	115	46.14	79.26
7200	120	46.2	78.63

Preliminary temperature profiles at U_m = 0.85 m/s (6d)

Time (Sec)	Time (min)	Dead- leg (°C) Maximum	Loop (°C) Maximum
0	0	26.6	81.22
300	5	26.71	78.85
600	10	27.05	79.14
900	15	28.98	79.14
1200	20	34.56	78.94
1500	25	41.15	79.14
1800	30	46.08	78.75
2100	35	51.34	79.12
2400	40	57.61	79.12
2700	45	61.11	79.09
3000	50	61.7	79.15
3300	55	65.37	78.84
3600	60	64.79	79.12
3900	65	64.69	78.77
4200	70	66.63	79.1
4500	75	66.89	79.27
4800	80	66.3	79.25
5100	85	66.95	78.9
5400	90	67.34	79.19
5700	95	67.48	79.19
6000	100	67.77	79.17
6300	105	67.4	79.21
6600	110	67.51	79.04
6900	115	67.59	79.12
7200	120	67.13	78.89

Temperature profiles at U_m = 0.19 m/s (6d)

Time (Sec)	Time (min)	Loop (°C) Maximum	Dead-leg (°C) Maximum
0	0	19.56	16.42
300	5	22.2	16.67
600	10	25.08	16.97
900	15	27.65	17.15
1200	20	30.24	17.38
1500	25	32.84	17.53
1800	30	35.53	17.74
2100	35	38.2	17.97
2400	40	40.79	18.2
2700	45	43.25	18.33
3000	50	45.97	18.51
3300	55	48.39	18.67
3600	60	51.05	18.86
3900	65	53.7	19.04
4200	70	56.12	19.2
4500	75	58.82	19.33
4800	80	61.23	19.49
5100	85	63.72	19.65
5400	90	66.29	19.86
5700	95	68.78	20
6000	100	71.17	20.15
6300	105	73.58	20.29
6600	110	76.05	20.42
6900	115	78.42	20.58
7200	120	79.14	20.71
7500	125	78.9	20.89
7800	130	78.58	21.04
8100	135	79.23	21.18
8400	140	79.08	21.29
8700	145	78.76	21.45
9000	150	78.48	21.56
9300	155	79.25	21.67
9600	160	79.1	21.83
9900	165	78.76	21.85
9999	166.65	78.62	21.74

3.4.2 Temperature profiles

Temperature profiles at U_m = 0.28 m/s (6d)

Time (Sec)	Time (min)	Loop (°C) Maximum	Dead-leg (°C) Maximum
0	0	23.05	20.75
300	5	25.87	20.91
600	10	28.81	21.07
900	15	31.77	21.16
1200	20	34.79	21.29
1500	25	37.81	21.42
1800	30	40.77	21.58
2100	35	43.64	21.76
2400	40	46.46	21.94
2700	45	49.18	22.09
3000	50	52.18	22.34
3300	55	54.98	22.52
3600	60	57.74	22.72
3900	65	60.39	22.94
4200	70	63.12	23.16
4500	75	65.8	23.45
4800	80	68.37	23.66
5100	85	70.8	23.75
5400	90	73.29	23.75
5700	95	74.04	23.79
6000	100	73.9	23.81
6300	105	73.52	23.79
6600	110	73.23	23.88
6900	115	73.36	24.15
7200	120	75.48	24.06
7500	125	76.33	24.15
7800	130	76.41	24.28
8100	135	76.13	24.35
8400	140	75.74	24.46
8700	145	76.15	24.53
9000	150	78.48	24.55
9300	155	79.23	26.8
9600	160	79.21	25.02
9900	165	78.52	24.86
9999	166.65	78.31	24.79

Temperature profiles at U_m = 0.56 m/s (6d)

Time (Sec)	Time (min)	Loop (°C) Maximum	Dead-leg (°C) Maximum
0	0	33.06	20.13
300	5	35.9	20.35
600	10	38.53	20.66
900	15	41.28	21.07
1200	20	43.91	21.54
1500	25	46.7	22.12
1800	30	49.55	22.83
2100	35	52.18	23.43
2400	40	54.77	23.99
2700	45	57.55	24.64
3000	50	60.14	25.2
3300	55	62.75	25.84
3600	60	65.37	26.38
3900	65	67.9	26.96
4200	70	70.42	27.52
4500	75	72.81	28.03
4800	80	75.36	28.59
5100	85	77.79	29.12
5400	90	79.73	29.66
5700	95	79.35	30.19
6000	100	79.04	30.61
6300	105	78.72	31.02
6600	110	78.42	31.42
6900	115	79.47	31.81
7200	120	79	32.21
7500	125	78.76	32.58
7800	130	78.6	32.75
8100	135	79.53	33.19
8400	140	79	33.54
8700	145	78.64	33.71
9000	150	79.19	34.09
9300	155	79.39	34.31
9600	160	78.86	34.44
9900	165	78.56	34.46
9999	166.65	78.46	34.35

Temperature profiles at U_m = 0.85 m/s (6d)

Time (Sec)	Time (min)	Loop (°C) Maximum	Dead-leg (°C) Maximum
0	0	32.45	20.04
300	5	35.33	21.2
600	10	38.11	22.34
900	15	40.81	23.45
1200	20	43.51	24.57
1500	25	46.2	26.02
1800	30	48.88	27.29
2100	35	51.49	28.79
2400	40	54.06	30.37
2700	45	56.65	31.79
3000	50	59.22	33.21
3300	55	61.93	34.31
3600	60	64.5	35.18
3900	65	66.93	35.84
4200	70	69.58	36.73
4500	75	72.18	37.85
4800	80	74.53	40.02
5100	85	77.08	43.51
5400	90	79.29	45.2
5700	95	79.35	45.97
6000	100	78.9	46.8
6300	105	78.6	47.9
6600	110	78.84	48.35
6900	115	80.73	48.3
7200	120	78.92	48.39
7500	125	78.64	49.1
7800	130	78.68	49.42
8100	135	79.45	49.57
8400	140	78.98	49.29
8700	145	78.74	49.44
9000	150	78.46	50.04
9300	155	79.29	50.42
9600	160	79	52.29
9900	165	78.7	53.13
9999	166.65	78.62	53.13

Temperature profiles at U_m = 1.03 m/s (6d)

Time (Sec)	Time (min)	Loop (°C) Maximum	Dead-leg (°C) Maximum
0	0	24.95	23.25
300	5	27.79	24.88
600	10	30.63	26.51
900	15	33.39	27.99
1200	20	36.25	32.01
1500	25	39.08	36.01
1800	30	41.77	38.97
2100	35	44.49	40.42
2400	40	47.28	44.13
2700	45	49.97	45.76
3000	50	52.65	48.15
3300	55	55.3	51.45
3600	60	57.95	53.83
3900	65	60.59	54.71
4200	70	63.14	56.69
4500	75	65.74	59.7
4800	80	68.25	62.57
5100	85	70.7	63.93
5400	90	73.23	59.78
5700	95	75.72	65.92
6000	100	78.15	70.28
6300	105	79.47	73.34
6600	110	79.12	73.01
6900	115	78.9	73.66
7200	120	78.6	72.95
7500	125	79	73.44
7800	130	79.41	73.74
8100	135	78.96	73.66
8400	140	78.72	73.96
8700	145	78.46	72.28
9000	150	79.53	73.76
9300	155	79.21	71.07
9600	160	78.92	72.95
9900	165	78.66	71.33
9999	166.65	78.54	69.56

Temperature profiles at U_m = 1.22 m/s (6d)

Time (Sec)	Time (min)	Loop (°C) Maximum	Dead-leg (°C) Maximum
0	0	34.07	31.4
300	5	36.84	34.66
600	10	39.86	36.71
900	15	42.54	40
1200	20	45.43	42.54
1500	25	48.26	44.45
1800	30	51.01	47.08
2100	35	53.78	49.5
2400	40	56.5	52.88
2700	45	59.26	55.78
3000	50	61.87	58.02
3300	55	64.5	60.45
3600	60	67.24	63.12
3900	65	69.93	63.37
4200	70	72.4	67.3
4500	75	74.87	68.45
4800	80	77.34	72.61
5100	85	79.71	73.8
5400	90	79.57	75.85
5700	95	79.27	76.17
6000	100	79.02	76.01
6300	105	78.76	76.03
6600	110	79.71	75.89
6900	115	79.47	76.39
7200	120	79.23	76.55
7500	125	78.9	76.07
7800	130	78.92	75.82
8100	135	79.69	76.45
8400	140	79.33	76.53
8700	145	79.1	76.21
9000	150	78.84	75.97
9300	155	79.73	76.39
9600	160	79.55	76.72
9900	165	79.27	76.61
9999	166.65	79.12	76.29

Temperature profiles at U_m = 1.5 m/s (6d)

Time (Sec)	Time (min)	Loop (°C) Maximum	Dead-leg (°C) Maximum
0	0	34.17	32.03
300	5	37.02	34.81
600	10	39.95	37.54
900	15	42.67	40.57
1200	20	45.58	42.91
1500	25	48.3	45.67
1800	30	51.09	47.92
2100	35	53.7	50.67
2400	40	56.52	53.45
2700	45	59.09	55.68
3000	50	61.87	58.25
3300	55	64.52	60.18
3600	60	66.99	62.75
3900	65	69.5	65.02
4200	70	72.06	66.97
4500	75	74.53	68.86
4800	80	77.04	71.13
5100	85	79.47	73.05
5400	90	79.83	74.25
5700	95	79.55	74.31
6000	100	79.19	74.27
6300	105	78.96	73.74
6600	110	79.87	74.75
6900	115	79.49	74.53
7200	120	79.23	74.79
7500	125	78.84	75.4
7800	130	79.67	75.8
8100	135	79.45	76.09
8400	140	79.17	76.09
8700	145	78.94	75.82
9000	150	79.65	75.56
9300	155	79.75	76.15
9600	160	79.35	76.07
9900	165	79.08	76.01
9999	166.65	78.92	75.97

Temperature profiles at U_m = 0.19 m/s (4d)

Time (Sec)	Time (min)	Loop (°C) Maximum	Dead-leg (°C) Maximum
0	0	28.16	25.44
300	5	30.8	24.59
600	10	33.69	24.04
900	15	36.52	23.59
1200	20	39.36	23.28
1500	25	42.05	22.96
1800	30	44.86	22.76
2100	35	47.6	22.74
2400	40	50.33	22.81
2700	45	52.98	23.01
3000	50	55.64	23.1
3300	55	58.33	23.28
3600	60	60.9	23.41
3900	65	63.6	23.59
4200	70	66.23	23.86
4500	75	68.76	24.12
4800	80	71.49	24.44
5100	85	74.04	24.59
5400	90	76.61	24.82
5700	95	79.21	25.08
6000	100	79.73	25.33
6300	105	79.43	25.62
6600	110	79.14	25.95
6900	115	78.78	26.25
7200	120	79.55	26.56
7500	125	79.49	26.74
7800	130	79.1	27.05
8100	135	78.8	27.34
8400	140	79.59	27.72
8700	145	79.47	27.99
9000	150	79.08	28.19
9300	155	78.76	28.54
9600	160	79.53	28.81
9900	165	79.43	28.95
9999	166.65	79.29	28.95

Temperature profiles at U_m = 0.28 m/s (4d)

Time (Sec)	Time (min)	Loop (°C) Maximum	Dead-leg (°C) Maximum
0	0	31.48	28.59
300	5	34.15	29.79
600	10	36.84	28.86
900	15	39.73	29.41
1200	20	42.48	30.54
1500	25	45.33	32.01
1800	30	47.96	33.28
2100	35	50.5	34.77
2400	40	53.09	35.6
2700	45	55.74	36.67
3000	50	58.21	38.53
3300	55	60.84	39.6
3600	60	63.43	40.53
3900	65	65.84	42.61
4200	70	68.53	44.73
4500	75	70.93	46.63
4800	80	73.5	48.13
5100	85	75.8	49.82
5400	90	78.13	50.98
5700	95	79.61	51.95
6000	100	79.59	54.12
6300	105	79.23	56.16
6600	110	78.94	56.16
6900	115	78.6	55.53
7200	120	79.35	55.07
7500	125	79.29	55.03
7800	130	79.02	55.34
8100	135	78.74	56.02
8400	140	78.9	56.56
8700	145	79.49	56.44
9000	150	79.37	57.03
9300	155	79.04	57.51
9600	160	78.7	57.24
9900	165	78.4	57.32
9999	166.65	78.23	57.3

Temperature profiles at U_m = 0.56 m/s (4d)

Time (Sec)	Time (min)	Loop (°C) Maximum	Dead-leg (°C) Maximum
0	0	31.55	29.95
300	5	34.26	32.16
600	10	36.91	34.68
900	15	39.56	37.3
1200	20	41.92	39.43
1500	25	44.6	42.07
1800	30	47.06	44.51
2100	35	49.63	46.89
2400	40	52.18	49.16
2700	45	54.65	50.92
3000	50	57.26	53.55
3300	55	59.7	56.04
3600	60	62.2	58.12
3900	65	64.71	60.61
4200	70	67.07	62.86
4500	75	69.54	64.56
4800	80	71.96	67.24
5100	85	74.39	68.8
5400	90	76.72	71.72
5700	95	78.9	73.44
6000	100	79.61	74.65
6300	105	79.14	74.45
6600	110	78.84	74.19
6900	115	78.6	74.12
7200	120	79.41	74.79
7500	125	79	74.87
7800	130	78.64	74.35
8100	135	79.47	74.21
8400	140	79.27	74.49
8700	145	78.94	74.61
9000	150	78.58	74.25
9300	155	79.43	74.25
9600	160	79.17	74.47
9900	165	78.8	74.47
9999	166.65	78.66	74.21

Temperature profiles at U_m = 0.85 m/s (4d)

Time (Sec)	Time (min)	Loop (°C) Maximum	Dead-leg (°C) Maximum
0	0	31.35	29.5
300	5	33.98	32.14
600	10	36.78	34.72
900	15	39.47	37.35
1200	20	41.94	39.6
1500	25	44.6	42.18
1800	30	47.25	44.49
2100	35	49.87	47
2400	40	52.42	49.07
2700	45	54.86	51.62
3000	50	57.43	53.95
3300	55	60	55.97
3600	60	62.38	58.44
3900	65	64.79	60.55
4200	70	67.34	62.59
4500	75	69.69	65
4800	80	71.96	67.11
5100	85	74.49	69.3
5400	90	76.72	71.09
5700	95	78.96	73.48
6000	100	79.39	74.1
6300	105	79.04	74.17
6600	110	78.74	73.86
6900	115	78.8	73.62
7200	120	79.51	73.98
7500	125	79.08	73.92
7800	130	78.82	73.56
8100	135	78.52	73.23
8400	140	79.49	73.52
8700	145	79.17	73.5
9000	150	78.86	73.38
9300	155	78.58	73.01
9600	160	79.49	73.38
9900	165	79.21	73.42
9999	166.65	79.04	73.21

Temperature profiles at U_m = 1.03 m/s (4d)

Time (Sec)	Time (min)	Loop (°C) Maximum	Dead-leg (°C) Maximum
0	0	32.4	30.08
300	5	35.22	32.4
600	10	37.98	34.83
900	15	40.64	37.22
1200	20	43.46	39.73
1500	25	46.08	42.01
1800	30	48.71	44.43
2100	35	51.36	46.7
2400	40	54.06	49.14
2700	45	56.69	51.15
3000	50	59.3	53.7
3300	55	61.79	55.95
3600	60	64.32	58.16
3900	65	66.79	60.47
4200	70	69.38	62.57
4500	75	71.88	64.58
4800	80	74.41	66.95
5100	85	76.76	68.95
5400	90	79.21	71.01
5700	95	79.49	71.82
6000	100	79.1	72
6300	105	78.82	71.88
6600	110	78.56	71.72
6900	115	79.47	71.86
7200	120	79.19	72
7500	125	78.92	71.94
7800	130	78.68	71.74
8100	135	79.45	71.9
8400	140	79.29	72.04
8700	145	79	72.04
9000	150	78.74	71.86
9300	155	78.72	71.7
9600	160	79.45	72.06
9900	165	79.14	72.02
9999	166.65	79.06	72.02

Temperature profiles at U_m = 1.22 m/s (4d)

Time (Sec)	Time (min)	Loop (°C) Maximum	Dead-leg (°C) Maximum
0	0	18.7	18.31
300	5	21.89	21.29
600	10	24.77	23.88
900	15	27.76	26.51
1200	20	30.61	29.04
1500	25	33.5	31.61
1800	30	36.32	34.17
2100	35	39.16	36.6
2400	40	42.01	39.03
2700	45	44.81	41.52
3000	50	47.6	43.81
3300	55	50.35	46.12
3600	60	53.13	48.58
3900	65	55.83	50.86
4200	70	58.4	53.17
4500	75	61.21	55.51
4800	80	63.8	57.74
5100	85	66.5	59.83
5400	90	68.99	61.93
5700	95	71.65	64.11
6000	100	74.1	66.21
6300	105	76.78	68.45
6600	110	79.25	70.6
6900	115	79.91	71.68
7200	120	79.57	71.82
7500	125	79.35	71.92
7800	130	79.06	71.92
8100	135	79.83	71.74
8400	140	79.77	72
8700	145	79.49	72.08
9000	150	79.23	71.98
9300	155	78.96	71.65
9600	160	80.05	70.54
9900	165	79.77	70.78
9999	166.65	79.57	70.76

Temperature profiles at U_m = 1.5 m/s (4d)

Time (Sec)	Time (min)	Loop (°C) Maximum	Dead-leg (°C) Maximum
0	0	32.93	32.05
300	5	35.71	34.81
600	10	38.55	37.15
900	15	41.3	39.84
1200	20	44.15	42.22
1500	25	46.83	44.68
1800	30	49.63	47.04
2100	35	52.4	49.67
2400	40	55.05	51.89
2700	45	57.7	54.69
3000	50	60.41	56.73
3300	55	62.94	58.65
3600	60	65.39	61.79
3900	65	68.14	64.34
4200	70	70.68	66.27
4500	75	73.13	68.51
4800	80	75.56	71.33
5100	85	77.93	72.44
5400	90	79.69	74.73
5700	95	79.47	74.97
6000	100	79.19	74.67
6300	105	78.92	74.47
6600	110	78.68	74.23
6900	115	79.77	74.91
7200	120	79.45	75
7500	125	79.17	74.47
7800	130	78.9	73.94
8100	135	79.08	73.84
8400	140	79.71	74.19
8700	145	79.33	74.12
9000	150	79.1	73.98
9300	155	78.82	73.86
9600	160	79.63	73.84
9900	165	79.69	74.35
9999	166.65	79.45	74.25

Temperature profiles at U_m = 0.19 m/s (2d)

Time (Sec)	Time (min)	Loop (°C) Maximum	Dead-leg (°C) Maximum
0	0	18.58	18.45
300	5	22.18	21.36
600	10	25.02	24.15
900	15	27.94	26.8
1200	20	30.67	29.28
1500	25	33.56	31.77
1800	30	36.23	34.31
2100	35	39.14	36.91
2400	40	42.01	39.64
2700	45	44.83	42.14
3000	50	47.6	44.62
3300	55	50.44	47.19
3600	60	53.22	49.85
3900	65	55.93	52.67
4200	70	58.8	55.47
4500	75	61.39	57.95
4800	80	64.19	60.53
5100	85	66.76	62.57
5400	90	69.48	65.53
5700	95	72.06	67.73
6000	100	74.61	69.83
6300	105	77.1	72.42
6600	110	79.21	74.35
6900	115	79.21	75.02
7200	120	78.8	74.39
7500	125	79.31	74.91
7800	130	79.21	74.91
8100	135	78.64	74.35
8400	140	79.29	74.91
8700	145	78.94	74.81
9000	150	78.72	74.41
9300	155	79.27	74.75
9600	160	78.82	74.51
9900	165	78.54	74.41
9999	166.65	78.38	74

Temperature profiles at U_m = 0.28 m/s (2d)

Time (Sec)	Time (min)	Loop (°C) Maximum	Dead-leg (°C) Maximum
0	0	24.04	23.7
300	5	26.67	26.22
600	10	29.44	28.77
900	15	31.88	31.15
1200	20	34.68	33.87
1500	25	37.24	36.34
1800	30	39.78	38.79
2100	35	42.31	41.15
2400	40	44.75	43.59
2700	45	47.34	46.01
3000	50	49.87	48.37
3300	55	52.5	50.92
3600	60	54.88	53.26
3900	65	58	56.33
4200	70	61.09	59.43
4500	75	63.39	61.83
4800	80	65.9	64.19
5100	85	68.37	66.76
5400	90	70.72	69.07
5700	95	73.11	71.37
6000	100	75.5	73.64
6300	105	77.73	75.78
6600	110	79.45	77.48
6900	115	79.47	77.53
7200	120	79.23	77.44
7500	125	78.86	76.94
7800	130	78.54	76.74
8100	135	79.23	77.24
8400	140	79.35	77.36
8700	145	79.08	77.14
9000	150	78.76	76.94
9300	155	78.42	76.63
9600	160	79.33	77.38
9900	165	79.17	77.32
9999	166.65	79.1	77.18

Temperature profiles at U_m = 0.56 m/s (2d)

Time (Sec)	Time (min)	Loop (°C) Maximum	Dead-leg (°C) Maximum
0	0	32.34	32.03
300	5	35.22	34.79
600	10	37.72	37.3
900	15	40.47	40.02
1200	20	42.93	42.46
1500	25	45.43	44.98
1800	30	48.22	47.64
2100	35	50.8	50.18
2400	40	53.28	52.71
2700	45	55.97	55.32
3000	50	58.27	57.55
3300	55	60.84	60.1
3600	60	63.29	62.51
3900	65	65.78	64.87
4200	70	68.37	67.38
4500	75	70.52	69.54
4800	80	72.99	71.96
5100	85	75.24	74.14
5400	90	77.53	76.41
5700	95	79.31	78.25
6000	100	79.21	78.15
6300	105	78.88	77.89
6600	110	78.6	77.63
6900	115	79.41	78.34
7200	120	79.35	78.34
7500	125	79.1	78.09
7800	130	78.78	77.81
8100	135	78.7	77.63
8400	140	79.45	78.38
8700	145	79.25	78.21
9000	150	78.94	77.95
9300	155	78.62	77.65
9600	160	79.47	78.36
9900	165	79.37	78.34
9999	166.65	79.27	78.21

Temperature profiles at U_m = 1.03 m/s (2d)

Time (Sec)	Time (min)	Loop (°C) Maximum	Dead-leg (°C) Maximum
0	0	32.93	32.73
300	5	35.99	35.71
600	10	38.94	38.59
900	15	41.9	41.54
1200	20	44.77	44.34
1500	25	47.66	47.17
1800	30	50.44	49.97
2100	35	53.28	52.73
2400	40	56.06	55.6
2700	45	58.88	58.46
3000	50	61.68	61.21
3300	55	64.4	63.88
3600	60	67.09	66.54
3900	65	69.81	69.21
4200	70	72.53	71.88
4500	75	75.16	74.47
4800	80	77.81	77.12
5100	85	79.71	78.94
5400	90	79.49	78.76
5700	95	79.25	78.5
6000	100	78.96	78.25
6300	105	79.49	78.72
6600	110	79.63	78.88
6900	115	79.33	78.6
7200	120	79.04	78.31
7500	125	78.78	78.31
7800	130	79.89	79.12
8100	135	79.51	78.82
8400	140	79.23	78.52
8700	145	78.96	78.23
9000	150	79.63	78.84
9300	155	79.73	78.96
9600	160	79.37	78.6
9900	165	79	78.27
9999	166.65	78.94	78.17

Temperature profiles at U_m = 1.5 m/s (2d)

Time (Sec)	Time (min)	Loop (°C) Maximum	Dead-leg (°C) Maximum
0	0	31.77	31.66
300	5	34.79	34.59
600	10	37.68	37.48
900	15	40.42	40.23
1200	20	43.46	43.14
1500	25	46.2	45.93
1800	30	49.07	48.75
2100	35	51.81	51.49
2400	40	54.58	54.18
2700	45	57.32	56.9
3000	50	60.06	59.62
3300	55	62.77	62.2
3600	60	65.47	65
3900	65	68.1	67.51
4200	70	70.68	70.02
4500	75	73.21	72.69
4800	80	75.87	75.14
5100	85	78.44	77.71
5400	90	80	79.23
5700	95	79.71	79.04
6000	100	79.39	78.76
6300	105	79.17	78.46
6600	110	78.86	78.19
6900	115	79.91	79.23
7200	120	79.57	78.92
7500	125	79.33	78.62
7800	130	79.02	78.34
8100	135	79.89	79.14
8400	140	79.79	79.04
8700	145	79.45	78.74
9000	150	79.12	78.44
9300	155	78.88	78.23
9600	160	79.73	79.04
9793	163.2167	79.53	78.84

3.4.3 Temperature Distribution data (6d)

Um = 0.19 m/s		Um = 0.56 m/s		Um = 0.85 m/s	
Position (mm)	Temperature (^{0}C)	Position (mm)	Temperature (^{0}C)	Position (mm)	Temperature (^{0}C)
300	22	0	80.8	300	53.2
290	22.5	50	80.6	295	57
280	22.8	100	80.6	290	60
270	23.2	150	80.6	285	62.3
260	23.8	180	80	280	64.7
250	24.5	190	78.6	275	67.4
240	25.5	200	78.4	270	72
230	26.7	210	78	265	75
220	28.3	220	75	260	76
210	30.1	230	73	255	77
200	32.3	240	66	250	77.6
190	35.1	250	58.5	240	78.4
180	38.7	260	51.4	230	78.5
170	42.9	270	46.4	220	78.4
160	48.6	280	42.2	210	79
150	54	290	38.5	200	79.2
140	61.5	300	35.16	150	79.8
130	70.5			100	80
125	75			50	80
120	77			0	80
115	77.8				
110	78.4				
105	78.8				
100	78.9				
50	79.5				
0	80.1				

Temperature distribution data conti. (6d)

Um = 1.03 m/s		Um = 1.22 m/s		Um = 1.5 m/s	
Position (mm)	Temperature (^{0}C)	Position (mm)	Temperature (^{0}C)	Position (mm)	Temperature (^{0}C)
300	68.6	300	76	300	75.2
295	70.3	297.5	76.7	290	77.6
290	73.25	295	77	280	78.5
285	73.8	290	77	270	79
280	75.6	285	77	260	79.2
275	76.2	280	77	250	79.7
270	76.35	275	78	200	80.2
265	77.1	270	78	150	80.5
260	77.5	265	78.5	100	80.5
255	78	260	78.5	50	80.5
250	78	250	78.6	0	80.6
240	78	240	78.6		
230	79.63	230	78.6		
220	80.1	220	79		
210	80	200	79.4		
200	80.1	150	80.2		
150	80.5	100	80.5		
100	80.7	50	80.7		
50	80.7	0	81		
0	80.9				

Temperature distribution data (4d)

Um = 0.19 m/s			Um = 0.28 m/s			Um = 0.56 m/s	
Position (mm)	Temperature (^{0}C)		Position (mm)	Temperature (^{0}C)		Position (mm)	Temperature (^{0}C)
200	29		200	58.12		200	74
190	31.5		195	63.3		195	77.67
180	34.9		190	67.5		190	78
170	39.2		185	72		185	78.58
160	44.1		180	75.4		180	78.9
150	50		175	77		175	79
140	57		170	77.6		170	79.45
130	65.3		165	78		165	80.19
120	72		160	78.6		160	80.15
115	75		155	78.7		155	80.25
110	77.6		150	78.9		150	80.15
105	78.3		145	79		100	80.25
100	78.7		140	79.3		50	80.25
90	79.6		135	79.7		0	80.43
80	80		130	79.8			
70	80.21		120	80.3			
60	80.3		110	80.4			
50	80.25		100	80.5			
0	80.8		50	80.65			
			0	81.2			

Um = 0.85 m/s			Um = 1.03 m/s			Um = 1.22 m/s	
Position (mm)	Temperature (^{0}C)		Position (mm)	Temperature (^{0}C)		Position (mm)	Temperature (^{0}C)
200	72.8		200	72		200	70.5
197.5	76.1		197.5	75.2		197.5	72.8
195	77.36		195	77.2		195	76.4
190	78.6		190	78.3		190	78.3
185	79.4		185	78.8		185	78.9
180	79.63		180	79.1		180	79.2
175	79.7		175	79.3		175	79.4
170	79.8		170	79.4		170	79.7
165	79.8		165	79.6		165	79.8
160	79.8		160	79.6		160	79.9
155	79.7		155	80		150	80.1
150	79.9		150	80.7		100	80.1
140	80.6		140	80.8		50	80.1
130	80.6		100	80.8		0	80.25
110	80.6		50	80.8			
100	80.6		0	80.9			
50	80.6						
0	80.7						

Temperature distribution data conti. (4d)

Um = 1.5 m/s	
Position (mm)	Temperature (^{0}C)
200	74.4
197.5	77
195	78.42
190	79
185	79.4
180	79.8
175	79.9
170	80
165	80.2
160	80.2
150	80.3
100	80.35
50	80.35
0	80.4

Temperature distribution data (2d)

Um = 0.19 m/s	
Position (mm)	Temperature (^{0}C)
100	72.77
97.5	75.04
95	76.6
90	77.8
85	78.5
80	79
75	79.2
70	79.3
65	79.5
60	79.5
55	79.5
50	79.41
40	79.43
30	79.45
20	79.8
10	80
0	80.1

Um = 0.28 m/s	
Position (mm)	Temperature (^{0}C)
100	76.4
97.5	77.3
95	77.7
90	79.5
85	79.8
80	80.1
70	80.4
60	80.5
50	80.55
0	80.7

Um = 0.56 m/s	
Position (mm)	Temperature (^{0}C)
100	78.15
97.5	78.7
95	79.04
90	79.6
85	79.93
80	80.11
75	80.25
70	80.35
65	80.4
60	80.45
55	80.45
50	80.45
40	80.45
20	80.51
0	80.55

Um = 1.03 m/s	
Position (mm)	Temperature (^{0}C)
100	78.3
97.5	79.4
95	79.7
90	80
70	80.7
50	80.9
0	81

Um = 1.5 m/s	
Position (mm)	Temperature (^{0}C)
100	78.78
97.5	79.08
95	79.5
90	79.7
85	80
80	80.2
70	80.45
50	80.6
0	80.65